Czech Technical University in Prague
Faculty of Electrical Engineering
Department of Measurement

Magnetic calibration by using non-linear optimization method

Doctoral Thesis

Aleš Zikmund

Prague, December 2014

Ph.D. Program:	Electrical Engineering and Information Technology
Branch of study:	Measurement and Instrumentation
Supervisor:	Prof. Ing. Pavel Ripka, CSc.
Supervisor-Specialist:	Doc. Ing. Antonín Platil, Ph.D.

Acknowledgement

I would like to thank everybody who has helped me with this work, mainly to my supervisor prof. Pavel Ripka for his advice and feedback. I would like to also express the appreciation to cooperative laboratories that allowed me to make experiments in their facilities. My thanks also go to my colleagues from the MagLab group. Finally, I wish to appreciate the support and patience of my family and my girlfriend.

The research presented here has been performed in collaboration with the following institutions:

Physikalisch-Technische Bundesanstalt Braunschweig, Braunschweig, Germany
GFZ Helmholtz Centre Postam, Niemegk, Germany
Institute of Geophysics, Academy of Sciences of the Czech Republic
Czech Metrology Institute, Laboratory of Fundamental Metrology, CZ
Billingsley Aerospace & Defense Inc., Germantown, MD, USA
Brownline, Meerkerk, NL

The research has been funded, or partially funded, by following grants:

Czech Science Foundation
102/09/H082 “Sensors and intelligent sensor systems”
Czech Technical University in Prague
SGS12/194/OHK3/3T/13 “Application of magnetic sensors for precise measurements”

Abstract

This thesis deals with optimization methods in magnetic measurements. It is focused on two important complex non-linear problems: calibrations of coil systems and magnetic tracking. Both mentioned magnetic problems do not have analytical solution, and therefore it is necessary to use non-linear optimization algorithms. The work contains theoretical research of the magnetic problems and their solutions which are designed with respect to minimizing measurement uncertainty.

Tri-axial magnetometers can be calibrated in tri-axial coil systems which have a specific magnetic homogeneity given by the arrangement and dimensions of the coils. The important parameters are coil constants and orthogonality which have to be calibrated in order to achieve a very precise metrological traceability.

In this work, I describe a novel calibration procedure that eliminates weak points of standard methods. The developed method is based on a measurement of a scalar magnetic field during a specific excitation of the coils. An appropriate number of current combinations has to be applied to obtain measurements enabling calculation of all parameters of the coil system by using the Levenberg-Marquardt optimization method. Due to the iterative method of calculation, the standard uncertainty analysis cannot be exploited. Therefore, I have chosen the Monte Carlo method for estimating the uncertainty. Experimental calibrations proved that the procedure can achieve uncertainty below 100 ppm.

A coil system, calibrated by the novel method, can be utilized for calibration of tri-axial magnetometers. Since it is very complicated to build a conventional field-nulling system because of various drifts, I designed a new calibration approach. The Earth's field is monitored by a precise scalar magnetometer and the field-cancellation system is inactive. Based on a sequence of precisely measured currents applied to the coils and measurements of the magnetometer response, the parameters (sensitivities and orthogonalities) of the tri-axial magnetometer can be calculated by using a non-linear optimization method. I have carried out an experimental calibration of a digital tri-axial magnetometer with the uncertainty of 350 ppm for sensitivities and 0.045 degree for the orthogonality.

I have also designed and tested a new principle of magnetic tracking based on non-linear optimization. A coil, generating magnetic field, causes a response of a tri-axial magnetic sensor depending on their mutual position. Based on magnetometer values, the arbitrary position is estimated by using a non-linear optimization. However, this calculation principle does not cover all possible situations, and so a tracker for a real application needs to be extended by an inertial navigation unit. After solving the symmetry problem, the magnetic tracker is used for horizontal drilling where it determines a mutual position of two approaching drill heads. The achieved precision is 0.3 meters in range of 10 meters.

Abstrakt

Tato dizertační práce se zabývá použitím optimalizačních metod v magnetických měřeních. Zaměřuje se na dva nelineární problémy: kalibrace cívkových systémů a určování polohy z magnetického pole. Oba problémy nemají analytické řešení a výpočty se provádí pomocí nelineárních optimalizačních metod. Práce obsahuje teoretický rozbor magnetických problémů a navrhuje jejich aplikaci s ohledem na minimalizaci nejistot měření.

Pro kalibrace magnetických senzorů se používá tříosých cívek, které mají významnou homogenitu magnetického pole danou jejich uspořádáním a rozměry. Důležitými parametry cívek jsou především jejich citlivosti a vzájemná kolmost os cívek. Ty musí být kalibrovány, aby bylo dosaženo velmi přesné metrologické návaznosti.

Práce podrobně popisuje novou kalibrační metodu, která překonává nevýhody stávajících kalibračních postupů. Je založena na měření skalární hodnoty magnetického pole cívek během jejich excitace sekvencí proudů. Parametry cívek jsou pak počítány pomocí optimalizační metody Levenberg-Marquardt. Jelikož se však jedná o iterační metodu, pro odhad nejistot měření musela být použita metoda Monte Carlo. Provedené experimenty prokázaly, že metoda je schopna měřit s nejistotou pod 100 ppm.

Standardní principy kalibrací tříosých magnetometrů spoléhají na vynulování zemského pole, ale takový přístup je komplikovaný kvůli přítomnosti různých nestabilit parametrů regulační smyčky. Proto jsem navrhl metodu, která odstraňuje regulační nulovací smyčku a snižuje tak chyby měření. Kalibrovaný magnetometr se vystaví sekvenci magnetických polí, která je generována tříosým cívkovým systémem, přičemž zemské magnetické pole je monitorováno přesným skalárním magnetometrem. Vhodnou volbou sekvence proudů tekoucích do cívek se zaručí, že je možné odhadnout parametry tříosého magnetometru pomocí optimalizačního algoritmu. Při vzorové kalibraci digitálního magnetometru jsem dosáhl nejistot 350 ppm pro citlivost os a 0.045 stupně pro vzájemné kolmosti os.

V rámci této práce jsem vyvinul vylepšený princip určování pozice z magnetického pole. Cívka, generující definované magnetické pole, způsobí odezvu na měřicím tříosém magnetometru odpovídající vzájemné pozici. Z hodnot měření magnetometru a znalostí parametrů cívky lze vypočítat libovolnou vzájemnou pozici cívky a magnetometru díky optimalizační iterační metodě. Výpočet pozice pouze z magnetického měření však nedokáže podchytit všechny možné polohy a je nutné doplnit zařízení o inerciální navigační jednotku. Po vyřešení problému symetrie magnetického pole byl tento magnetický princip nasazen jako navigační systém pro měření vzájemné polohy dvou horizontálně vrtacích hlavic a bylo dosaženo přesnosti 0.3 metru v rozsahu 10 metrů.

Contents

1 State of the art 1
1.1 Magnetic sensor calibration 1
Coil system 1
Calibration of the coil system 6
1.2 Magnetic tracking 9
1.3 Non-linear optimization method 11
Convergence of optimization methods 12
Line search 13
Curve fitting 13
Gradient Descent (GD) 14
Steepest descent 14
Newton's method for multidimensional problems 15
Variable metric method 16
Levenberg-Marquardt modification 16
Trusted region method 17
2 Objectives of the dissertation 18
2.1 Calibration of coil systems 18
2.2 Magnetic tracker application 19
3 Scalar calibration of coil systems 20
3.1 Scalar magnetometers 20
Proton magnetometers 20
Alkali vapor magnetometer (optically pumped) 22
Overhauser magnetometer 22
3.2 Principle of scalar calibration 23
Single coil - Sensitivity 24
Double coil - orthogonality 25
Triple coil 26

Non-linear optimization algorithm....28
3.3 Uncertainty analysis....28
Type A uncertainty....28
Type B uncertainty....28
Estimating the uncertainty of sensitivity calibration....30
Estimating the uncertainty of orthogonality calibration....30
3.4 Procedure....34
3.5 Testing scalar calibration....37
The coil system in Pruhonice....37
Braunbek coil system at PTB Braunschweig....42
Coil constant calibration....45
Calibration of orthogonality....47
Helmholtz coil system – GFZ Niemegk, Postdam....50
4 Calibration of tri-axial magnetometer....56
4.1 New calibration method....56
4.2 Uncertainty analysis....59
4.3 Experimental calibration of a magnetometer....59
5 Magnetic tracker....63
5.1 Principle....63
Source of the magnetic field....63
Magnetic sensor....65
The mathematical point of view....65
Excitation sequence....66
5.2 Distance sensor....67
5.3 Magnetic tracker – hybrid system....72
Inertial measurement unit (IMU)....74
Coil – the source of the magnetic field....74
Symmetry problem....75
Excitation sequence:....77

Error analysis of the calculation 77
5.4 Magnetic tracker for horizontal directional drilling (HDD) – system design .. 79
Power and communication 81
Mechanical construction of the chain 81
Magnetic tracker units 83
Coil unit 84
Magnetometer unit 85
Excitation sequence 87
Synchronization 87
Symmetry problem – horizontal directional drilling 89
Measurement procedure: 90
Precision of the hybrid magnetic tracker 91
6 Conclusions 94
6.1 Scalar calibration of the coil system 94
6.2 Magnetic tracker 94
6.3 Achieved objectives 95
6.4 Issues for further research 96
7 Publications, whit author's share in % 97
7.1 Peer reviewed publications – journals indexed in JCR 97
7.2 Publications in journals excerpted by WoS 98
7.3 Other publications 98
7.4 Projects 98
8 Bibliography 99
9 Abbreviations 102

1 State of the art

1.1 Magnetic sensor calibration

Magnetic sensors used in practical applications have to be calibrated. They suffer from many specific error parameters that cannot be suppressed or that can change over a long-term period of time. Typical cases are the fluxgate sensor (Ripka, 2001) or the AMR magnetometer (Ripka, 2001). It is necessary to know their offset, sensitivity and orthogonality values (in a 3D setup) in order to make an accurate measurement of the magnetic field. A major task in the calibration procedure is to establish these parameters. Basic calibration procedures are summarized in (Ripka & Zikmund, 2013).

The presence of the Earth's magnetic field all over the world complicates the calibration of sensors. It is therefore very complicated to measure some parameters of magnetic sensors (e.g. offsets).

For this purpose, magnetic shielding creates a near-zero magnetic field. This can be used for offset and for stability measurements including noise measurement.

Coil system

Coil systems, in their essence, create a defined magnetic field in terms of direction and magnitude. If the coil axis is precisely oriented in the direction of the Earth's field vector, a "magnetic vacuum" can be formed by the coil current which is controlled by the feedback remote magnetic sensor. The same task can be achieved by a tri-axial coil system in arbitrary orientation with respect to the Earth's field. The coil system can additionally create a defined, arbitrarily oriented, magnetic field. (Hakkinen & Ryno, 1990) present magnetometer calibration in a supposedly ideal orthogonal coil system. They used the 2-meter coil system and precisely positioned theodolite to calibrate tri-axial magnetic sensors.

We can divide coil systems into two groups: a one-dimensional group, having only one axis and a three-dimensional group with three perpendicular axes that are more complex. Not only the sensitivity but also the orthogonality has to be known (or calibrated) in order to ensure precision of the coil system, since the manufacturing process of the coil system does not guarantee the perpendicular angles.

The main consideration is homogeneity of the magnetic field of the coil. When a magnetic sensor is calibrated with coils, homogeneous magnetic field is assumed within the volume of the coil and the homogenous volume has to be dimensioned to at least the size of the sensor. The greater the volume is, the more precise calibration can be achieved. The homogeneity of the coil system is evaluated by calculating the

magnetic field in each point of the coil volume. In the simple case of square coils, the magnetic field vector produced at an arbitrary position in the space of the coil can be evaluated using the Biot-Savart law as the sum of the magnetic fields of each linear coil segment. The equations are presented in (Herceg, et al., 2009). However, a problem appears when studying the homogeneity of circular coils, because the off-axis values have very complex calculations.

In the 1940s, this problem was expressed by the elliptical integral of first and second order, which approximates the mathematical function of the magnetic field of coils with a polynomial within the relative error of 10^{-8}.

An elliptical description formulates the magnetic field in the cylindrical coordinate system. Due to rotational symmetry, the third coordinate can be neglected and thus the radial B_r and axial B_a components are described as:

$$B_r = \frac{\mu_0 I}{2\pi} \frac{z}{r\sqrt{(a+r)^2+z^2}} \left[-K(k) + \frac{a^2+r^2+z^2}{(a-r)^2+z^2} E(k) \right] \quad (1)$$

and

$$B_z = \frac{\mu_0 I}{2\pi} \frac{z}{\sqrt{(a+r)^2+z^2}} \left[K(k) + \frac{a^2-r^2-z^2}{(a-r)^2+z^2} E(k) \right] \quad (2)$$

where a - axial distance
r – radial distance
z - distance

Another way to investigate the homogeneity is by using FEM simulation. Large models and precise meshing can be used for the calculation because present-day computers have high enough calculating performance to solve an appropriate number of model elements. The simulation can involve the finite size of the coil caused by winding, and thus provides a more accurate approximation of a real coil system.

Several configurations of coils producing a homogeneous field will now be discussed.

Helmholtz coils

These coils consist of a pair of circular (optionally square) coils each having N turns. Each coil carries a current I and they are separated by a distance which is equal to the radius of the coil. The design is derived from the first and second spatial derivatives of

the magnetic field on the mid plane and these derivatives are zeroed. In the mid plane between the two coils, a homogeneous magnetic field B is produced (Bronaugh, 1990).

$$B = \left(\frac{4}{5}\right)^{\frac{3}{2}} \frac{\mu_0 NI}{r} \qquad (3)$$

where r is the radius of the coil (the distance between coils) and B is the magnetic field that is generated.

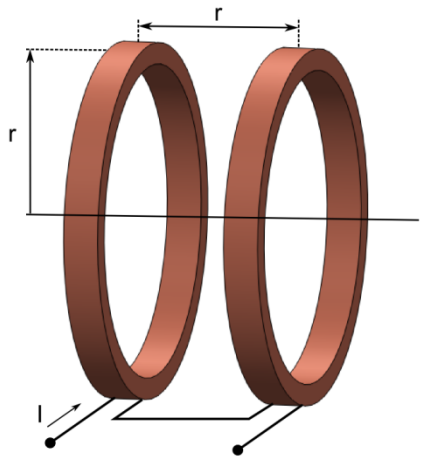

Figure 1. *Configuration of Helmholtz coils.*

The adverse ratio homogeneous area versus the coil radius rules the Helmholtz coil out for many applications (i.e the coils must be too large for given homogeneous area size). The homogeneous space size also depends on the allowable field tolerance - see Figure 4 below. The Maxwell configuration or some other multi-sectional coil system brings an improvement.

Maxwell coils

This setup has a more homogeneous magnetic field inside the coils, at the expense of complexity. The coil pair has a different distance and additionally the third coil is in the mid plane. The coils approximate the surface of a sphere (spherical coil would provide an ideal homogeneity). The main coil is placed in the middle, according to the picture below, and its radius is R. The side coils have a radius of $R\sqrt{4/7}$ and have a distance of $R\sqrt{3/7}$ from the middle.

The side coils should be wound with $N(49/64)$ turns, where N is the nominal number of turns of the middle coil.

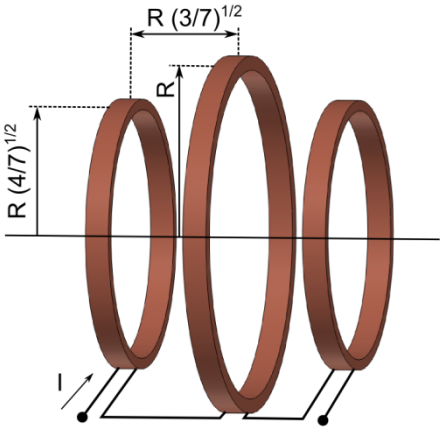

Figure 2. *Maxwell coil setup.*

Braunbek coils

Another way to improve the homogeneity of a coil system is to use a four-coil arrangement based on the Fanselau setup (Fanselau, 1929). The circular outer coils (square coils can also be used) have a smaller radius a_1 distanced from the middle d_1 by and the inner coils have a radius a_2, distanced by d_2. The ratios are then:

$$\frac{d_1}{a_1} = 1.107, \qquad \frac{a_2}{a_1} = 1.309, \qquad \frac{d_2}{a_1} = 0.364, \qquad \frac{d_2}{a_2} = 0.278,$$

The number of turns is equal in each coil and the current exciting the coil is also the same.

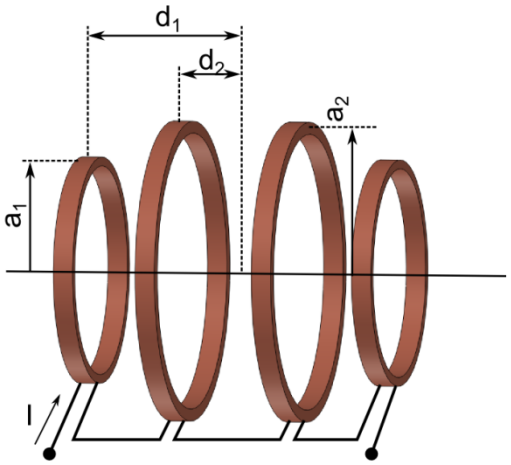

Figure 3. *Braunbek coil system.*

Homogeneity, an important parameter of the coils, is compared in Table 1 and Table 2.

Table 1. Non-homogeneity in the axis direction (taken from (Braunbek, 1934)).

Coil setup	r/R = 0.1	r/R = 0.2	r/R = 0.8
Simple coil	$-1.5\cdot10^{-2}$	$-6\cdot10^{-2}$	$-1.2\cdot10^{-1}$
Helmholtz coils	$-2\cdot10^{-4}$	$-3\cdot10^{-3}$	$-1.3\cdot10^{-2}$
Fanselau coils	$8\cdot10^{-7}$	$5\cdot10^{-5}$	$6\cdot10^{-4}$
Braunbek coils	$-3\cdot10^{-8}$	$-9\cdot10^{-6}$	$-2\cdot10^{-4}$

Table 2. Non-homogeneity in the direction perpendicular to the axis(taken from (Braunbek, 1934)).

Coil setup	r/R = 0.1	r/R = 0.2	r/R = 0.8
Simple coil	$7.5\cdot10^{-8}$	$3\cdot10^{-2}$	$7\cdot10^{-2}$
Helmholtz coils	$-7\cdot10^{-5}$	$-1\cdot10^{-3}$	$-6\cdot10^{-3}$
Fanselau coils	$-2.5\cdot10^{-7}$	$-1.6\cdot10^{-5}$	$-2\cdot10^{-4}$
Braunbek coils	$-9\cdot10^{-9}$	$-2.4\cdot10^{-6}$	$-6\cdot10^{-5}$

Numerous improvements have been developed subsequently to produce a larger uniform magnetic field. They have been established from the derivatives of higher orders using a 3-coil or higher order coil setup. For simplicity of machining, most of them are designed as rectangular coils, and their ampere-turns ratio is adjusted to be an integer number. A summary of the coils systems is presented in (Kirschvink, 1992). Table 3 presents possible setups of the coils.

An FEM simulation was performed to compare the homogeneity of a number of setups. Figure 4 compares among the Helmholtz, Lee-Whiting and square 4-coil Merrite setups.

Table 3. An overview of the coils setup for a homogenous magnetic field (taken from (Kirschvink, 1992)).

Coil design	Coil shape	No. of coils	Coil length or dia	Coil spacing w.r.t center	Ampere-turn ratios	Homogeneity at r/R=0.1 (FEM)
Helmholtz	circle square	2 2	d,d d,d	-0.25d,+ -0.2726d,+	1/1 1/1	$1.1 \cdot 10^{-4}$ $(1 \cdot 10^{-4})$
Lee-Whiting	circle	4	d,d,d,d	-0.4704d, -0.1216d, +, +	9/4/4/9	$2.67 \cdot 10^{-5}$ $(1.34 \cdot 10^{-5})$
Merritte et. all	square	3	d,d,d	-0.4106d, 0, +	39/20/39	
Alldred & Scollar	square	4	0.955d, d,d, 0.955d	-0.5254d, -0.1441d, +, +	21/11/11/21	
Merrite et. al.	square	4	d,d,d,d	-0.5055d, -0.1281d, +, +	26/11/11/26 85/36/36/85	$5.66 \cdot 10^{-8}$ $(1.32 \cdot 10^{-5})$
Rubens	square	5	d,d,d,d,d	-0.5d, -0.25d, 0, +, +	19/4/10/4/19	

Calibration of the coil system

Coil systems are assembled from copper wire wound on a support. Although the theoretical model for coils is precisely derived, manufacturing imperfections can cause that the parameters do not fit the model, mainly in the matter of sensitivity. Another difficulty with the three-dimensional coil system concerns perpendicularity. Previous works, e.g. (Hakkinen & Ryno, 1990), neglected this parameter with respect to dimensions of coil systems, and the coils were assumed to be perpendicular. Due to increasing requirements on sensor parameters, this assumption is no longer acceptable and all the calibration coil parameters have to be found. The calibrated parameters of coil systems are listed in Table 4. The main parameters are the sensitivity of each axis and the mutual orthogonality. Other angular parameters included in the list represent the orientation between the coil axes and the Earth's magnetic vector.

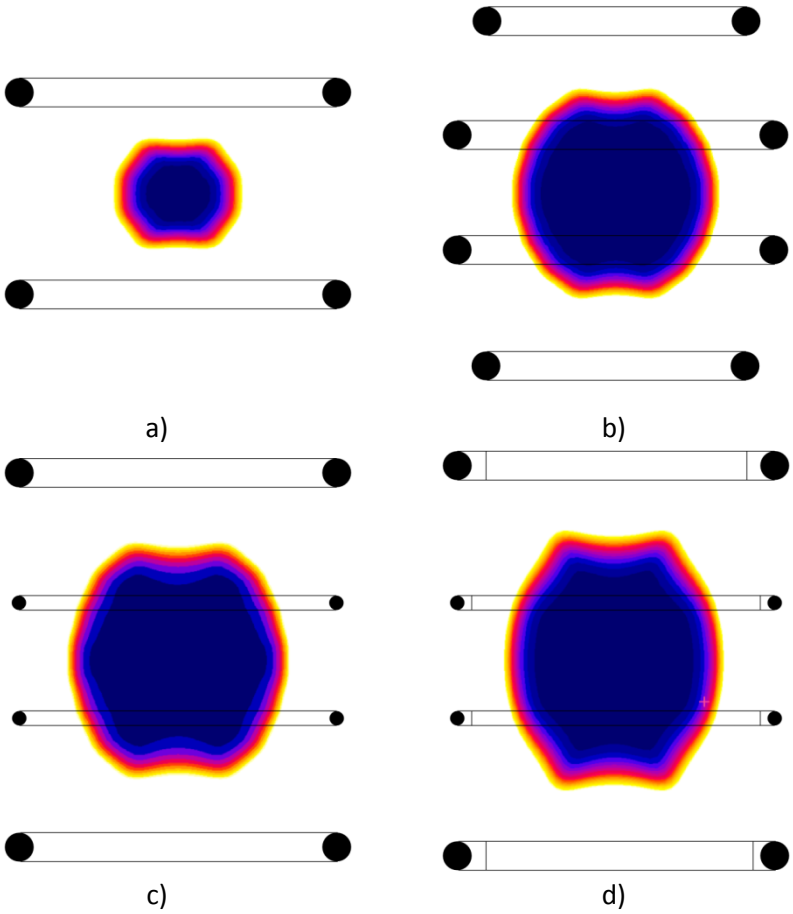

Figure 4. *Comparison of coil homogeneity for the same diameter (cross-section of coils): a) Helmholtz coils (circular), b) Braunbek coils (circular), c) Lee-Whiting (circular) and d) Merrite (square) coils. Color map of homogeneity (blue 0.1% and yellow is 1%).*

A simple procedure was developed in (Stupak Jr, 1995) for calibrating one-axial Helmholtz coils used for measuring permanent magnet moments. The gaussmeter, that Stupak recommends, measures the flux by crossing a coil of known area and known turns. The Helmholtz coil is supplied with the current source and the gaussmeter measures the magnetic flux density. The sensitivity of the coil is determined by dividing the magnetic flux by the current.

A one-dimensional coil can also be calibrated in a coil system of known constants. The tested coil is placed in the middle of the known coils and the magnetometer, usually a fluxgate magnetometer, is aligned to measure in the direction of the magnetic field that is created. In fact, the fluxgate indicates a zero magnetic field because the magnetic field created by the known coils should be compensated by the calibrated coil. The two currents are balanced to reach a zero magnetic field. The

constant is then given by the ratio of the currents and the known coil constant. These methods are sorted into comparative methods, which are summarized in (Jankowski & Sucksdorff, 1996).

A very precise calibration can be made by using a scalar magnetometer and an active cancelation system which suppresses the Earth's magnetic field. The precise scalar magnetometer measures the magnetic field excited by the measured coil, while the comparatively huge cancelation coil system compensates the Earth's field. The sensitivity of the coil is calculated by dividing the magnetic field by the coil current.

The most widely used method for calibrating a tri-axial coil system is based on a tri-axial magnetometer and a theodolite. It is a similar method to DI flux measurement (Hemshorn, et al., 2009). The magnetometer anchored and aligned on the theodolite is placed in the homogeneous area of the system of coils. The magnetometer is precisely positioned into known positions thanks to the high accuracy of the theodolite. The sensitivities of the coil and the angles between the coils are extracted from the measured values by an analytical expression. This type of calibration is dependent on the tri-axial magnetometer which has to be calibrated to a superior standard, and so it carries an extra unwanted uncertainty. Since the theodolite has to be perfectly leveled or aligned to the coil system, the weakness of this method is obvious. Moreover, the theodolite typically has a limited positional range in the vertical direction, and this can reduce the accuracy of the calibration.

We have introduced a new group of coil calibration procedures based on a scalar approach. The scalar methods should eliminate problems related to the principle of the theodolite. The original scalar calibration method was published in a paper by (Zikmund & Ripka, 2010), and it forms the main topic of this thesis.

Briefly, the method is based on scalar magnetic field measurements during a sequence of various coil current excitations. The synchronized measurements (scalar magnetic field and current) are processed by an optimization algorithm, which evaluates the parameters of the coil system according to the mathematical description.

In (Heillig, 2012), the scalar calibration procedure was modified to be able to evaluate the parameters analytically. To determine parameters of the coil system, they use positive and negative currents flowing sequentially through the coils. The magnetic fields measured with the scalar magnetometer are substituted into a cosine law equation, and the parameter is calculated analytically.

Using this approach, they were able to double check the resulting angle, because they obtained four values and the calculating expression needs only two. The

observed error of the 2 angular minutes (0.04 degrees) is explained by uncertainties of the magnetometer readings (stability of the magnetic field).

However, the method is conditioned by the assumption of identical currents flowing into the coils during the whole sequence. This assumption could cause a grave problem if it is not met.

If we assume a relatively high coil constant, for example 50 µT/A, even small changes of the current (in the order of hundreds µA, e.g. 200 µA) can affect the measured field by an error of around 10 nT, and this causes an additional error of 200 ppm (0.02 degrees). The stability of the current is not discussed here.

Table 4. The calibration parameters of 3D coil systems.

Parameter	Symbol	Note
Sensitivity of coil X (usually NS)	S_X	(nT/A)
Sensitivity of coil Y (usually EW)	S_Y	(nT/A)
Sensitivity of coil Z (usually Vert.)	S_Z	(nT/A)
Angle between the X and Y axis	α_1	(degree)
Angle between the Y and Z axis	α_2	(degree)
Angle between the X and Z axis	α_3	(degree)
Additional		
Angle between X and the projection of B_{EARTH} into the XY plane	γ	(degree) see Figure 7
Angle between X and B_{EARTH}	δ	(degree) see Figure 7

1.2 Magnetic tracking

Magnetic trackers are devices which measure a distance and a position based on magnetic measurement. It is suitable to apply them when other methods, e.g. an ultrasound, optical or radio-frequency method cannot localize the position because their signal is suppressed or attenuated by the environment.

Tracking has industrial as well as medical applications. (Tomek, et al., 2007) describe an implantable magnetic distance measurement system for stomach volume estimation. The system was based on 2 mm diameter transmission and detection coils, and it worked at 3 kHz frequency. The basic accuracy was 1 mm at 5 cm distance and 5 mm at 10 cm distance. The main source of error was angular mismatch and lateral displacement between the coils. In a single-source, single-sensor system these effects cannot be corrected and they can cause gross errors: in an extreme case (when the angular mismatch is 90°) the signal is completely lost. A tri-axial detection coil (Tomek, et al., 2008) was employed to reduce this error below 10 % for any angular

position. A magnetic tracker can be used e.g. for wall thickness measurements or for borehole displacement tracking in the building industry and in archeology.

Magnetic trackers are exploited in horizontal directional drilling, where the task is to make a precisely-located hole below the surface (e.g. crossing under highways) for pipes or electrical cables. These drill jobs are usually performed from one side and the goal point is achieved by positioning the drill head on the basis of inertial measurement unit (IMU) information. Although an optical gyro has excellent precision of ±0.03 degrees, in the course of long distance jobs (more than 3 km) the drilling head cannot accurately meet the goal point. These jobs are therefore solved by drilling from two sides. This means that drilling takes place both from the starting point and from the goal point, and they should meet somewhere in the middle. The situation is depicted in Figure 5.

Previous work (Raab, et al., 1979) was also focused on the magnetic principle. The tri-axial magnetic source and the tri-axial magnetic sensor were exploited to track small changes in mutual position and orientation. The excitation represents a quasi-static signal, and it is separated into three parts to obtain 9 linearly independent measurements. The resulting position is analytically calculated from a linearized model. The method exploits a relative model, so the initial position (the reference point) and the rotation have to be defined before starting the system. The subsequent positions are established with the previous shift of the reference values as a new start position. The system designed in (Liu, et al., 2004) uses a similar principle: three orthogonal coils and a tri-axial sensor. To eliminate the rotation error, two accelerometers (as inclinometers) serve to establish the two orientation angles. The third orientation angle is calculated from the DC part of the magnetometer signals. The magnetic source (coil) is excited by an AC current with amplitude modulation, and its magnetic field is detected by the magnetic sensor, and is demodulated using a digital phase sensitive detector. The resulting position is then analytically determined from a combination of the known mutual rotation and the AC magnetic field of the sensor. This approach does not take into account the distortion of the magnetic field when there are magnetic or conducting materials in the vicinity. The magnetic field is measured with magneto-resistive sensors, so the precision is limited due to the noise of the sensor.

Another way to establish the position by the magnetic principle is mentioned in (Song, et al., 2013). The principle uses a rotating magnetic dipole magnetic field generated by two 2 orthogonal coils. The coils are fed by in phase and quadratic signals which make the rotating magnetic field. The tri-axial orthogonal coils sense the magnetic field. The phase and amplitude of the voltage from coils are values from

which the orientation and the position are calculated. The calculation is derived from an analytical equation. The method can obtain the results in one period of the excitation signal. The authors achieved 1 mm error in localization and 5 degrees in orientation within a space of 250 mm.

Another magnetic tracker for human motion tracking was developed in (Roetenberg, et al., 2007). It utilizes orthogonal coils and 3D magnetic sensors fixed on a human body. They achieved poor accuracy because of the magnetic noise signal ratio and limited source strength. During tests, their system achieved precision of 8 mm in distance and 5 degrees in orientation within a range of 0.5 meter.

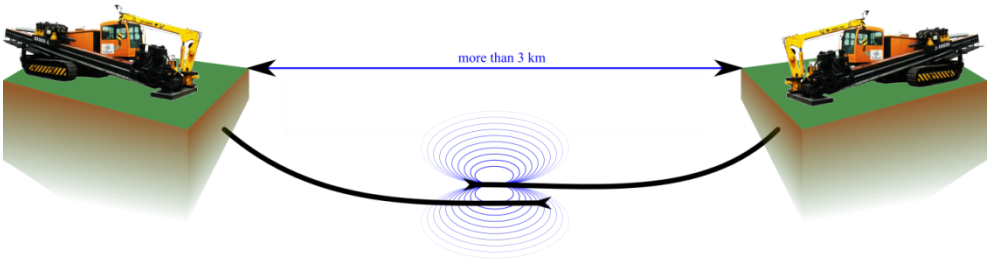

Figure 5. *Horizontal directional drilling from two sides.*

1.3 Non-linear optimization method

The methods, briefly mentioned in previous sections, do not have analytical solution if any simplification (linearization, etc.) is not applied. In order to calibrate the coil system or to calculate the position (in the case of a magnetic tracker), non-linear equations have to be solved. Therefore, the thesis presents their solutions by a numerical way. A review of numerical optimization methods for solving the nonlinear problem is therefore outlined.

The numerical algorithms are, in their essence, an iterative procedure. In our case, we find

$$\min\{f(x)\};\ x \in \boldsymbol{R}^n \qquad (4)$$

Numerical methods are able to find a solution with the required precision in a finite count of computations. In each step of iteration, new results $x_{(t+1)}$ of the optimization problem are generated according to certain rules which specify the next iteration based on local information I_t of the problem collected along the previous iterations. The procedure thus produces a sequence of approximated solutions.

$$x_{t+1} = X_{t+1}(I_t, I_{t-1}, \dots) \quad (5)$$

The information obtained from the actual iterative step *t* can be gradient or higher-order derivatives of these functions at x_t. The search rules are specific for different types of optimization method.

- zero-order routines, using only values of the objective and the constraints and not using their derivatives;
- first-order routines, using the values and the gradients of the objective and the constraints;
- second-order routines, using the values, the gradients and the Hessians (i.e., matrices of second-order derivatives) of the objective and the constraints.

Higher derivatives (third and higher) are not used in practice because they cause computing difficulties in multi-variable problems.

Convergence of optimization methods

A nonlinear problem cannot be expected to be solvable exactly in a finite number of steps. The methods attempt to iterate to a solution in a finite time. The convergence of any type of optimization is important for solving any specific problem. Convergence is however not the only required indicator for validating an optimization algorithm.

Another issue is the rate of convergence, which provides information on how fast a result with specific precision will be reached. The rate can be considered as a quality pointer of the convergence, and can also serve as a recommendation for the practical usage of any method. In the traditional nonlinear optimization, the rate is resolved by asymptotic rates. This is defined by an error function which measures the quality of an approximate solution. The sequence $r_t=err(x_t)$ should converge to zero if the result of the optimization is achieved. There are several types of error evaluation function, e.g. the residual principle. The rate of the convergence of iterative numerical routines is evaluated as the rank of the corresponding sequence r_t. It should be emphasized that the convergence rate does not state whether convergence is achieved for a particular problem.

The difficulty with the numerical nonlinear method is the possibility that the algorithm will find a minimum without knowledge as to whether it is local or global. The global minimum can be found by choosing of a proper initial condition.

Line search

A line search is a simple example of one-dimensional unconstrained optimization for

$$\min\{f(x)\};\ x \in \boldsymbol{R} \qquad (6)$$

where f is at least continuing. This line search principle forms the basis for many multidimensional optimizations. The unconstrained method involves the following procedure:

- Look at the local information of a function in the current iteration step
- Choose a direction for the next iteration, normally a descending direction
- Perform step x_{t+1}

It has to be ensured that f(t+1) < f(t) in order to maintain progress in the minimizing procedure.

First order methods (a line search, a Fibonacci search, or a Golden search) use only minimal information about the function and its values. They are very simple and converge with a linear, rate but they are able to solve problems with unimodal functions.

Curve fitting

Curve fitting exploits more information about a function f by approximating it by a simple function with an analytically computable minimum. A good way is to approximate f by a polynomial (a Taylor polynomial) which comes from derivatives of the function.

The algorithm iterates as follows:

- At the beginning of the iteration, certain initial points are known and the derivatives are calculated at these points. The polynomial is determined from these conditions.
- A new minimum is expressed from the polynomial by an analytical search and that point is taken as a new search point.
- The algorithm then computes the value of the function at the new search point found in the previous step and the procedure is repeated.

Newton's method is very well known. The principle of the method assumes that the function is twice continuously differentiable and the polynomial is a Taylor polynomial of the second order.

$$p(x) = f(x_{t-1}) + f'(x_{t-1})(x - x_{t-1}) + \frac{1}{2}f''(x_{t-1})(x - x_{t-1})^2 \quad (7)$$

This means that the minimizing step is

$$x_t = x_{t-1} - \frac{f'(x_{t-1})}{f''(x_{t-1})} \quad (8)$$

This is a simplification (using the one-dimensional case), but the method works for multidimensional functions as well.

Gradient Descent (GD)

The gradient descent method, which assumes computable $f(x)$ and $\nabla f(x)$ iterates according to the direction $g = -\nabla f(x)$ (a descent direction) of f at x. It means that the next step of iteration algorithm is carried out as an opposite direction to the gradient direction with step size γ_t.

$$x_t = x_{t-1} - \gamma_t \nabla f(x_{t-1}) \quad (9)$$

The generic gradient descent method is a recurrence with a specific rule for choosing step size γ_t, which specifies the length of the future step. The gradient method forms the essence of other methods that search the step size (γ_t) in some way.

Steepest descent

The steepest descent is one of the most famous implementations of gradient descent methods. The method is described in (Meza, 2010). It is based on the optimized coefficient γ_t (the step size) according to the following equation:

$$\arg\min_{\gamma}\{x_{t-1} - \gamma_t \nabla f(x_{t-1})\} \quad (10)$$

It can be proved that gradient methods have global convergence if the trajectory is bounded. Gradient methods have strong points:

- a broad family of problems for which global convergence to critical points can be guaranteed.
- simplicity: for each step of the method, there is a single evaluation of $\nabla f$and a small number of evaluations of f. Note that each evaluation of f is accompanied by small number of arithmetic operations.

- However, an important weakness of GD is the relatively low (linear) rate of convergence. Even if a problem is a strongly convex quadratic case, the method converges linearly. The convergence is affected by the number of conditions.

Proceeding in the direction of the steepest descent at each iteration is not necessarily the most effective strategy. The recorded path of the algorithm can be jagged because the steepest descent algorithm must tack at each turn.

An improvement comes with the conjugate gradient, a modification of steepest descent. The algorithm stores information from the previous steps and the information is used in the following step to successively negotiate functions with narrow valleys.

Newton's method for multidimensional problems

This method is based on the same principle as the one-dimensional Newton method but the derivatives are replaced by the Jacobian $\nabla f(x)$ and Hessian $\nabla^2 f(x)$ matrix of the function. The minimization procedure is controlled by the following iterations:

$$x_{t+1} = x_t + [\nabla^2 f(x_t)]^{-1} \nabla f(x_t) \qquad (11)$$

The initial point x_0 is given before starting the iterations.

Its convergence is locally quadratic if the non-degenerated case is supposed but the Newton method does not have global convergence. If the initial point is not close to the minimal optimum, it may also diverge, because it is not guaranteed that the Hessian is positive definite over the whole function. We cannot rely on this method for convergence, and for this reason several modifications have been developed.

Newton's method has defined the search direction and also the step size of the direction. To make this method more robust (convergence to minimum), the step size is chosen by a kind of line search method (gradient method). A significant progress is achieved in the iteration. This means that the method is described by:

$$x_{t+1} = x_t + \gamma_{t+1}\, e(x_t), \qquad e(x_t) = [\nabla^2 f(x_t)]^{-1} \nabla f(x_t) \qquad (12)$$

where the step size $\gamma_{t+1} \geq 0$ is calculated from a line search principle. Specifically, the steepest descent method can be exploited.

$$\gamma_{t+1} \in \operatorname{Argmin} \left\{ f\,(x_t + \gamma e(x_t)) \middle| \gamma \geq 0 \right\} \qquad (13)$$

Variable metric method

This method combines the gradient descent and Newton methods. There is an additional parameter (matrix A) which influences the optimization direction of the Newton method. The positive definite matrix A substitutes the anti-gradient direction, which is an approximation of the Hessian function, and it entails possible effective convergence. The Hessian matrix is approximated in such a way that matrix A remains positive definite and symmetric. The method routine (the generic metric method) is performed:

- Initialization: choose a starting point x_0 and set $t = 0$
- Step t: given by previous iterate x_{t-1}
  - Compute $f(x_{t-1})$, $\nabla f(x_{t-1})$
  - Choose positive definite symmetric matrix A_t
  - Compute the anti-gradient direction
$$d_t = -A_t^{-1}\nabla f(x_{t-1})$$
  - Perform line search x_{t-1}, from the direction d_t the new iteration is
$$x_t = x_{t-1} + \gamma_t d_t = x_{t-1} - \gamma_t A_t^{-1}\nabla f(x_{t-1})$$

Levenberg-Marquardt modification

In the Levenberg-Marquardt modification (Marquardt, 1963), matrix A_{t+1} is chosen as the controlled Hessian matrix. It calculates the direction of iteration

$$A_{t+1} = \epsilon_t I + H_t \qquad (14)$$

from the actual Hessian, where the regularization $\epsilon_t \geq 0$ is chosen to make the matrix A_{t+1} positive definite in order to ensure that $A_{t+1} \geq \delta I$, where δ is a positive threshold.

The desired ϵ_t is sought over the Hessian of the function in each step. When the requirement $H_t \geq \delta I$ is satisfied, we empirically take $\epsilon_t \geq 0$ and $A_{t+1} = H_t$, thus getting the pure Newton direction.

If the previous condition is not confirmed, the Hessian matrix is adjusted according to

$$A(\epsilon) = \epsilon I + H_t - \delta I \qquad (15)$$

To ensure shifting of the matrix toward the positively defined area ϵ is calculated by the bisection method to find the upper bound. Optimized ϵ is installed into equation 15.

Trusted region method

The trusted region method forms an alternative class of algorithms that combine desirable global convergence with the local super-linear rate of Newton method convergence. In addition, trust-region methods contain information on whether the algorithm iterates too far away from the solution for fast local convergence.

In each step of iteration, the algorithm proceeds with searching step direction and step length. If the new found direction and step length, carried out by the Newton method or the quasi-Newton method, does not pass the trust condition (region), another direction should be searched. Therefore, the algorithm always searches a new iteration in the area of the chosen trust region.

From the mathematical point of view, the method periodically calculates:

- Newton and quasi-Newton at each step (approximately) solve the minimization problem

$$\min m(x_k + s) = f(x_k) + \nabla f(x_k)s + \frac{1}{2}s^T H_k s$$

  in the case that H_k is symmetric and positive definite (SPD) and a Hessian matrix.
- In the case that H_k is SPD the minimum is

$$s = -H_k^{-1} g_k, \qquad g_k = \nabla f(x_k)^T$$

  and s is the quasi-Newton step.
- if $H_k = \nabla^2 f(x_k)$ and is SPD, then $s = -H_k^{-1} g_k$ is the Newton step.
- if H_k is not positive definite, the search direction $-H_k^{-1} g_k$ may fail to be a descent direction and the previous minimization problem can have no solution.
- The problem is that the model $m(x_k + s)$ is an approximation of $f(x)$ and this approximation is valid only in the near vicinity of x_k.
- So that an alternative minimization problem is the following

$$\min_s m(x_k + s) = f(x_k) + \nabla f(x_k)s + \frac{1}{2}s^T H_k s$$

Subject to $\|s\| \leq \delta_k$ is the trust region of the model, i.e. the region where we trust that the model is valid.

Numerical methods are frequently exploited in mathematical computation of non-linear models. They serve mainly for calculating control engineering problems and also for economic optimization. A concrete implementation is found e.g. in Matlab (a mathematical software), where the *fsolve* function is implemented for solving non-linear optimization. The trust-region method is a default set for solving problems. However, Levenberg-Marquard can be optionally specified to prefer the calculation routine.

2 Objectives of the dissertation

As shown in chapter 1, for magnetic field problems such as coil system calibration and calculation of the position in magnetic tracking, the describing equations are non-linear, and this makes it impossible to express the case analytically.

The main objective of this thesis is therefore to solve these specific magnetic field problems by using non-linear optimization algorithms and verify their applicability in terms of accuracy and solvability.

Further objectives are to provide a mathematical description of the magnetic model and to express the accuracy and the uncertainty of the calculation.

Secondary objectives are to develop measurement setups for the magnetic problem (magnetic tracker and scalar calibration) and to test the setups in real situations and verify the developed methods.

2.1 Calibration of coil systems

Coil systems are used for calibrating magnetic sensors, but the coils themselves have to be calibrated in order to guarantee metrological traceability. Standard calibrating methods use vectorial magnetometers, typically fluxgate sensors, which do not measure the absolute magnetic field. The ability to use a very precise absolute magnetic field sensor in the calibration would therefore offer numerous advantages. The problem is that absolute magnetometers measure the scalar of the magnetic field, though with excellent uncertainty.

Since scalar magnetometers measure the norm of the vectorial field, the coil parameter solution is non-linear.

The particular goal of this part of the dissertation is to develop a calibration procedure for establishing the coil sensitivity and orthogonal angles based on scalar magnetometer measurements. This goal will be achieved by the following steps:

- describe the coil system mathematically, and to express the scalar value that is measured during coil excitation
- find a suitable algorithm for solving nonlinear equations of scalar principle.
- evaluate the uncertainties of the calculated parameters
- test the procedure by making real measurements

2.2 Magnetic tracker application

The magnetic field generated by a magnetic dipole, which is used as a field source for the principle of the magnetic tracker is described by non-linear equations with respect to the spatial coordinates. In addition, the rotational transformation has to be taken into account.

Previous works have eliminated the nonlinearity by local linearization, or have neglected some parameters when solving the complex non-linear problem. In this way they have obtained an analytical solution, but it is necessary to know the initial conditions.

The specific goals of this part of the dissertation are to:

- write equations completely characterizing the principle of the magnetic tracker based on the magnetic dipole source
- verify whether the optimization algorithm is able to converge and solve this problem
- design a measurement setup and verify the basic principles
- modify the magnetic tracker principle for horizontal directional drill navigation, and to design the measurement electronics including programmed firmware
- design a measurement system for an industrial application and verify the developed procedures and methods and achievable accuracy.

3 Scalar calibration of coil systems

As was briefly mentioned in the chapter on the State of the Art, our novel method utilizes a scalar magnetometer and current measurement. The current is sequentially applied into the coil, or into a combination of the coils and the resulting field is measured by a scalar magnetometer, which is placed in the homogeneous space of the system of coils. The method measures the total field of a combination of two vectors: the Earth's magnetic field and the magnetic field generated by the coils during whole excitation sequence.

In order to express the magnetic field generated by any coil and subsequently to calculate the coil parameters, a sufficient number of current combinations have to be applied to cover the space dimension of the unknown variable. Since the total magnetic field is a norm of magnetic field components, the parameters have to be established by non-linear algorithms.

This method relies on the stability of the Earth's magnetic field during the calibration sequence. This requirement is limiting, because it is necessary to choose a suitable sequence duration that will reduce the uncertainty due to the instability of the Earth's field, or due to vicinity of some source of magnetic noise.

3.1 Scalar magnetometers

A very important aspect of the measurement is a scalar magnetometer itself. Its parameters influence the measurement uncertainty. A fundamental weakness is the orientation error, i.e. the error caused by a sensor that is not aligned with respect to the magnetic field vector. This is a very important consideration, because the magnetic field during calibration can have an arbitrary direction. The scalar magnetometer should be independent from the orientation, but in some instruments there are intensive directions limiting the operational freedom.

The gradient tolerance and sample rate have to be taken into account because of the inhomogeneity of the Earth's magnetic field, the variations, and also the environmental noise.

A short overview of scalar magnetometers will therefore be presented in order to compare their suitability for this application.

Proton magnetometers

Magnetic resonance magnetometers belong to the group of precise magnetic field instruments that measure weak magnetic fields like Earth's field. Magnetometers of

this type exploit a phenomenon known as nuclear magnetic resonance (NMR). NMR was discovered in the 1940s and is based on the properties of nuclei (protons), their magnetic moment and precession.

An interesting aspect of the NMR effect is its ability to measure a weak absolute magnetic field (Earth's field about 50 000nT) with accuracy of 10^{-7} (Waters & Phillips, 1956). The principle is based on picking up the ac-magnetic NMR signal by a coil surrounding a sample of atomic nuclei after suitable excitation.

Nuclear resonance magnetometers have a well-defined sample of nuclei with a precisely known gyromagnetic constant. The resonant frequency of a magnetometer is defined by

$$f = \frac{B \cdot \gamma_P}{2\,\pi} \qquad (16)$$

The emitted resonance frequency of the signal is given by the gyromagnetic ratio γ_P of the individual nuclei samples, and so the frequency is proportional to the magnetic field. The most important parameter of scalar nuclear magnetometers is the stability and accuracy of the gyromagnetic constant. The constant is derived from the atomic parameters, and it is determined very accurately. The currently accepted gyromagnetic ratio value for a proton is (from NIST CoData)

$$\gamma_p = (2.675\,222\,005 \pm 0.000\,000\,063) \cdot 10^8\ (s \cdot T)^{-1}$$

In metrological praxis, the gyromagnetic ratio is defined for a spherical aqueous sample whose value differs from the theoretical γ_P, then we use modified (shielded) gyromagnetic ratio γ'_P (from NIST CoData)

$$\gamma'_p = (2.675\,153\,268 \pm 0.000\,000\,066) \cdot 10^8\ (s \cdot T)^{-1}$$

Since the gyromagnetic ratio is determined very accurately, the proton magnetometer can measure the magnetic field with high precision and reproducibility.

A classical proton magnetometer (free precession) has a cylindrical chamber filled with a pure water sample (some hydrocarbons are also used). The chamber is surrounded by pick-up coils and an excitation coil. A current step is fed into the excitation coil to make a strong polarization of the nuclei sample. When the excitation stops, the protons start to create a precession signal by their rotation. The rotation corresponds to equation 16, and in the pick-up coil an exponentially decaying sinusoidal signal will appear. Its frequency is dependent on the magnetic field. The frequency is detected by a signal conditioning and processing system, and is recalculated to the magnetic field.

Due to directional polarization, the classical proton magnetometer is influenced by the direction of the measured magnetic field. The strongest (most reliable) signal is

when the measured field is perpendicular to the polarization vector. If perpendicularity is violated, the precision of proton magnetometers deteriorates.

As the time response of a proton magnetometer (greater than 5 sec) is not ideal, this type of scalar magnetometer is not suitable for the scalar calibration principle.

Alkali vapor magnetometer (optically pumped)

The resonance effect is not limited to protons, but can be found in an analogous manner for electrons as so-called electron spin resonance (ESR). Since electrons have a much higher spin resonance frequency, a more sensitive rapidly-responding scalar magnetometer can be constructed. The gyromagnetic constant of a free electron is

$$\gamma_e = (1.760\,859\,708 \pm 0.000\,000\,039) \cdot 10^{11}\ (s \cdot T)^{-1}$$

Alkali vapor (optically pumped) magnetometers contain a medium of evaporated alkali metal with atoms having a set distribution of valence electrons which can change energy state. These electrons are populated in two low energy levels (1 and 2).

A transfer between the two energy levels of electrons can be induced by a resonance magnetic field with a frequency that is the Larmor frequency about the ambient field. The frequency itself is determined on the basis of excitation by a light source. The light of the specific wavelength, absorbed by electrons residing on level 2, forces the electrons to occupy the highest energy level 3 (polarization). Due to the non-stability of the electrons at level 3, they decay back mainly to level 1 which caused that the vapor stop absorb the light. For back depolarization into the original electron distribution (to absorb the light), the RF depolarizing signal has to be applied. The frequency is of RF depolarizing field correspond to Larmor frequency.

However, the optically pumped magnetometers are much more complicated devices, they are described in detail in (Ripka, 2001).

Overhauser magnetometer

The normal classical proton magnetometer is usually excited by a pulsed DC-magnetic field and uses the measurement of the frequency of the decaying resonance spin signal, but an optically pumped magnetometer uses light in resonance with an optical spectral line of the sample. It therefore produces a continuous ESR signal.

The Overhauser effect combines these two phenomena. The magnetometer is based on a specific liquid where a free radicals exists and energy transfer (electron to proton) are present at the atomic level. In terms of their construction, a magnetometer is very similar to a proton magnetometer.

The radio frequency produces ESR excitation of the electrons, which transfer their excitation to the protons through a collision mechanism. In this way, continuous

excitation of the protons is ensured through the electrons, and the proton resonance signal can be measured continuously because there is a frequency gap between the excitation (RF) and the useful detected signal.

The Overhauser magnetometer offers the advantages of a rapid response and lower consumption, together with excellent precision in contrast with the classical proton magnetometer.

The choice of a scalar magnetometer depends on the principle of the calibration method of coil systems. The most adequate magnetometer is the Overhauser magnetometer, for the following reasons, above all

- a faster response
- resistance to field gradients
- simplicity
- lower influence of the direction of the magnetic vector
- higher sensitivity
- measurement in the range of 20 μT to 120 μT

3.2 Principle of scalar calibration

The main idea of the method is to:

- measure the magnetic field with a scalar magnetometer placed in a homogeneous area of the coil system.
- excite the coils by a current sequence to get linearly independent results
- establish the coil parameters from measured values.

One way to obtain description of all calibration parameters of a coil system is to create a general case which describes the magnetic field dependent on all possible combinations of all coil currents. By generating convenient combinations of currents we will be able to calculate these parameters.

This approach would be advantageous if the calculation algorithm had simple solutions. A simpler way is to calculate the parameters of the coil system progressively. In this way, we limit the requirements on the optimization method (convergence) by decreasing the high number of unknown variables. This approach leads to the use of an optimization method only when we need to evaluate the orthogonal angle.

Single coil - Sensitivity

First, the case of a single coil case is considered in order to establish the sensitivity of the coil. A current sequence is applied only to one coil, the parameter of which (only sensitivity) should be calculated. Thus we need to express only three unknown variables, and they can be calculated analytically. The resulting field B_{TOT}, measured with a scalar magnetometer, is given by

$$B_{TOT}^2 = (I_L S + B_E \sin(\varepsilon))^2 + (B_E \cos(\varepsilon))^2 \qquad (17)$$

where S is the sensitivity of any individual coil, I_L is the coil current, B_E is the amplitude of the Earth's magnetic field vector, and ε is the angle between the coil axis and the Earth's magnetic vector.

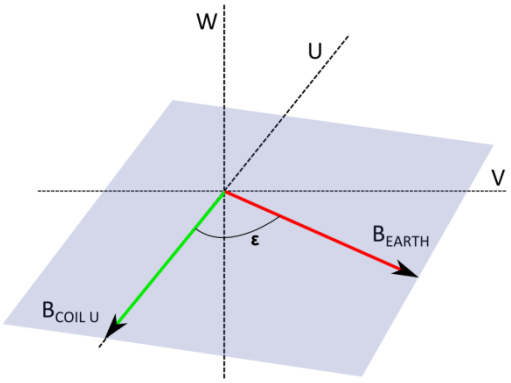

Figure 6. *The assumed arrangement of the single coil setup.*

There are only three unknown variables (B_E, S, ε) in equation 17, and so we need three different calibration currents into coil to establish these variables. The Earth's magnetic field can be measured when the current is not being applied, I_L=0 (B_E), and so two variables remain to be calculated. Two current sequences are therefore needed. The simplest choice is the sequence when the polarity of a current with the same level is reverted (B_- and B_+) and B_E is measured during an interval when the current is not flowing into the coil. The current should be chosen with respect to the scalar magnetometer range. Then the sensitivity is calculated according to:

$$S = \sqrt{\frac{B_-^2 + B_+^2 - 2B_E^2}{2I_L^2}} \qquad (18)$$

Due to many effects, it is in fact impossible to generate the same current in both polarities with precision of 10 ppm. The sensitivity expression comes from two equations which assume different current levels.

$$B_1^2 = (I_1 S + B_E \sin(\varepsilon))^2 + (B_E \cos(\varepsilon))^2$$
$$B_2^2 = (I_2 S + B_E \sin(\varepsilon))^2 + (B_E \cos(\varepsilon))^2 \quad (19)$$

The analytical solution is given by the following equation

$$S = \sqrt{\frac{I_1 B_2^2 - I_2 B_1^2 - I_1 B_E^2 + I_2 B_E^2}{I_1 I_2 (I_2 - I_1)}} \quad (20)$$

In case of tri-axial coil system, the sensitivities of all three coils need to be known before going on to calibrate the orthogonality.

Double coil - orthogonality

In order to calculate the non-orthogonal angles between two coil axes, we have to excite both coils simultaneously.

This situation can be imagined as three vectors, where two of them (the coil axes) are placed in the same plane and form the important calibration angle. The third vector is the vector of the Earth's magnetic field, and it has an arbitrary orientation to the coil plane. The spatial interpretation is depicted in Figure 7. Then the equation can be described as follows:

$$B_{TOT}^2 = (B_{L1} + B_{L2} \cos(\alpha) + B_E \cos(\delta) \cos(\gamma))^2 + (B_{L2} \sin(\alpha) + B_E \cos(\delta) \sin(\gamma))^2 + (B_E \cos(\delta))^2 \quad (21)$$

where B_{TOT} is the magnetic field measured by a scalar magnetometer, B_{L1} is the magnetic field generated by the first coil, and B_{L2} is the magnetic field of the second coil. α is the unknown angle between the coils (orthogonality angle), δ and γ describe the direction of the Earth's field.

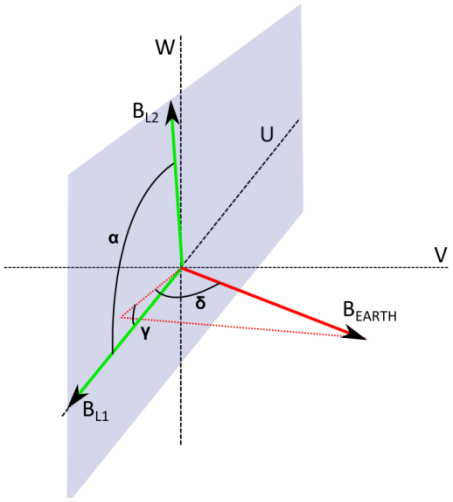

Figure 7. *The assumed arrangement of the double coil case.*

With respect to equation 21, B_{L1}, B_{L2} can be calculated from the calibrated sensitivities (for a single coil) and flowing currents, and B_E is measured while the calibration currents are not flowing. All three remaining angles α, δ and γ are unknown variables which need to be calculated. These variables cannot be derived analytically because the equation is non-linear. Therefore, at least three combinations of currents have to be chosen. Good practice is to combine all the possible polarities of the calibration currents flowing in the coils even if we get one extra measurement that can be used for checking the results. In this situation, the currents exciting the coils also have to comply with the condition that they must not exceed the range of the magnetometer.

If we use the single coil and double coil principle, we can establish all parameters of a 3D coil system (three sensitivities, and three orthogonality angles) but it is carried out step by step. We have potential possibility to determine the parameters in one step by using a triple coil excitation.

Triple coil

Establishing the parameters of a coil system is done with generating currents to all 3 coils. As has been shown above, this approach is not very practical due to the increased number of variables and related problems with the calculations. To be concrete, the equation has seven parameters that need to be established. To solve the problem, seven different current combinations need to be generated.

This could be realistic, but the solution would have to be optimized through seven variables. That could increase the residual error and lead to a complication with

convergence of the non-linear solver. This approach is therefore rejected, and single and double coil (step by step) is used for the calibration procedure.

Since all equations contain B_E while the whole current sequence is running, the background (Earth's magnetic field + environmental noise) should be as stable as possible over the measurement time. However, due to the variations in the Earth's field, and other field disturbances caused by electric current and movement of ferromagnetic objects, this condition cannot be satisfied. Nevertheless, we do have some ways to suppress the magnetic noise.

The obvious solution is to effectively attenuate the influence of ambient field variations by repeating the measurement sequence and by averaging. It will be shown that we can achieve low uncertainties by using this simple approach. A good technique is to create a time interval in the current sequence when the current will be zero, and to measure only the Earth's field in that interval. Then an approximation can be made from the Earth's field measured before, during and at the end of the sequence. In this way, slow variations in the magnetic field can be detected and compensated. If large variations appear, the measurement is not usable.

Another approach would be to make measurements of the Earth's field during the whole period using a remote magnetic sensor. The distance between the sensor and the coil system should be such that the coil field measured by the sensor is negligible. For example: If we suppose that the coil in the far distance is a dipole, and the magnetic field within 1 meter is the same as inside the coil (typical maximum B=100µT), we can calculated the moment of the coil, according to equation 36. Relative to this, we can calculate the distance needed to decrease the influence of the coil. From one meter distance we get the approximate coil moment

$$B = \frac{\mu_0 m}{2\,\pi\, r^3} \rightarrow 100 \cdot 10^3\, nT = \frac{4\cdot\pi\cdot 10^{-7}\cdot m}{2\cdot\pi\cdot 1^3} \cdot 10^9 = \frac{200\cdot m}{1^3} \rightarrow m = 500\, nT/m^3.$$

The minimum distance of the remote sensor, when the influence has to be below 2 nT, is

$$2\, nT = \frac{200\cdot m}{d^3} \rightarrow d = 36.8\, m.$$

The remotely measured ambient field can be included in the calculation to remove the field variation. The problem with this method is that it requires a very stable field gradient between the coil system and the remote sensor. We did not utilize this method as the gradient stability at the location of the calibrated coils was relatively poor.

Non-linear optimization algorithm

An adequate optimization method has to be selected. According to equation 21, three unknown variables have to be calculated. All three searched angles can be constrained by the upper and lower limit, because their approximate values are known and thus we can expect a band of convergence.

In addition, it is not necessary to generate the exact number of equations that enter into the solver: an overdetermined equation system could also refine the results.

The traditional Gauss-Newton optimization method works appropriately. It converges very quickly even if the problem is solved as an unconstrained one. The solution converges to very low residual limit (relatively 10^{-5}).

Improved modifications (e.g. Levenberg-Marquardt and or Trusted-region) also converge the problem, and even with higher rate of convergence.

3.3 Uncertainty analysis

In metrology, all measured or calibrated data has to be expressed with an uncertainty value that quantifies errors that arise during the measurement procedure. The international standardized method (GUM, 1994) describes two types of uncertainty. So called type A uncertainty is based on a statistical calculation of the measurement set. Type B uncertainty focuses on known sources that should be taken into consideration as potential sources of uncertainty. An analysis of scalar calibration is made in (Zikmund & Ripka, 2012).

Type A uncertainty

This type can be determined from a significant number of measurements, when the statistical law begins to operate. The measurement is carried out at least 20 times. Then the type A uncertainty is defined as the standard deviation of the measured set.

Type B uncertainty

According to (Taylor, 2009), the uncertainty of the coil sensitivities can be derived from the standardized method by a partial derivative of the analytical expression. Even if equation 21 is non-linear, which should lead to inaccuracy of the uncertainty estimation, the method works because we use very precise measurements and the Taylor approximation of the 1^{st} order is sufficient in that small vicinity of linearization. To check the principle, we used Monte Carlo method in the verification, as will be described below.

However, uncertainty analyses of the orthogonality of the coil system are a more complicated matter. Since the orthogonality is calculated by a non-linear optimization algorithm, an analytical solution cannot be achieved, and likewise analytical uncertainty analysis cannot be utilized. The only way to obtain the uncertainty is by simulation.

The measurements have two sources of uncertainty. The current measurement, which evaluates the exact current flowing into the coil during excitation, is the main source of uncertainty. It has higher uncertainty than the second source, i.e. magnetic field measurement.

A scalar magnetometer (an Overhauser magnetometer) measures with accuracy of 0.2 nT, which is an error of 10^{-5} with respect to the measured field (around 50 000nT).

However, this value cannot be taken as a basis for establishing the type B uncertainty, because during scalar calibration the measurements are usually carried out in the non-stable Earth's magnetic field.

Ideally, if the Earth's field was within the precision of the scalar magnetometer, Overhauser accuracy could be converted to the uncertainty of the magnetic field measurement. Unfortunately, according to the typical record of the magnetic field, depicted in Figure 8,

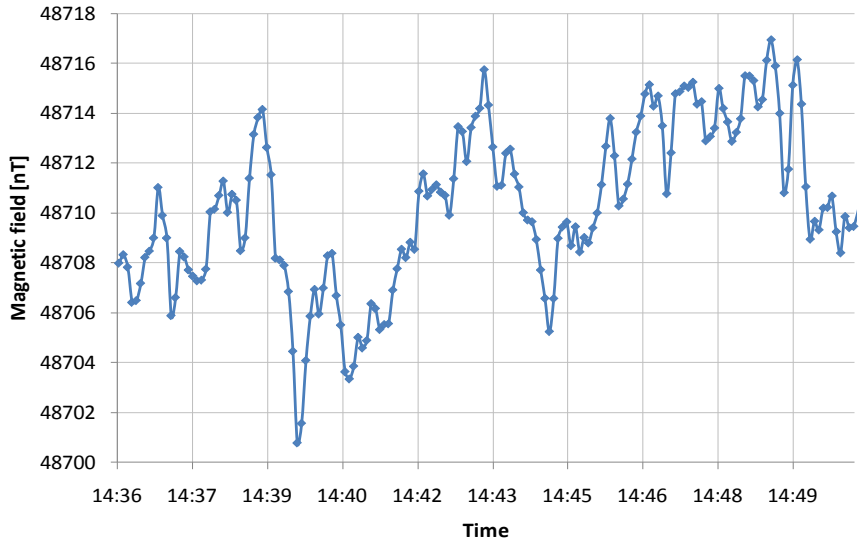

Figure 8. *Record of magnetic field in Pruhonice.*

the basic field variations, being affected by natural influences and also by industrial noise, cause higher uncertainty than the uncertainty of the device itself. The stability of the Earth's magnetic field is also given by the time interval which is confined to the calibration current steps when the magnetic field is measured. For example, if the

current steps are in 20 second time intervals, the magnetic field stability is ±5nT. This value is then substituted as the input uncertainty of the magnetic field.

Estimating the uncertainty of sensitivity calibration

The sensitivity is calculated from the analytical formula 20. The uncertainty can be established from the partial derivatives.

$$u_S^2 = \left(\frac{\partial S}{\partial B_1} u_{B_1}\right)^2 + \left(\frac{\partial S}{\partial B_2} u_{B_2}\right)^2 + \left(\frac{\partial S}{\partial B_E} u_{B_E}\right)^2 + \left(\frac{\partial S}{\partial I_1} u_{I_1}\right)^2 + \left(\frac{\partial S}{\partial I_2} u_{I_2}\right)^2 \qquad (22)$$

where the partial derivative with respect to B_1, B_2, B_E, I_1, I_2:

$$\frac{\partial S}{\partial B_2} = \frac{B_2\, z}{I_2(I_2 - I_1)} \qquad (23)$$

$$\frac{\partial S}{\partial B_E} = \frac{B_E\, z}{I_1 I_2} \qquad (24)$$

$$\frac{\partial S}{\partial I_1} = \frac{z\,((I_1^2 B_2^2 - (I_1 - I_2)^2 B_E^2 + B_1^2(I_2^2 - 2\, I_1 I_2))}{2 I_2 I_1^2 (I_2 - I_1)^2} \qquad (25)$$

$$\frac{\partial S}{\partial I_1} = \frac{z\,((I_1^2 B_2^2 - (I_1 - I_2)^2 B_E^2 + B_1^2(I_2^2 - 2\, I_1 I_2))}{2 I_2 I_1^2 (I_2 - I_1)^2} \qquad (26)$$

$$\frac{\partial S}{\partial I_2} = \frac{z\,(I_2^2 B_1^2 - (I_1 - I_2)^2 B_E^2 + B_2^2(I_1^2 - 2\, I_1 I_2))}{2 I_1 I_2^2 (I_2 - I_1)^2} \qquad (27)$$

and where z is given by $z = 1/S$.

Estimating the uncertainty of orthogonality calibration

Formula 22 is a strongly non-linear equation which could cause the standard derivation of uncertainty to fail due to an insufficient approximation by the partial derivatives, and due to the fact that the iteration method calculates the result. The Monte Carlo method (Angeles Herrador & Gonzalez, 2004) was exploited for this purpose to reveal the main source of the uncertainty.

Monte Carlo analysis is a numerical method which periodically solves the problem from the input sets of variables. The input sets are values with a probability

distribution representing a specific quantity. The individual value of the distribution is periodically sent to the solver, sorting out the equations, and the solver calculates and collects all results. The schematic principle is shown in Figure 9.

All input parameters from which the orthogonal angle is calculated are generated as a set of values that has a uniform probability distribution. The distribution is defined with maximum device errors or with maximum uncertainty of the previous calculated parameter.

The procedure starts by generating the uniform distribution for all input parameters within the interval of their errors (given by a device or determined by previous calculations). The uniform set is created by a pseudorandom generator. Then the values of the sets are sequentially inserted into the solving algorithm. In this way, we get many possible results according to the distribution of the inputs.

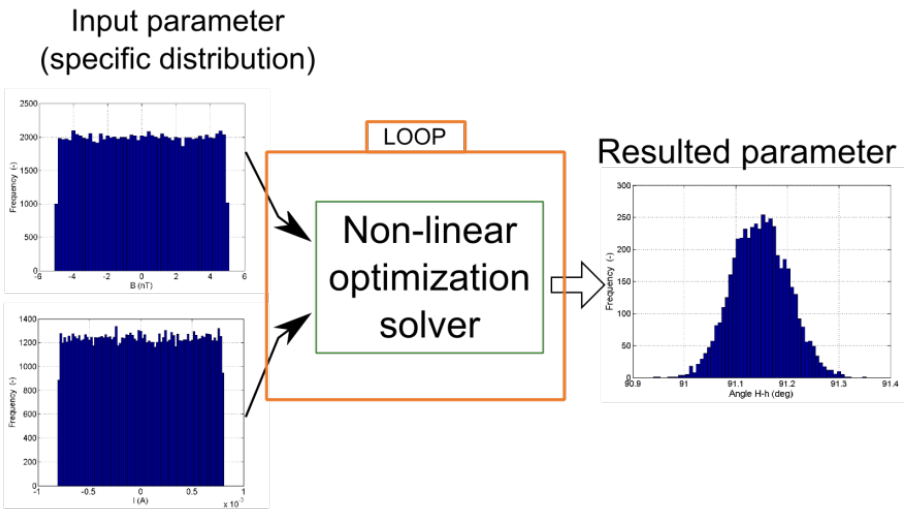

Figure 9. *Monte Carlo principle of uncertainty analysis.*

The length of the (generated) sets plays a role in the precision of the results. Since the uncertainty is calculated by the Monte Carlo method, the uncertainty is defined as the standard deviation of the resulting sets coming from the length of the inputs. The more items there are in the sets the better the establishment of the output parameter distribution will be.

When there are many inputs and a difficult solving procedure, the Monte Carlo method requires more calculating time. The optimal count of the Monte Carlo passes should be of the order of thousands.

A preliminary test of the uncertainty analysis was carried out on measurements made in Pruhonice (the first experimental application of the method is described in chapter 3.6). The current measurements were carried out using Agilent 34401 multimeter in current mode. The uncertainties of current are shown in Table 5 and the uncertainty of the magnetic field was established to be 5 nT, as discussed above. All uncertainties was calculated with the coverage factor k=1.

Table 5. Substituted uncertainty of the measured quantities (k=1).

Quantity	Value	Uncertainty	Uncertainty
I (N-S coil)	0.6135 A	746/√3 μA	702 ppm
I (E-W coil)	1.0007 A	1100/√3 μA	635 ppm
I (Vertical)	0.7051 A	753/√3 μA	617 ppm
B_-, B_+, B_E	20 to 80 μT	5/√3 nT	144 to 36 ppm

The resulting uncertainties are presented in Table 6 and Table 7.

Table 6. Analytically calculated uncertainty without the coverage factor (k=1).

Coil	Sensitivity (nT/A)	Uncertainty (nT/A)	Uncertainty (ppm)
H (N-S)	56929	39.2	688
h (E-W)	19311	15.3	792
Z (vert)	37121	26.3	710

Table 7. Simulated uncertainty of orthogonalities by the Monte Carlo method (k=1).

Coils	Angle (deg)	Uncertainty (deg)	Uncertainty (ppm)
H-h	91.15	0.055	598
Z-H	89.95	0.089	988
Z-h	89.97	0.088	987

The influence of measured quantities on results was studied. On the basis of the Pruhonice experiment, the main sources of error was identified current measurements which were suppressed in the subsequent measurement. Figure 10 shows the uncertainty of the calculated sensitivity affected by current and magnetic field uncertainties. The major influence is from the dominant component of the input uncertainties. If one of them (the current or the magnetic field) is higher than the other, then the sensitivity uncertainty is influenced mainly by the dominant part. To decrease the uncertainty of the sensitivity, we should at least equalize both input uncertainties and bring them to the same level.

As has been explained, the variation of the ambient magnetic field cannot be reduced, because it is due to the location. The current therefore has to be measured at least with uncertainty that is not greater than the uncertainty of the magnetic field. In the case of the Pruhonice experiment, the improvement is a more accurate measurement of the current.

An analysis of the propagation of the input uncertainty into the results is depicted in Figures 10 and 11. The uncertainty of the sensitivity is included because of the calculation of equation 22. According to the graphs, the resulting uncertainty cannot be decreased if the input current uncertainty is below 100 ppm. The behavior is very similar to the previous analysis. We should therefore follow the recommendation to measure all inputs with the lowest uncertainty, or with the same level of uncertainty.

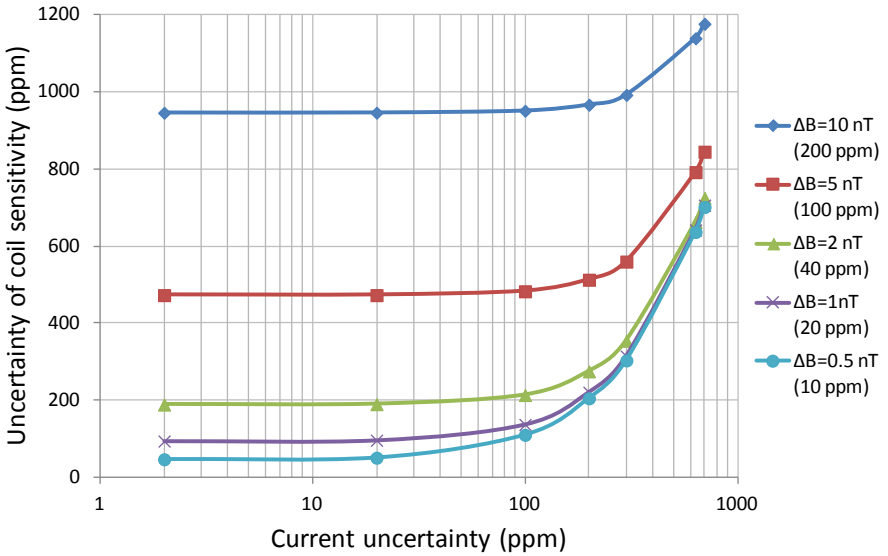

Figure 10. *Dependency of the uncertainty of the coil sensitivity on the input uncertainties (for the Z coil). The total magnetic field in range of 20 to 80 μT.*

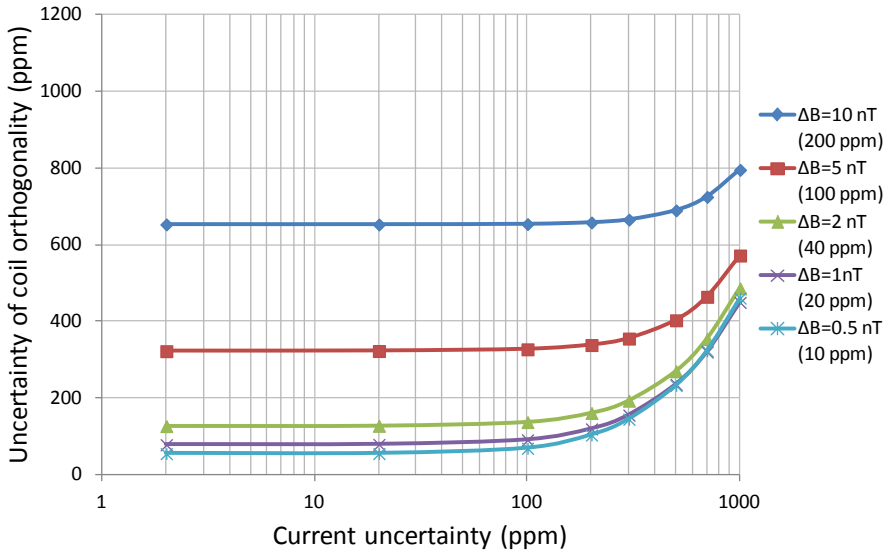

Figure 11. *Dependency of the uncertainty of the coil orthogonality on the input uncertainties. The sensitivity uncertainty is considered constant 100 ppm and the total magnetic field in range of 20 to 80 µT.*

3.4 Procedure

When a 3D coil system is calibrated using scalar calibration, certain requirements must be kept in mind. In this section, the best practice guide is outlined. This guide indicates how to perform the calibration procedure with the highest precision.

Measuring devices:

- a scalar Overhauser magnetometer with minimum range of 20 – 120 µT
- two very precise shunt resistors (min 5 ppm)
- two voltmeters (ideally 8 ½ digits)
- two current controlled sources (stability of the current at least 100 ppm)

Requirements:

A calibrated coil system should be at least big enough to prevent a gradient caused by non-homogeneity of the coil system reducing the precision of the scalar magnetometer measurement. The coil excitation currents have to be also chosen sufficiently.

Approximate coil constants should be known, or quick measurements should be made. This information is important for setting the current amplitude without over-ranging the scalar magnetometer.

Coil constant calibration

The measuring setup is shown in Figure 12. The voltmeter measures the voltage drop on the shunt resistor (caused by current). The Overhauser magnetometer is located in the middle of the coil system (homogeneous area).

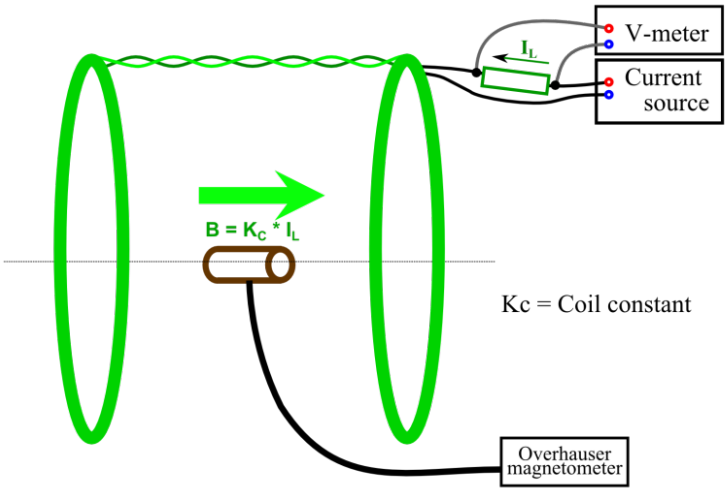

Figure 12. *Calibration of the coil sensitivity – measurement setup.*

Procedure:

1. A positive (I_1), negative ($-I_2$) and zero current (only the Earth's magnetic field is measured) are sequentially applied to the calibrated coil. To switch the currents we can use:
    a. a programmed current source, or
    b. an external H-bridge controlled by a computer.
2. The switching time should be long enough to get at least five measurements of the magnetometer within one step of the sequence. This means that if the OVH has a sample rate of 3 seconds between samples it would be appropriate to measure 20 seconds in each current step.

Table 8. Current sequence for coil sensitivity measurements.

Step	1. (20 sec)	2. (20 sec)	3. (20 sec)
Coil A	Without Current	Positive current (I_1)	Negative current ($-I_2$)
Measured values	B_E	B_{TOT1}	B_{TOT2}

B_E – the Earth's magnetic field
B_{TOT1} – magnetic field for positive excitation
B_{TOT2} – magnetic field for negative excitation

3. The whole sequence should be repeated at least 50 times and then we will obtain 50 measurements of the coil constant.
4. The constant is then calculated from equation 21.

The expanded uncertainty (k=2) of coil constant K_C is given as:

$$U_{Kc} = 2\,u_{Kc}, \tag{28}$$

where u_{Kc} – is the standard uncertainty of measurement
Standard uncertainty is defined as:

$$u_{Kc} = \sqrt{u_{KcA}^2 + u_{KcB}^2}, \tag{29}$$

u_{KcA} – standard type A uncertainty ,
u_{KcB} – standard type B uncertainty.
Both type A uncertainty and type B uncertainty are described in section 3.3.

Calibration of coil system orthogonality

The connection is shown in Figure 13. The voltmeters measure the voltage drops on both resistors and, as in the case of coil sensitivity, the Overhauser magnetometer is positioned in the middle of the coil system.

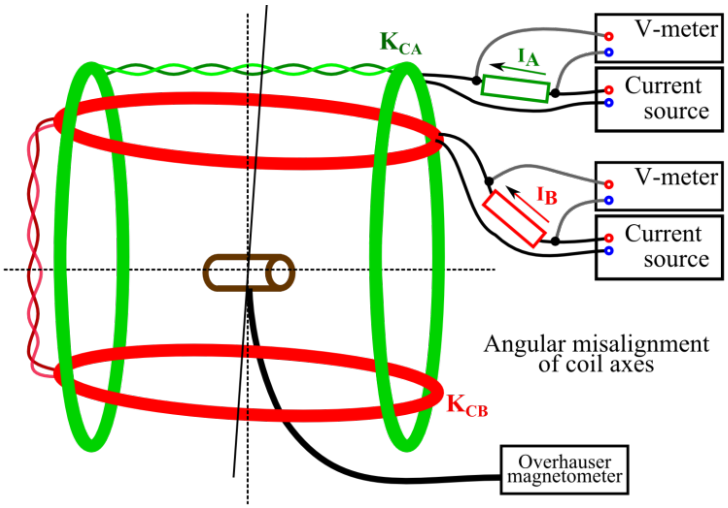

Figure 13. *Calibration of orthogonality – measurement setup.*

The result is calculated using the non-linear optimization method described in section 3.2.

The expanded uncertainty (k=2) of orthogonality angle α is given as:

$$U_\alpha = 2\, u_\alpha, \tag{30}$$

where u_α – is the standard uncertainty of measurement
The standard uncertainty is defined as:

$$u_\alpha = \sqrt{u_{\alpha A}^2 + u_{\alpha B}^2}, \tag{31}$$

$u_{\alpha A}$ is a standard type A uncertainty, and $u_{\alpha B}$ is a standard type B uncertainty.

3.5 Testing scalar calibration

The coil system in Pruhonice

This measurement was carried out as a preliminary trial, and the results are not as accurate as would be desirable.

The biggest coil *H* is placed in the North-South direction, and the second coil *h* has its axis parallel to the West-East direction, and is the smallest and the weakest. The third axis is vertical. In fact, coil *H* has 4 sections, the vertical coil has 3 sections, and coil *h* has only 2 sections. The coil parameters are shown in Table 9.

The Overhauser GSM-19 magnetometer (from GEM Systems, Inc.), a precise scalar magnetometer, was used. Its range is from 20 to 120 μT.

The currents had to be properly chosen to avoid overranging and to minimize the uncertainty and maximize the utilization of the magnetometer range. The coil currents were measured using 6.5-digit Agilent 34401A multimeter in ammeter mode. 100 PLC integration time was used to suppress AC interferences at the power line frequency.

Figure 14. *The Braunbek squared coil system in Pruhonice.*

Table 9. Approximate parameters of the Pruhonice coil system.

Coil	H	h	Z
Orientation	North-South	East-West	Vertical
(roughly) Coil constant	57 (μT/A)	19 (μT/A)	37 (μT/A)
Resistance	75 Ω	28 Ω	64 Ω
Earth's magnetic field	20300 (nT)	0 (nT)	44100 (nT)

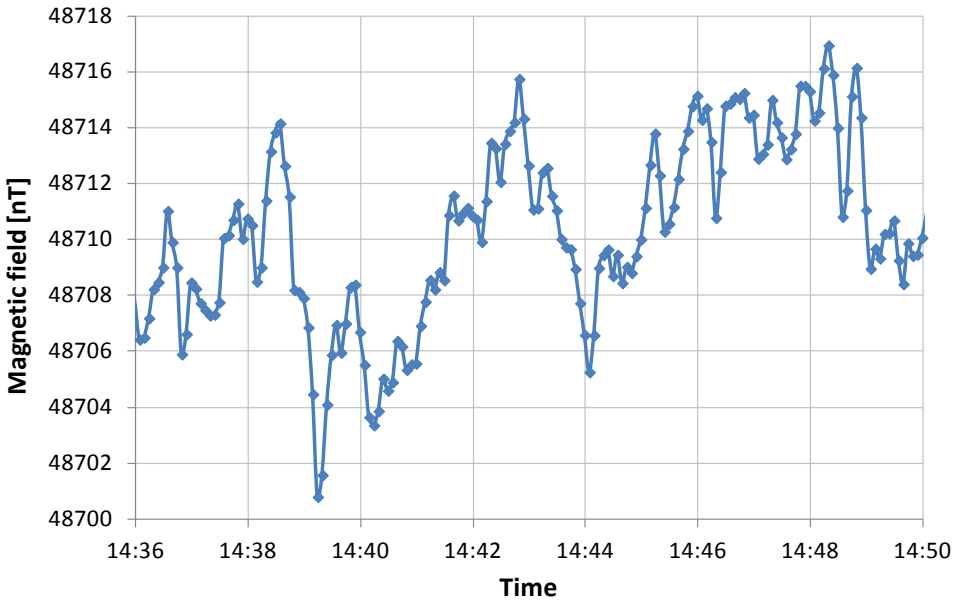

Figure 15. *Record of the magnetic field in Pruhonice's location.*

As has been mentioned, the uncertainty is affected by the magnetic field noise. To achieve a better noise level value, a short time observation has to be performed before the calibration procedure (ideally, it should be performed again after the calibration procedure). The scalar magnetometer is in the coil system, and no current flows into the coil. The measured set of magnetic field values is analyzed, and the peak-peak value of the magnetic field record within a time interval of 5 minutes is the value that is further used for the uncertainty calculation. In the Pruhonice experiment, see Figure 15, the magnetic field noise was determined as ±5 nT.

An example of sensitivity calibration is depicted in Figure 16. Current with both polarities was applied to the coil. Each step of the current was followed by an interval of zero current. The magnetic field measured in this interval is only the ambient field. Since the ambient magnetic field is contained in the three equations, the average of the ambient field (before positive current, between positive current and negative current, and after negative current) is calculated and substituted into the equation.

There was a similar situation when calibrating the angle (see the example in Figure 17). The ambient magnetic field was measured after each current step. The current and magnetic field measurements were not perfectly synchronized, and it could happen that the current did not always correspond to the magnetic field. We therefore had to manually select the right values from the record. This problem was removed in further experiments by using a trigger signal.

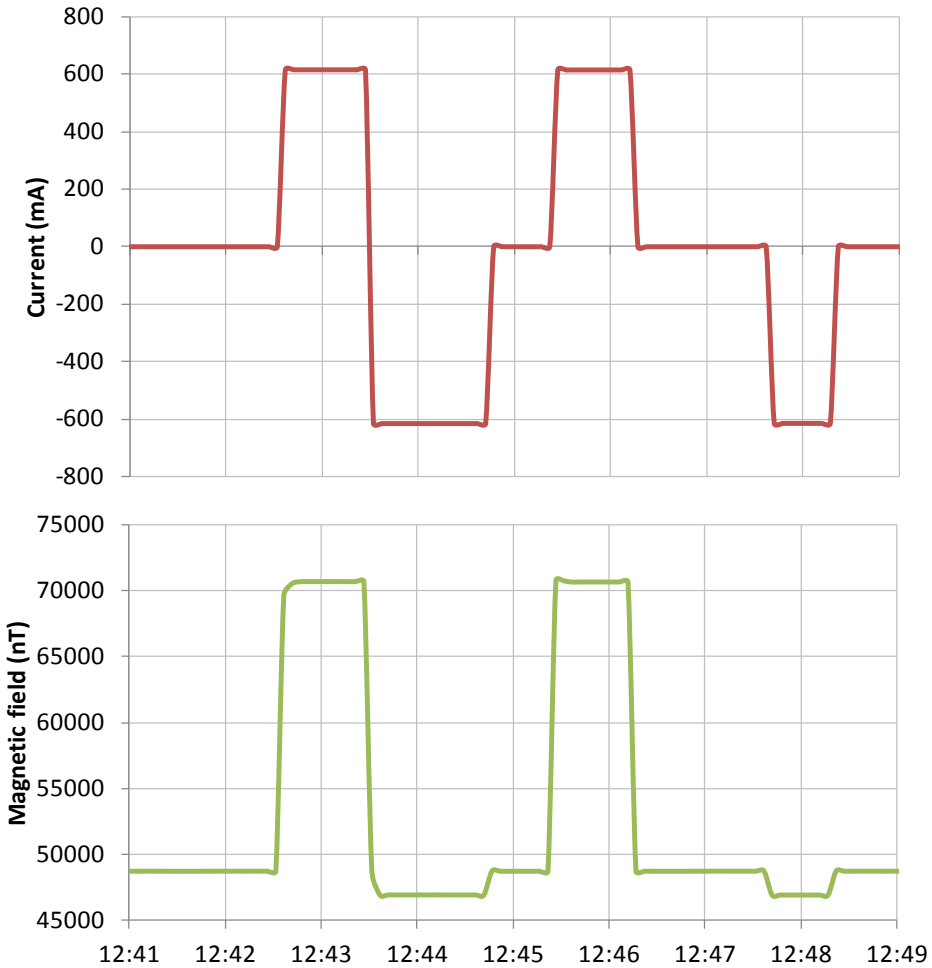

Figure 16. *Time record of the magnetic field and applied current during coil sensitivity calibration (coil H).*

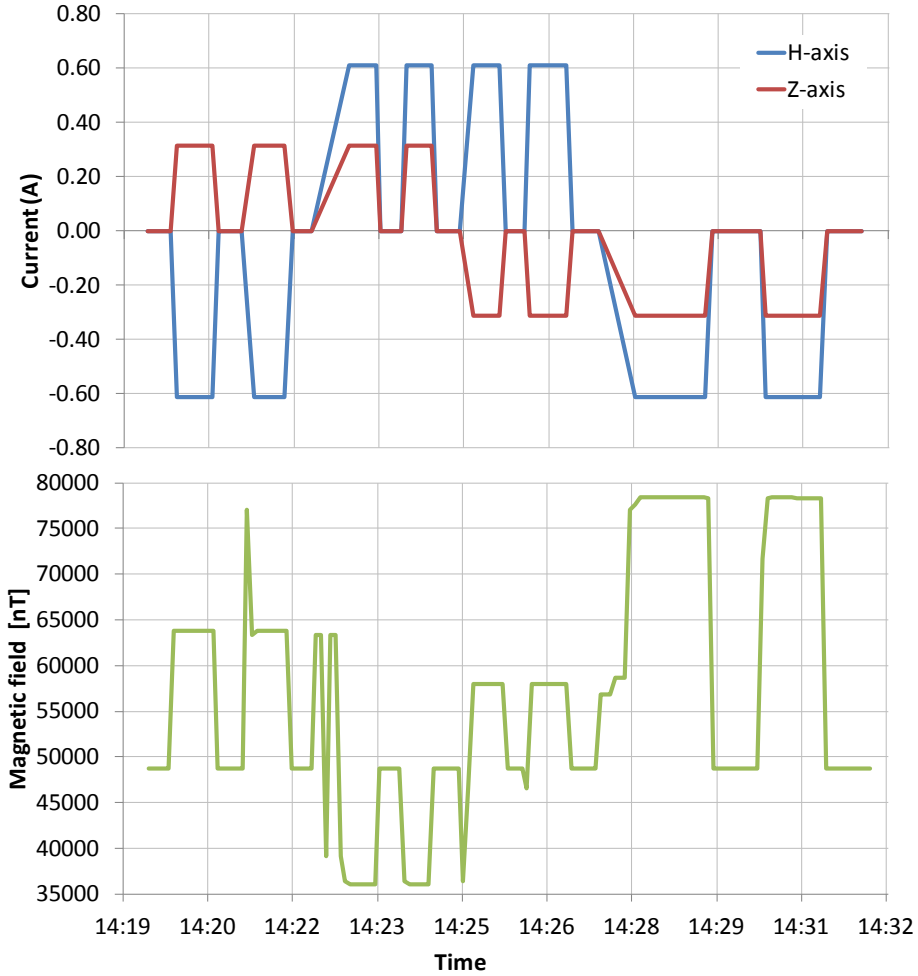

Figure 17. *Time record of the magnetic field and applied current during orthogonality calibration (H-Z coil axis).*

The calibration results are presented in Table 10 and 11. In this experiment, the type A uncertainty was not evaluated, because we had carried out only a few measurements, and statistical processing was therefore not appropriate.

Table 10. Coil constant calibration results.

Coil	H (N-S)	h (E-W)	Z (Vert.)
Constant OVH (nT/A)	56929	19311	37121
Uncertainty B (nT/A)	39.2	15.3	26.3
Uncertainty B (ppm)	688	792	710

Table 11. Orthogonality calibration results.

Coils	H-h	Z-H	Y-Z
Angle (deg)	91.15	89.95	89.97
Uncertainty B (deg)	0.055	0.089	0.088
Uncertainty B (ppm of 90 degrees)	611	989	978

Due to non-optimal choice of measuring devices (current measurement, current source) and poor ambient magnetic field stability, the precision of the calibration was low. The short measurement time had a significant impact, so averaging could not be exploited. This measurement was carried out as a preliminary trial to test the algorithms that had been developed and to identify the main sources of uncertainty (see Section 3.3).

Braunbek coil system at PTB Braunschweig

A major test of the procedure was carried out at PTB Braunschweig, a world level calibration facility. The PTB coil system has a Braunbek structure. The three-meter coils are depicted in Figure 18. The location of the non-magnetic facility is advantageous since the laboratory, unlike the Pruhonice facility, is away from the city and the short-term magnetic field disturbance is relatively low at ±2nT, see Figure 19.

The coil constants of the Braunbek system (Table 12) were known approximately from a previous measurement. The current excitation sequence could therefore be planned to avoid over-ranging of the magnetometer (20-120 μT).

The orientation of the individual axis, the magnitude of the Earth's magnetic field (49 160 nT) and the inclination of its vector (67.5 deg) were used for establishing the current sequence.

Table 12. Preliminary parameters of the axis of the Braunbek system.

Coils	X	Y	Z
Orientation	North-South	East-West	Vertical
(approx.) Coil constant	46.5 (μT/A)	48 (μT/A)	49.7 (μT/A)
Resistance	13.32 Ω	13.42 Ω	12.49 Ω
Earth's magnetic field	18800 (nT)	0 (nT)	45400 (nT)

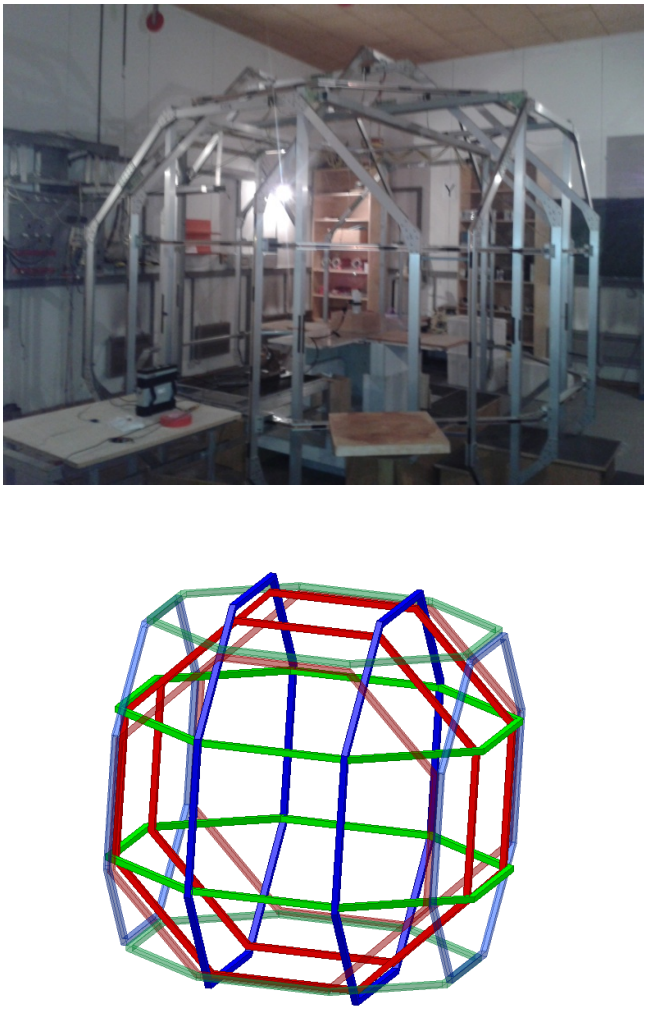

Figure 18. *Braunbek coil system in PTB Braunschweig.*

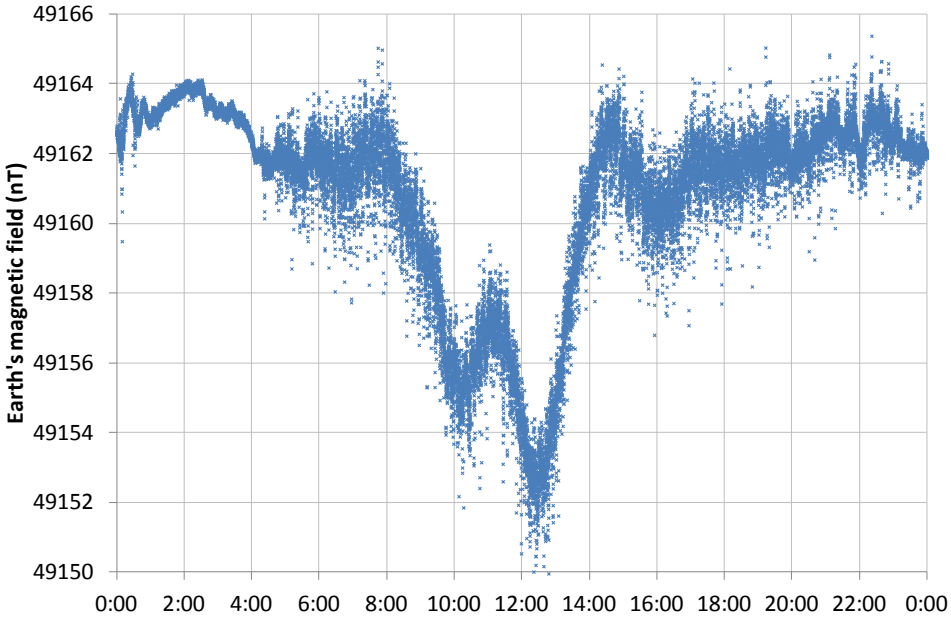

Figure 19. *The Earth's magnetic field was measured in the location of the coil system to establish its variation.*

Measurement devices and equipment.

Overhauser magnetometer: GSM-19, GEM Systems, Sensitivity: 0.022 nT @ 1 Hz,
Absolute Accuracy: +/- 0.1 nT, Range – 20,000 to 120,000 nT
Gradient Tolerance: Over 10,000 nT/m.

Resistors:
R_1 = 1.0003175 ± 0.000001 Ω
R_2 = 0.0999381 ± 0.000005 Ω

Voltmeters:
2 x Agilent 3458: 8½ digits multimeter – set in the range of 1 V
its uncertainty in the 1 V range is (8 ppm*Reading + 0.3 ppm*Range)

Current sources:
ADCMT 6243 – DC/Voltage/Current source – set in current mode in the 2 A range, its accuracy in the 2 A range is 100 µA.

All devices were connected with the GPIB bus, so the measurements were fully automatically controlled by LabView software. The current sources were set in the desired sequence and the voltmeters were triggered by the same signal in order to measure at the same time. All data was logged into a file in a computer and stored for further calculation. The OVH magnetometer could not be connected to the measuring chain. We used time stamps to merge the data in a post-processing step.

Coil constant calibration

Table 13. Applied current for coil constant estimation.

Coil = Current (A)	X = 0.95	X = -0.95	Y = 0.95	Y = -0.95	Z = 1	Z = -0.2
Magnetic field (μT)	77.65	52.02	67.02	67.02	96.96	40.17

The measurements were carried out over a longer time in order to obtain at least 80 readings. Figure 20 and 21 illustrate that while the variation of the ambient field depends on the time of day (correlate with Figure 19), variations of the coil constant are time independent. This is due to the relatively short time taken for the measurements (the whole sequence took around 40 seconds). If the time was suitably short, the ambient magnetic field was not changed and the result did not vary even when there were larger ambient disturbances of the magnetic field.

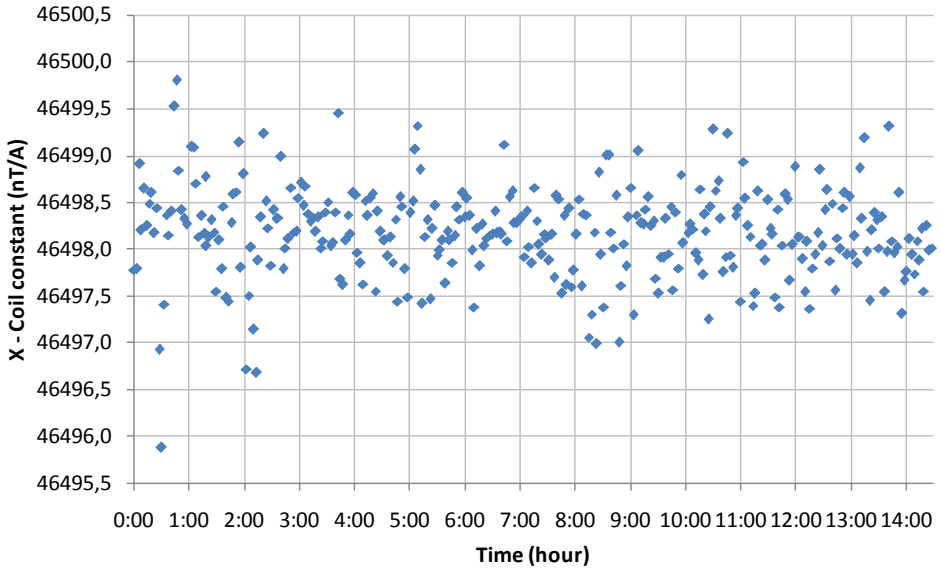

Figure 20. *Calculated constant of the X coil.*

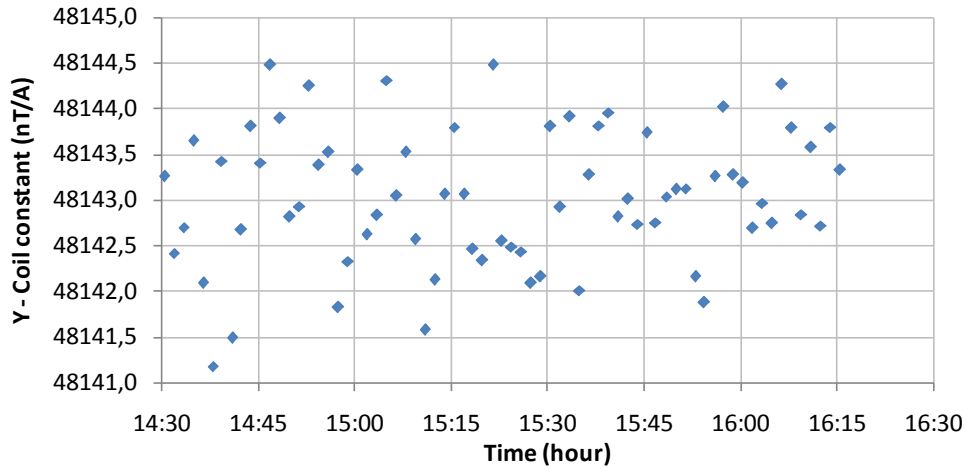

Figure 21. *Calculated constant of the Y coil.*

To check the results, a control measurement was performed using a technique developed at PTB. These measurements were based on a proton magnetometer.

The proton magnetometer sensor head is oriented perpendicularly to a calibrated axis inside the homogeneous area of the Braunbek system. The calibrated coil of the field cancellation system is substituted by an extra 1-meter Helmholtz coil, which replaces the axis in the cancellation system. This means that the cancellation system is still able to compensate the Earth's magnetic field, but one axis (replaced by the Helmholtz coil) can be calibrated. During the measurements the Earth's field is suppressed to very low values (a maximum of 10nT due to gradient field variations), and the NMR magnetometer measures only the field generated by the calibrated Braunbek coil. In order also to decrease the influence of the residual magnetic field (after compensation), both polarities of the current are applied to the calibrated axis, and the average value is adopted. To calibrate another axis, the setup has to be rotated to the other coil – the direction of the extra Helmholtz coil and the NMR magnetometer.

The results are presented in Table 14. The OVH marking is the scalar calibration and NMR means the calibration made by PTB. The uncertainties were calculated according to section 3.3. This means that the type A uncertainty was calculated as the standard deviation of the measurement set and the type B uncertainty was estimated analytically.

Table 14. Coil constant calibration – results, uncertainty, comparison with NMR.

Coil	X (N-S)	Y (E-W)	Z (Vert.)
Constant OVH (nT/A)	46498,16	48143,03	49848,24
Uncert. A (ppm)	11	15	6
Uncert. B (ppm)	21	19	25
Combin. Uncert. (nT) k=1	1.07	1.15	1.28
Constant NMR (nT/A)	46499,14	48143,59	49848,21
Uncert. A (ppm)	4	5	6
Uncert. B (ppm)	30	30	30
Combin. Uncert. (nT) k=1	1.4	1.5	1.5

As is shown in Figure 22, the two calibrating techniques have the same results, as regards their combined (k=1) uncertainty band (their tolerance bands have an overlap).

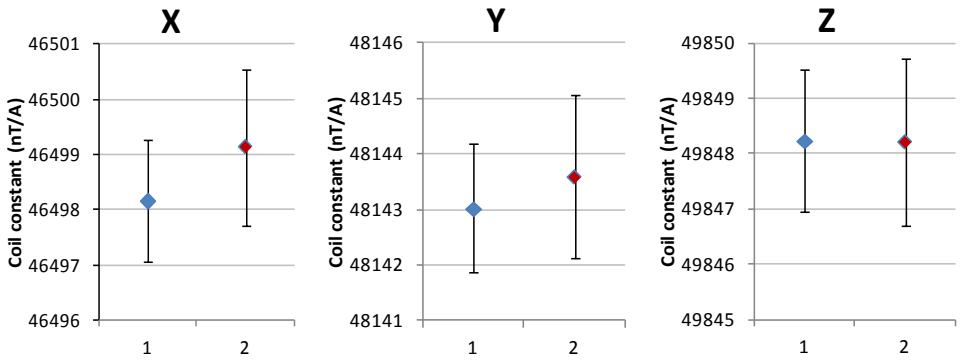

Figure 22. *Comparison of the calibration methods for sensitivity – PTB Braunschweig. (1 – scalar calibration carried out with the Overhauser magnetometer, 2 – PTB calibration principle carried out with the NMR).*

Calibration of orthogonality

When planning the current sequence for estimating the orthogonality of the coil, the situation was a little easier because two coils are excited. The combination of currents can therefore be adjusted so that the total magnetic field is in the range of the magnetometer and the current measurement complies with the uncertainty requirements.

Table 15. Current sequence for XY orthogonality calibration.

Coil X current (A)	-0.96	-0.95	0.8	0.9
Coil Y current (A)	1.2	1.3	1.3	-1.5
Magnetic field (µT)	77.80	81.27	95.41	104.58

Table 16. Sequence for XZ orthogonality calibration.

Coil X current (A)	-1.75	1.2	-1.4	1.2
Coil Z current (A)	-0.9	-0.8	0.8	0.6
Magnetic field (μT)	62.71	74.98	96.99	106.07

Table 17. Sequence for YZ orthogonality calibration.

Coil Y current (A)	1.4	-1.6	1.2	-1.3
Coil Z current (A)	-0.95	-0.9	0.5	0.8
Magnetic field (μT)	71.43	80.43	92.14	106.35

Each current sequence was followed by zero excitation to measure the total Earth's magnetic field. The current steps were sequentially switched according the table. Each step took 50 seconds, in order to settle the magnetometer and obtain enough valuable measurements. An example of excitation is depicted in Figure 23.

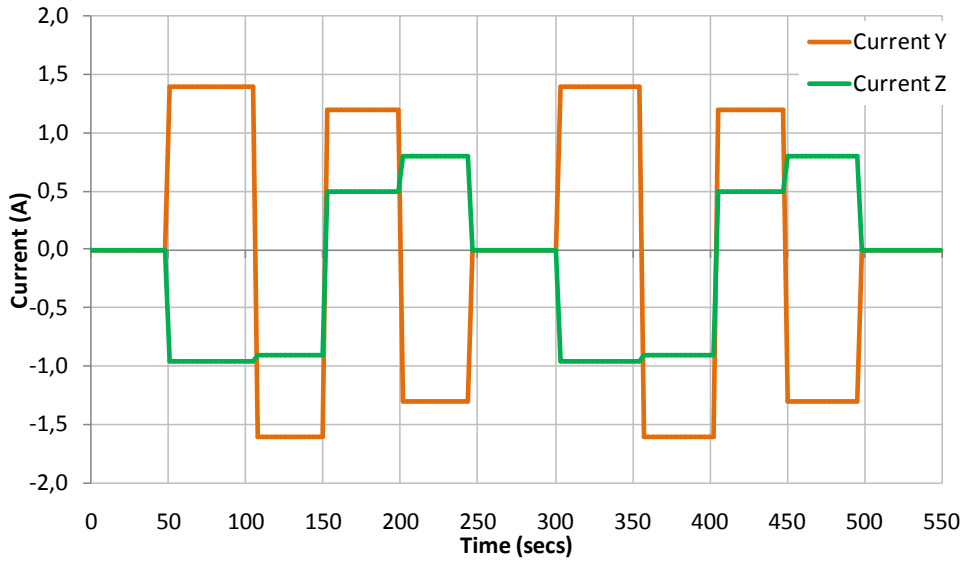

Figure 23. *Excitation sequence for XY calibration.*

Figures 24, 25 and 26 show the variation of the calculated orthogonal angles. The time dependency can be seen. During the measurements, the best time was at night from 1 am to 4 am, because the time variation of the ambient magnetic field is at its daily lowest level. This differs from the sensitivity calibration, due to the measurement time for one sequence. When carrying out the sensitivity calibration, the measurement time for one sequence was 40 seconds, but during the orthogonal angle calibration the measurement time was 250 seconds, which is more than six times longer. The magnetic field changed in the course of this long period of time and the

assumption that the magnetic field was stable was disrupted. The variation of the results was therefore lowest between 1 am and 4 am.

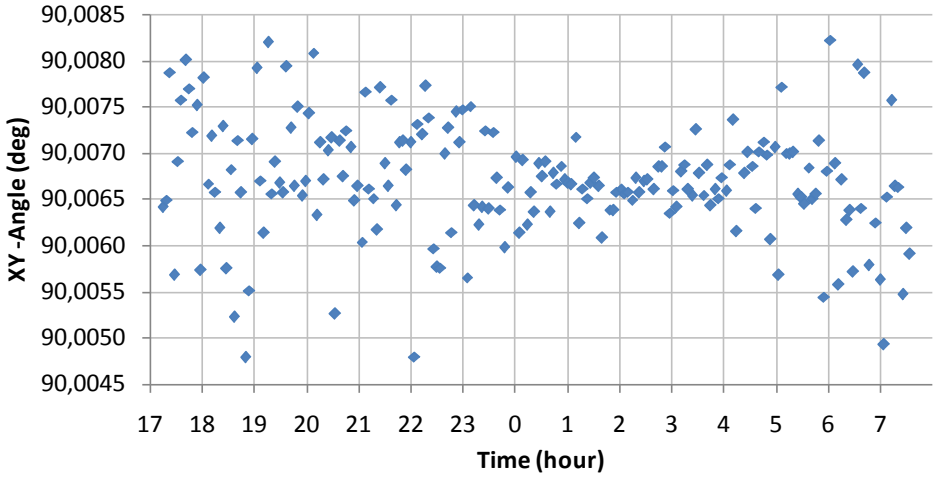

Figure 24. *Orthogonality X-Y calibration.*

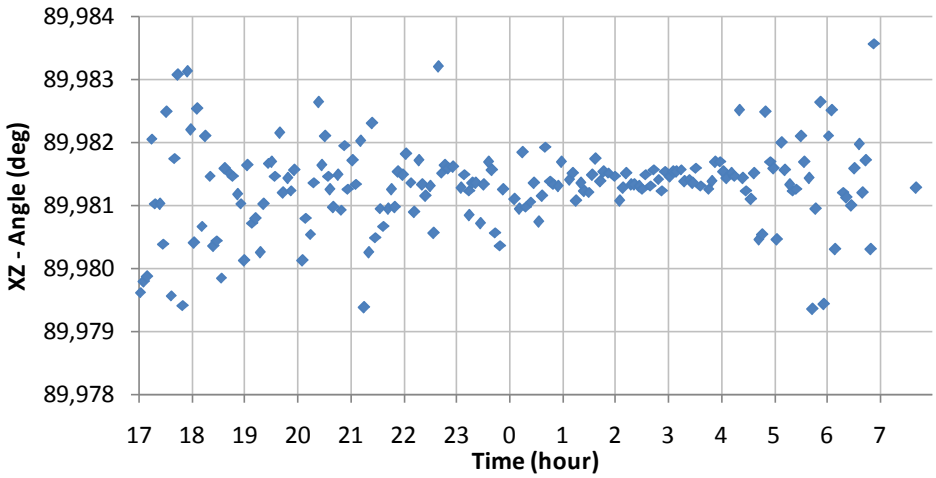

Figure 25. *Orthogonality X-Z calibration.*

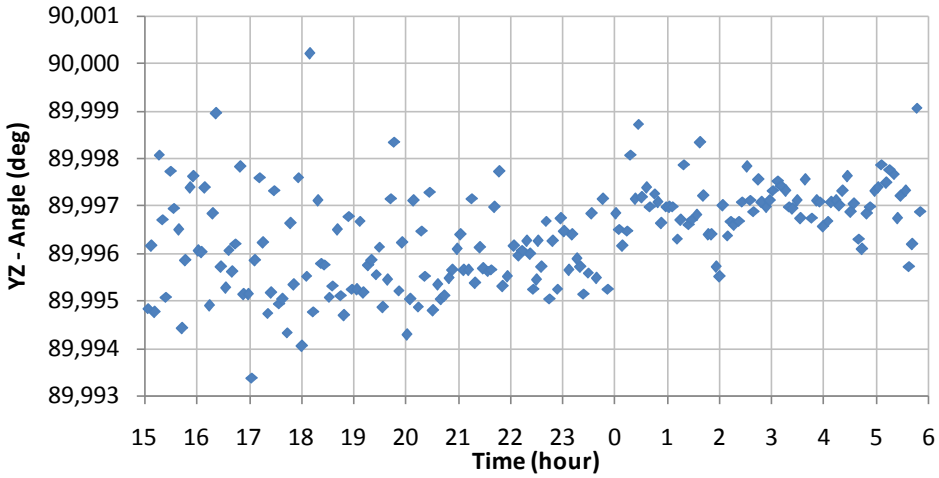

Figure 26. *Orthogonality Y-Z calibration.*

The results and their uncertainty are presented in Table 18. The type A uncertainty was determined from the standard deviation, and the type B uncertainty of the angles was expressed by the Monte Carlo method, as has been explained above.

Table 18. Orthogonality calibration – results, uncertainty (PTB Braunschweig coil system).

Coils	X-Y	X-Z	Y-Z
Angle (deg)	90.0067	89.9813	89.9963
Uncert. A (ppm)	7	9	11
Uncert. B (ppm)	32	31	33
Uncert. (deg)	0.0036	0.0037	0.004

Unfortunately, it was not possible to calibrate the orthogonal angles using the PTB methods because the ambient magnetic field has to be cancelled when NMR measurements are made, and the measured magnetic field has to be oriented perpendicular to the NMR sensor.

Helmholtz coil system – GFZ Niemegk, Postdam

The coil system is a three-dimensional Helmholtz setup. The biggest coil is about three meters in diameter (see Figure 27). The system serves mainly to calibrate the tri-axial sensor by the AC procedure. The approximate parameters of the coil are shown in Table 19.

Table 19. Parameters of the Niemegk observatory's coil system.

Coil	X	Y	Z
Orientation	North-South	East-West	Vertical
(roughly) Coil constant	8.5 (μT/A)	8.2 (μT/A)	5.5 (μT/A)
Resistance	54.2 Ω	57.5 Ω	82.5 Ω
Inductance	5.5 (mH)	5.8 (mH)	8.5 (mH)
Earth's magnetic field	18900 (nT)	0 (nT)	45300 (nT)

Figure 27. *Coil system in the Niemegk observatory.*

The coil constants are very small, and a high current could not be applied to the coil because of the small cross-section of the wire of the coil. Therefore, only small changes of the magnetic field were applied compared with the Earth's magnetic field, the variation of which was not negligible. Nevertheless, Figures 28 and 29 show that

the field variation was much smaller than in Pruhonice and even much smaller than in the PTB measurement. On the basis of this measurement, the uncertainty of the magnetic field measurement was established as 0.1 nT.

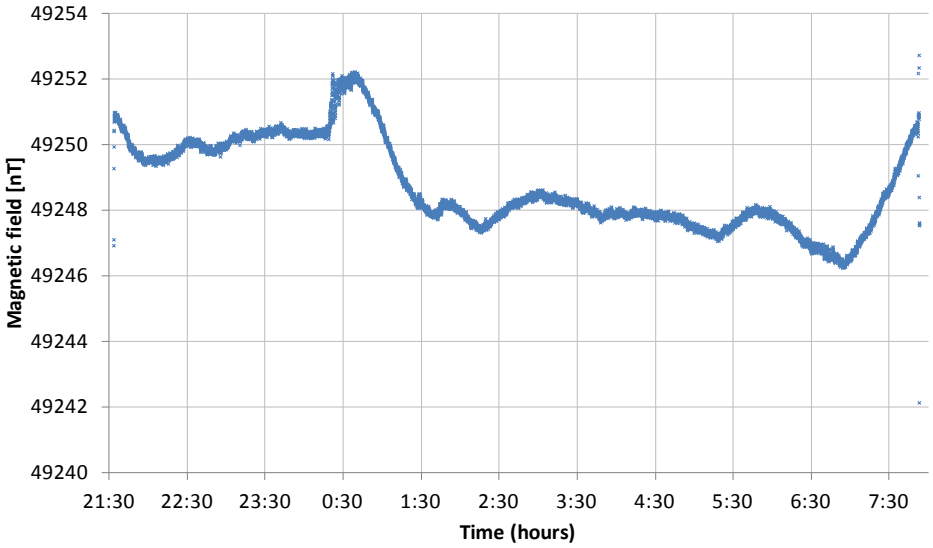

Figure 28. *The variation of the Earth's magnetic field during the day.*

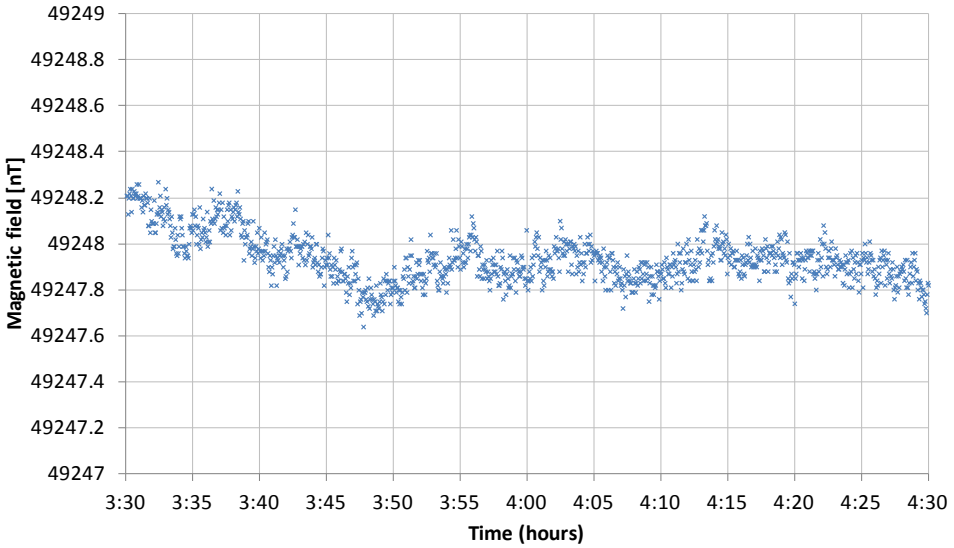

Figure 29. *Short-time variation of the Earth's magnetic field.*

The measurement setup was the same as for the PTB measurements. The results are depicted in the following tables.

Table 20. Results of the coil constant calibration (Niemegk coil system).

Coil	X (N-S)	Y (E-W)	Z (Vert.)
Constant OVH (nT/A)	8506.3	8132.2	5499.1
Uncertainty A (nT/A)	0.52	0.34	0.60
Uncertainty B (nT/A)	0.73	0.74	1.12
Combined uncertainty (nT/A)	0.89	0.81	1.27
Combined uncertainty (ppm)	105	100	231

Table 21. Results of the orthogonality calibration (Niemegk coil system).

Coils	X-Y	X-Z	Y-Z
Angle (deg)	89.91	89.98	89.92
Uncertainty A (deg)	0.02	0.02	0.01
Uncertainty B (deg)	0.03	0.04	0.04
Combined uncertainty (deg)	0.04	0.05	0.05

The precision of the calibration was strongly influenced by the impossibility to excite the coils properly.

The GFZ Niemegk observatory calibrates the coil constants with the scalar principle using a Cesium magnetometer, and the orthogonality is determined by using a theodolite and searching zero AC responses on the fluxgate magnetometer:

The magnetometer is aligned with the theodolite, which is leveled in the homogeneous space of the coil. One of the horizontal coils is excited by the AC current. The theodolite is settled up at the angle where the magnetometer measures the minimal value at the known frequency. This is a new zero angle of the theodolite. Then the second horizontal coil is excited and the theodolite is rotated to the angle at which the magnetometer indicates zero. The difference of the angles (the base angle and the newly-obtained angle) is the angle between two coils projected into the horizontal plane. This can be repeated many times to reduce the uncertainty by averaging.

It is somewhat complicated to calibrate the angles related to the vertical axis of the coil systems, because the theodolite has to be set up in the vertical plane. This calibration was therefore not carried out.

The results of the Niemegk calibration procedure are depicted in Table 22.

Table 22. Results of the coil constant calibration (carried out by the Niemegk observatory).

Coil	X (N-S)	Y (E-W)	Z (Vert.)
Constant OVH (nT/A)	8508	8132	5498
Uncertainty A (nT/A)	1.1	1.2	1.4
Uncertainty A (ppm)	120	150	250

Table 23. Results of the orthogonality calibration (carried out by the Niemegk observatory).

Coils	X-Y
Angle (deg)	89.92
Uncertainty A (deg)	0.05

Figure 30 compares the results obtained for the scalar calibrations carried out by the Overhauser magnetometer and by the Niemegk observatory's Cesium magnetometer.

There is an overlap of the tolerance bands in each of the axes, so we can summarize that within the uncertainty the constants were met.

A comparison of the orthogonal angles is depicted in Figure 31. Since the Niemgek observatory provided only the orthogonal angle of horizontal axes X and Y, we compared only this. It can be seen that the results are comparable.

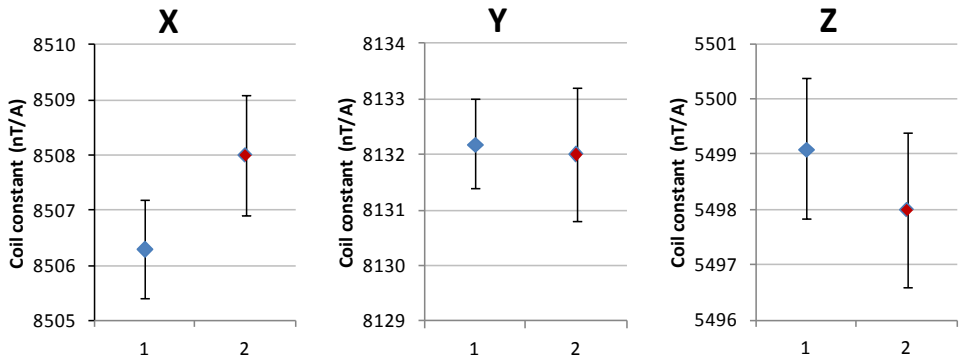

Figure 30. *Results of sensitivity - comparison of the calibration methods - Niemegk. (1 – scalar calibration carried out with the Overhauser magnetometer, 2 – Niemegk calibration principle carried out with the Cesium magnetometer).*

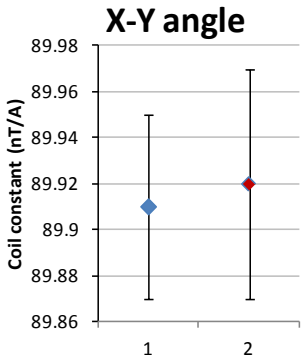

Figure 31. *Results of orthogonality - comparison of the calibration methods - Niemegk. (1 - scalar calibration carried out with the Overhauser magnetometer, 2 – Niemegk calibration principle carried out with a fluxgate magnetometer).*

4 Calibration of tri-axial magnetometer

If parameters of a coil system are calibrated, the coil system can be exploited for calibration of tri-axial magnetometers.

Coil systems usually cancel the Earth's magnetic field in order to reach zero magnetic field and they can also produce a defined magnetic field in order to establish parameters of the magnetometers. In most cases, the cancellation system works as an open-loop control. A reference tri-axial magnetometer that measures remotely the Earth's magnetic field controls currents flowing into the coils to keep a magnetic "vacuum". The reference sensor has to be far enough from the coil system to avoid any mutual influences. A typical distance is in range of 40 - 60 meters.

A tri-axial magnetometer to be calibrated is then placed in the middle of the coil system, where zero magnetic field is maintained, and it is calibrated by a sequence of known additional magnetic fields generated by the coils. The parameters of the tri-axial magnetometer can be calculated based on measured values.

It is very complicated task to setup such cancellation system (Risbo, et al., 2003) because the cancellation loop has to be tuned to minimize any influence of noise (a current source, magnetic noise etc.). Especially, huge problems are temperature drifts of various offsets, non-stability of current sources and others.

Another approach to calibration of tri-axial magnetometers is the scalar calibration, which provides very good results (Olsen, et al., 2003), but it relies on mechanical rotations of the calibrated magnetometer in the Earth's field, and so it is very sensitive to field disturbances but also to any magnetic field gradient. In order to cancel disturbances, the magnetic field should be logged and a gradient of the magnetic field determined.

4.1 New calibration method

A new calibration procedure combines the scalar principle and the principle based on a tri-axial coil system. A calibrated magnetometer is placed in a coil system, and it is exposed to an arbitrary magnetic field that is generated by currents flowing in the coils. The Earth's magnetic field is not compensated during excitation, but it is remote measured by a scalar magnetometer. Since we measure the total field, the orientation of the Earth's field is not known and it is one of calculated parameters. The distance of the scalar magnetometer from a coils system has to respect the same rules as in the remotely tri-axial magnetometer. This means that magnetometer has to be at least 40 meters far to suppress influences of coil excitations.

Mathematically, each axis of the calibrated magnetometer can be related to the reference frame of the coil system according to Figure 32. The output value of each individual magnetometer axis is given as:

$$M = S\,[B_E \sin(\alpha_E) + B_X \cos(\alpha)\cos(\beta) + B_Y \cos(\alpha)\sin(\beta) + B_Z \sin(\alpha)] \qquad (32)$$

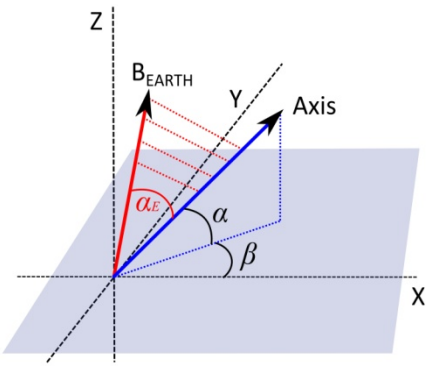

Figure 32. *Calibration of one axis of magnetometer with respect to a reference coil system – graphical representation.*

Unknown parameters: S is a sensitivity of sensor axis, α_E is a spatial angle of projecting the Earth's vector to the magnetometer axis, α and β are spatial angles between the magnetometer axis and the coil reference system.

Measured values: B_E is the Earth's magnetic field, measured by a scalar magnetometer at a distant location, B_X, B_Y and B_Z are the magnetic field components generated by the 3D coil system – they can be calculated by knowing the coil constants and applied currents.

Magnetometer offsets are not included as unknown variables in equation 32. They can be either assumed zero, or their values should be determined as M_{OFF}, preferably by measuring in a magnetic shield chamber. The reason is that the offsets are in the range of 10-100 nT which is a very small value compared to the other calculated parameters and so their influence on the calculation is negligible and the method converges even if the offsets are not precisely determined. Therefore, the measured offsets can be included to the calculation according to equation 33.

During the calibration, the total Earth's magnetic field (at the Overhauser location) and output M of a magnetometer axis are sampled simultaneously in each step of applied fields. Since the 40-meter distance is between the coil and the Overhauser location, the same inclination and declination are supposed on both place. This is a limiting point of this method because gradients of the Earth's magnetic field can change the homogeneity of the field and thus they can violate the assumption.

Therefore reduction of the gradient influence should be carried out by a preliminary measurement. At the beginning of the real calibration procedure, the gradient B_G is measured and this value is then included into the calculations. Nevertheless, then the stability of the gradient is expected within the calibration time.

$$M = M_{OFF} + S \begin{bmatrix} (B_E + B_G)\sin(\alpha_E) + B_X \cos(\alpha)\cos(\beta) \\ + \ \mathrm{B_Y}\cos(\alpha)\sin(\beta) + B_Z \sin(\alpha) \end{bmatrix} \qquad (33)$$

Another method of suppressing the gradient is analogous to the method mentioned in section 3.2. The Earth's field is measured directly in the coils in time intervals when coils are not excited but this way demands two scalar magnetometers.

Equation 33 is strongly non-linear and therefore it has to be solved by an optimization algorithm. It is obvious that equation is similar to equation 21 and so the same optimization method, the Levenberg-Marquardt method, was chosen.

At least four independent excitation currents have to be applied in order to calculate all unknown parameters from equation 33. Table 24 shows the typical sequence of applied fields created with the respective coil axes. Increasing the number of combinations shown in Table 24 increases the resulting precision, however, decreases the calibration speed.

Table 24. Applied current for coil constant estimation.

Step	1	2	3	4	5	6	7
B_X (μT)	25	-25	0	25	-25	-25	0
B_Y (μT)	-25	0	25	-25	25	25	-25
B_Z (μT)	0	25	-25	25	0	-25	25

If a tri-axial calibrated magnetometer is able to sample all three axes, (a data acquisition circuit is able to do so respectively), all calibration parameters can be established from one run of the calibration procedure. The resulting parameters of the tri-axial sensor are graphically explained in Figure 33.

In principle, the calibrated magnetometer can have arbitrary orientation with respect to coil system. However, practical experiences show that it is better to align approximately axes of the magnetometer with coil axes.

Since the calibration technique (Olsen, et al., 2003) uses a different notation of the non-orthogonal angles, the non-orthogonal angles are recalculated according to equation 34 in order to be able to compare results.

$$\begin{aligned}\Delta_1 &= \beta_U + \beta_V \\ \Delta_2 &= \alpha_U + \beta_W \\ \Delta_3 &= \alpha_V + \alpha_W\end{aligned} \tag{34}$$

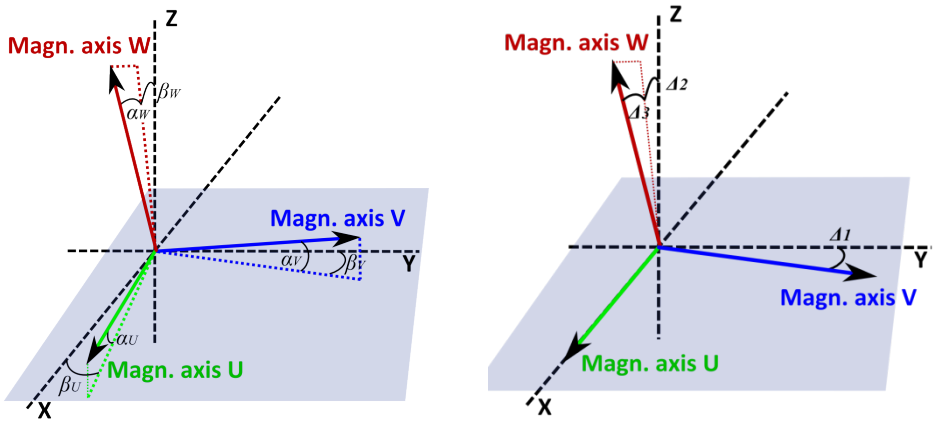

a) *b)*

Figure 33. *The resulting angle parameters - a) a representation of our method b) representation of the method described in (Olsen, et al., 2003).*

4.2 Uncertainty analysis

We had to select the same analysis as in the calibration of the coil system. Since calculation is carried out by the optimization method, the type B uncertainty is determined by the Monte-Carlo method. Known sources of uncertainty are current measurement, coil sensitivity and Earth's field measurement. The type A uncertainty is then calculated from a set of measurements.

4.3 Experimental calibration of a magnetometer

A tri-axial digital magnetometer was calibrated in one-meter Helmholtz coil system (Billingsley HELM-3) which is depicted in Figure 34.

As the first step, the coil system was calibrated by means the method described in chapter 3 and results are shown in Table 25.

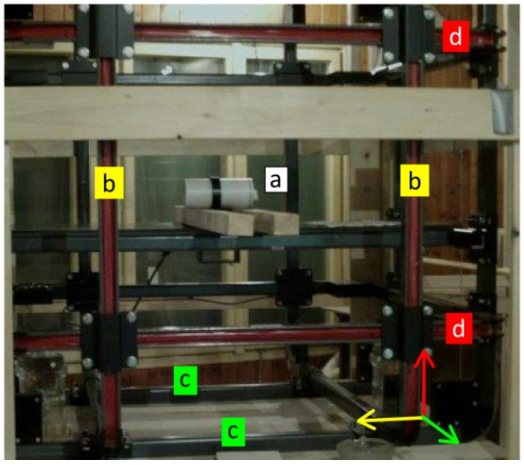

Figure 34. *a) The Overhauser magnetometer sensor placed in the tri-axial Helmholtz coils during calibration – a central position assures low field gradient, b) the coil pair oriented N-S, c) the coil pair oriented E-W d) the coil pair oriented vertically.*

Then the Overhauser magnetometer was moved to a location that was around 40 meters far and a gradient between this new location and the coil system was measured in order to minimize error. The digital magnetometer was placed to the center of the coil system, and it was approximately aligned respecting coil axes.

During measurement, all quantities were automatically measured by LabView program in synchronized intervals and a current sequence was generated by precise sources with stability of 60 µA.

We applied a current sequence suitable for the calibration (see Figure 35). The sequence contains current steps designed to have significant influence on the calibrated sensors in each perpendicular direction. The aim was to obtain a response at least 25 µT in each axis of the calibrated magnetometer.

Table 25. The calibration parameters of the Helmholtz coil system.

Parameter	Value	Uncertainty
Overhauser magn. (nT)	20 - 120 µT	0.2 nT
Coil constant (nT/A)	78788, 76648, 83016	204, 175, 286 ppm
Coil angles (degree)	90, 90, 90	0.02 degree
Sensing resistors values (Ω)	1.00006, 0.99989, 0.99993	30 ppm
Voltage measurement (V)	0 - 1	80 ppm

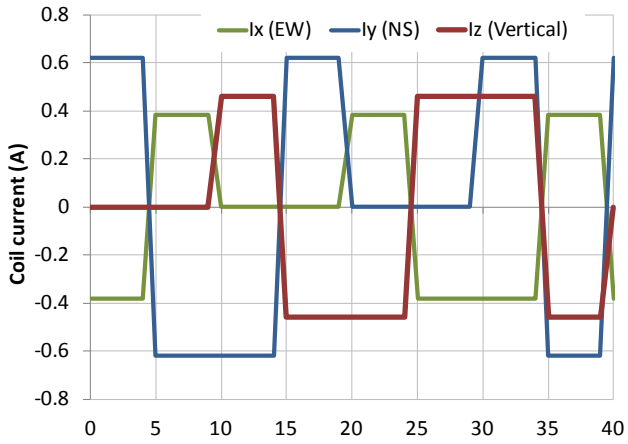

Figure 35. *The current sequence applied to respective coil axes during calibration of the digital magnetometer.*

The magnetometer output was measured correspondingly to the applied current sequence. Figure 36 shows a time record of magnetometers values as a response to the coils excitation. The magnetic axis orientation is significant because it correlates with the coil excitation. The V axis was vertical (Z coil), the W axis was oriented to North-South direction (Y coil) and U magnetometer axis was approximately aligned with East-West coil (X coil). The alignment was, however, not ideal as we can see small cross-field reactions, but this does not poses a problem for the calibration algorithm.

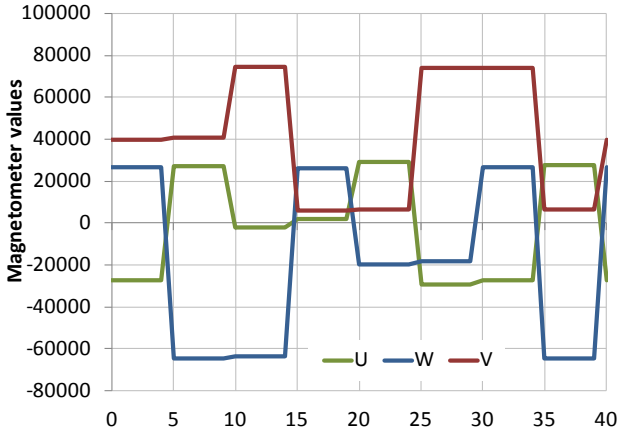

Figure 36. *A response of the digital magnetometer on an excitation of the reference coil.*

The calibration current sequence was repeated 12 times to obtain a minimal statistical set for averaging and calculation of the type A uncertainty, and therefore we found higher residuals of the optimization method in some combinations of the current. This was probably caused by vectorial components of the ambient magnetic noise which are different depending on the orientation - the higher residuals were

correlated with the situation when the vertical coil was excited which corresponds with a rule that the higher noise is in the vertical component.

The calculated sensitivities of magnetometer axes varied maximally of 210 ppm and the angles varied 0.028 degree which was designated as the type A uncertainty.

The B-type uncertainties were done by the Monte Carlo simulation using the parameters from Table 25. We set up the input parameters according to the real measured quantities and their values were scattered with their known uncertainties. The worst B-type uncertainty of 110 ppm appeared in the W axis because it was most affected by the magnetic field noise. We finally calculated the combined uncertainty as a norm of two A and B components and results are given together with the calibrated parameters in Table 26.

We calibrated the same sensor also by a different technique of the scalar calibration (Olsen, et al., 2003) and so we could compare the calibration results to our procedure. The data agree well supposing that also the scalar calibration has a significant uncertainty which is usually expressed as calibration residua.

Table 26. Comparison of the calibration techniques.

	Uncert. B	Uncert. A	Results with combined uncert., (k = 2)	Scalar method (Olsen, et al., 2003)
Offset U (nT)	2		-32.5 ±4	-30.5
Offset V (nT)	2		-37.5 ±4	-34.4
Offset W (nT)	2		-24.5 ±4	-27.6
Sensitivity U norm. (-)	88	132	0.9659 ±320 ppm	0.9666
Sensitivity V norm. (-)	68	116	0.9431 ±270 ppm	0.9436
Sensitivity W norm. (-)	110	185	0.9022 ±430 ppm	0.9021
Angle Δ_1 (deg)	0.002	0.016	0.205 ±0.034	0.167
Angle Δ_2 (deg)	0.001	0.024	0.531 ±0.048	0.603
Angle Δ_3 (deg)	0.003	0.031	0.104 ±0.062	0.107

5 Magnetic tracker

5.1 Principle

The position between two bodies is defined by six variables. These are the spatial position (distance, azimuth and elevation) and the mutual rotation (yaw, pitch and roll). Our specific situation is shown in Figure 37. The first part represents the source of a magnetic field (a coil system), and the second part is a precise tri-axial magnetic sensor).

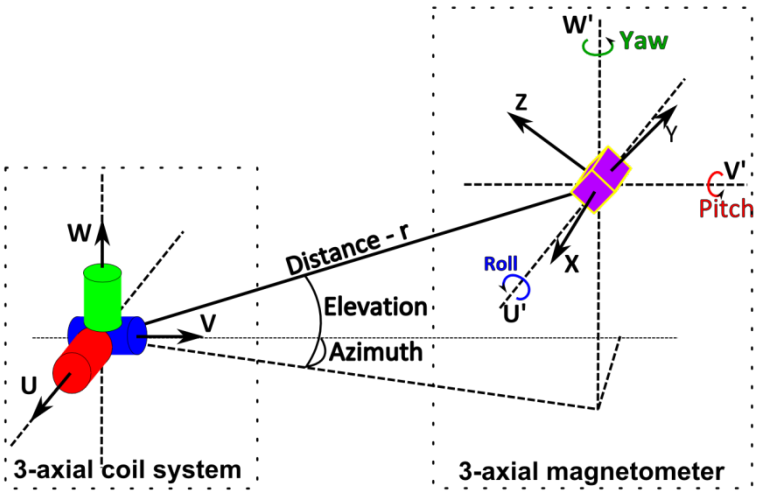

Figure 37. *Magnetic tracker – model situation.*

Source of the magnetic field

Some simple magnetic trackers, e.g. the system described in (Liu & Wang, 2011), use a permanent magnet as a magnetic marker. An inherent problem is that the DC field of the marker cannot be distinguished from the Earth's field. This causes gross errors in greater distances.

The magnetic source should have a mathematically describable model of the generated magnetic field. The simplest type is the magnetic dipole model. A solenoid coil is chosen as the excitation part, because it approximates the ideal dipole model with a magnetic model of

$$m = NIA \qquad (35)$$

where N is the number of turns, I is the excitation current and A is the average turn area. Then the ideal magnetic field has radial components

$$B_R = \frac{\mu_0 m \cos\phi}{2\,\pi\, r^3} \tag{36}$$

and tangential components

$$B_T = \frac{\mu_0 m \sin\phi}{4\,\pi\, r^3} \tag{37}$$

where ϕ is the angle between the coil axis and the direction to the measured point, and r is the distance to the point. If tri-axial excitation is considered, the equations can be rewritten to the matrix

$$M = T_\beta' T_\alpha' \frac{m}{2\pi r^3} \begin{bmatrix} 1 & 0 & 0 \\ 0 & -1/2 & 0 \\ 0 & 0 & -1/2 \end{bmatrix} T_\alpha T_\beta f_0 \tag{38}$$

where T are the matrices corresponding to the tangential and radial component of an individual coil and f_0 is the driving matrix. If vector f_0 is for example [1,0,0] then the only coil X is excited.

$$T_\alpha = \begin{bmatrix} \cos\alpha & \sin\alpha & 0 \\ -\sin\alpha & \cos\alpha & 0 \\ 0 & 0 & 1 \end{bmatrix} \qquad T_\beta = \begin{bmatrix} \cos\beta & 0 & -\sin\beta \\ 0 & 1 & 0 \\ \sin\alpha & 0 & \cos\beta \end{bmatrix} \tag{39}$$

To complete the transformation, matrices representing the sensor orientation in relation to the coil source have to be added

$$M = T_{YAW} T_{PITCH} T_{ROLL} T_\beta' T_\alpha' \frac{m}{2\pi r^3} \begin{bmatrix} 1 & 0 & 0 \\ 0 & -1/2 & 0 \\ 0 & 0 & -1/2 \end{bmatrix} T_\alpha T_\beta f_0 \tag{40}$$

The matrices are defined as

$$T_{YAW} = \begin{bmatrix} \cos\gamma & \sin\gamma & 0 \\ -\sin\gamma & \cos\gamma & 0 \\ 0 & 0 & 1 \end{bmatrix} \qquad T_{PITCH} = \begin{bmatrix} \cos\delta & 0 & -\sin\delta \\ 0 & 1 & 0 \\ \sin\delta & 0 & \cos\delta \end{bmatrix} \tag{41}$$

$$T_{ROLL} = \begin{bmatrix} 1 & 0 & 0 \\ 0 & \cos\varepsilon & \sin\varepsilon \\ 0 & -\sin\varepsilon & \cos\varepsilon \end{bmatrix}$$

Matrix M contains all magnetic field components which are generated from the three perpendicular coils.

Magnetic sensor

From the previous equations, one can recognize that we have to know all three components in order to establish the position. The magnetic field sensor should therefore be a tri-axial. In order to obtain the precise value of the measured distance, the magnetic sensor should have low noise. Offset variations can be compensated by using a bipolar excitation field. AMR sensors are small and cheap, but they have a noise level in the order of 5 nT (Ripka, et al., 2003), which is too high for the required accuracy in long distance measurement. GMR sensors also do not achieve an acceptable noise level. Even with AC excitation (Ripka, et al., 1999), their noise is at a level of 15 nT, which is not sufficient for a precise distance meter.

The noise of GMI sensors is below 10pT RMS/√Hz @1 Hz (Ding, et al., 2009) which would meet the requirements for distance sensor precision, but their sensitivity and offset are strongly temperature dependent (Malatek, et al., 2008). They are therefore not suitable for this application.

We therefore used tri-axial fluxgate sensors (Billingsley TFM100G2) with resolution of 0.1 nT and sufficient offset and gain stability. The noise power spectrum density is ≤12 pT RMS/√Hz @1 Hz, which drops below 4 pT at 10 Hz. The offset drift of ± 0.6 nT/K is still large, but its effect can be suppressed by calculating the field differences. The sensitivity temperature dependence is only 0.007%/K, which makes the sensors ideal for this application. Another advantage of these sensors is their large linearity (linearity error below ± 0.015% of the Full Scale). A disadvantage of fluxgate sensors is their large size. Even though the sensors that we use are “miniature”, the sensor head is approx. 3x3x3 cm in size, and there is a need for corrections, which will be discussed below.

The mathematical point of view

It is a complex problem to calculate the position of two points on the basis of the magnetic dipole model, because the solver has to sort out the equations for six variables. Additionally, the equations are strongly non-linear, and the model cannot be substituted by a linear model because the transform matrices contain the sin and cos

function and the point could theoretically be anywhere on the function wave. This problem leads to an optimization solver, which is based on a non-linear numerical technique.

It is necessary to find the global optimum, and the appropriate optimization method therefore has to be chosen. The pure Gauss-Newton method cannot be used because it does not guarantee global convergence. We therefore used the Trust-region or the Leveberg-Marquart method to calculate the problem.

The Trusted region method needs to solve the problem with the same number of equations as is the number of unknown variables. Since the tri-axial setup of the coil system generates a magnetic field in three different directions, nine equations are used to describe the situation. One option is to degrade the problem and express it only with reduced information (measurements from 2 coils).

However, the Levenberg-Marquart method is able to accept an overdetermined set of equations.

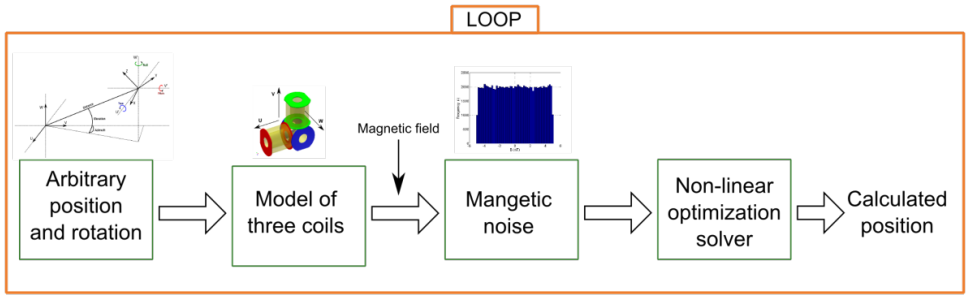

Figure 38. *Testing the solution method of the magnetic tracker.*

The tests proved that attempts to establish the exact position with the selected method do not work in the full range of positions. Difficulties come from the rotation matrices of the proposed model. In some non-ideal cases, the rotation angles can be misinterpreted. The method converges to a minimum, but the rotation angles are misinterpreted. This also influences the matrices of spherical angles. This problem is caused by the multimodality of the solution. The initial point of iteration would therefore have to be changed case-by-case, or would have to include the limitations.

Excitation sequence

The instrument could work in the vicinity of highly conductive objects. In order to avoid field distortion by eddy currents, we had to excite the magnetic field with a very low frequency – typically a square wave below 10 Hz. It is not practical to use a DC field (e.g. from a permanent magnet), as it cannot be distinguished from the Earth's field. The magnetic field is therefore excited by repetitive current pulses of both

polarities, which are sequentially sent to individual source coils U, V, and W. In this way, the Earth's magnetic field is eliminated after subtracting the response to positive and negative field pulses. This is an advantage of using vectorial sensors rather than the scalar magnetometers that we used for calibrating the coil systems.

5.2 Distance sensor

The existing design could not work robustly as a full-featured magnetic tracker. Nevertheless, radius r, which represents the direct distance between two points, is calculated very precisely.

A magnetic distance sensor based on this principle was described in (Zikmund & Ripka, 2012). The source of the magnetic field was a solenoid triplet in the configuration according to Figure 39. A 1D case was created to check the theoretical assumption that the solenoid can be mathematically replaced by a dipole description. One source and also the sensor were positioned perfectly axially, the sensor was moved axially by a defined distance, and the magnetic field was measured using the procedure described here of current pulses of both polarities.

The measured values (Figure 40) fit with the theoretical curve $B \sim 1/r^3$ for the ideal dipole source. Deviation from this rule is expected in the small distance where the size of the source coil cannot be neglected. For long distances the signal is very weak in comparison with the noise. By fitting, we can approximate the magnetic field of this coil and the error is spread in the whole range (see Figure 41).

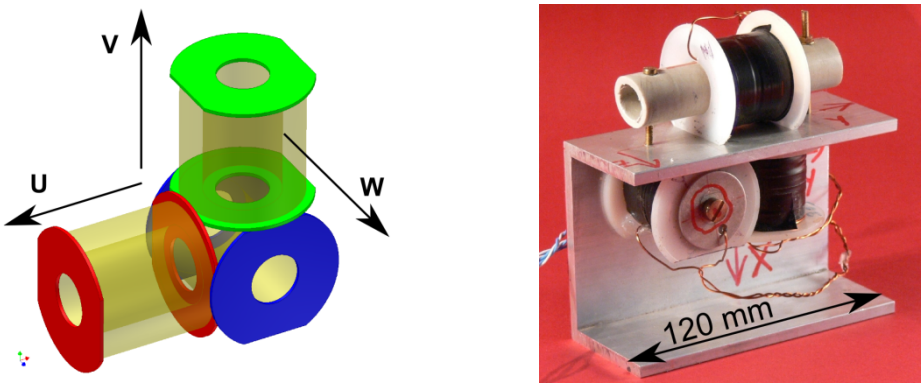

a) b)

Figure 39. *Configuration of the coil triplet from magnetic distance sensor.*

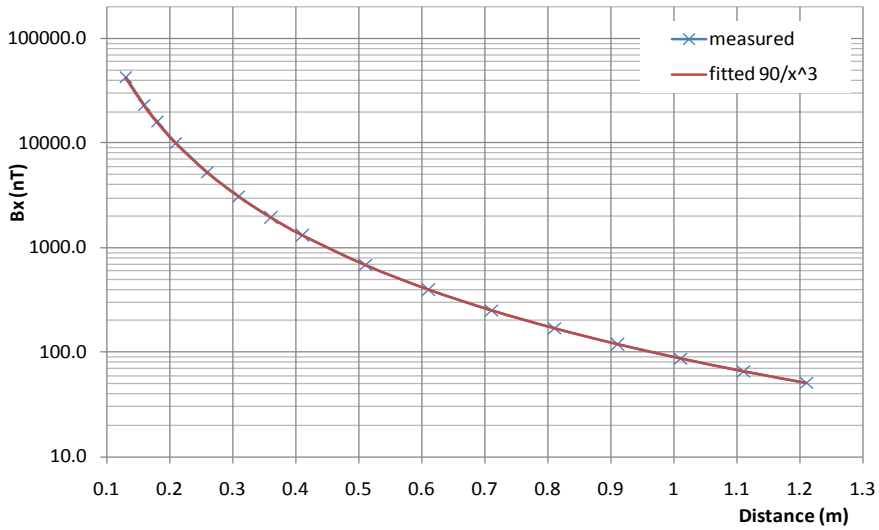

Figure 40. *The magnetic field in the 1st Gauss position.*

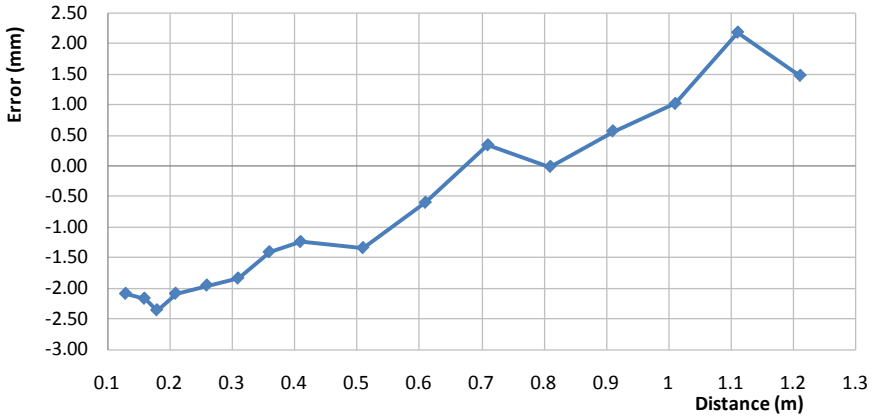

Figure 41. *The errors of the estimated distance.*

All measurements are influenced by ambient noise, because measurements are made in a magnetically noisy environment, unless very elaborate measures are taken. The main noise sources were from the external environment (mainly the movement of ferromagnetic objects and electric currents from trams). In our case, the magnetic field was measured by a tri-axial fluxgate magnetometer the own noise of which was in the range of 10 pT/√Hz@1Hz, which was negligible in comparison with the environmental noise. Figure 42 shows a typical record of the magnetic field captured during the measurement procedures.

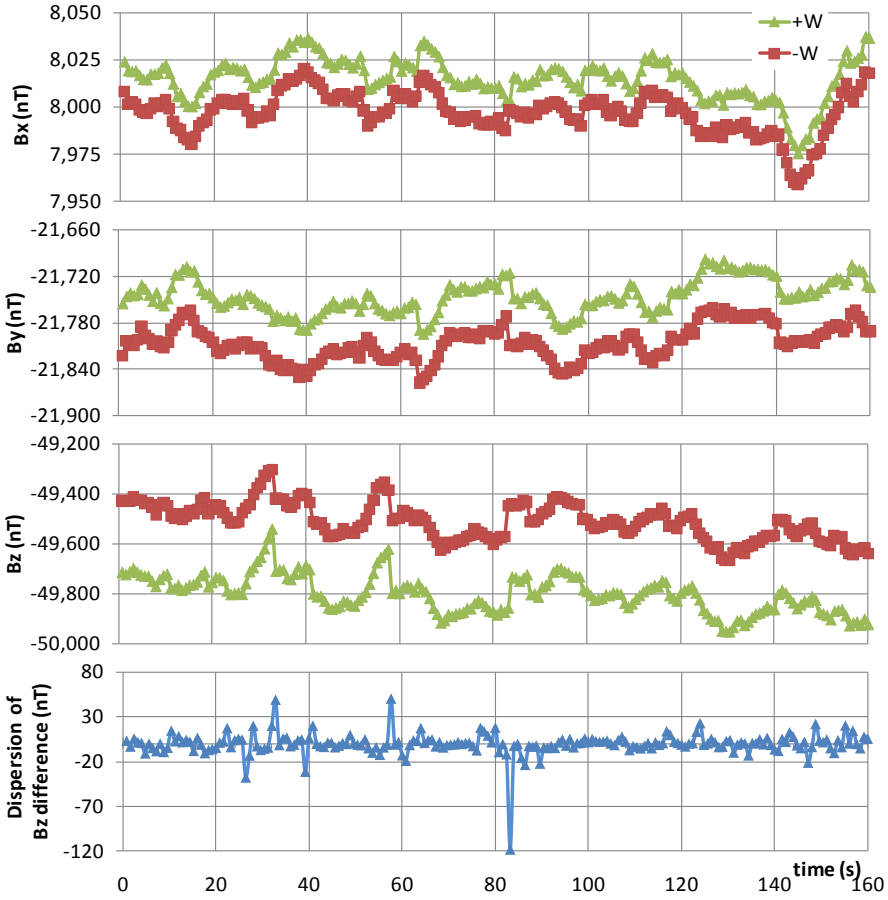

Figure 42. *The magnetic field while W coil is being excited, the dispersion in the Z axis.*

The magnetic variations are observable (mainly in the Z axis). The RMS noise of the external field was about 64, 98 and 345 nT in the X, Y and Z directions, respectively. Due to this, we used a long measurement lasting about 3 minutes, which contained 200 data items per coil source. The switching device was developed to achieve quick switching of the polarities and also of the coils. In this way, the noise was reduced to 1.5, 4.3 and 12.8 nT (X, Y and Z axis). The uncertainty can be further reduced below 1 nT by longer averaging.

The tests were carried out in a distance of 0.5 m, when the sensor head was rotated in the horizontal plane (azimuth angle). The magnetometer was permanently fixed in a stable position and the magnetic source placed on a theodolite was also rotated in the azimuth direction.

Each 1/8 radian, the magnetic field excited by all three coils was measured and average values were calculated from the 200 samples. These average values are

shown in Figures 43, 44 and 45 for each coil. The sinus wave is supposed to be in all magnetic field components during the rotate procedure.

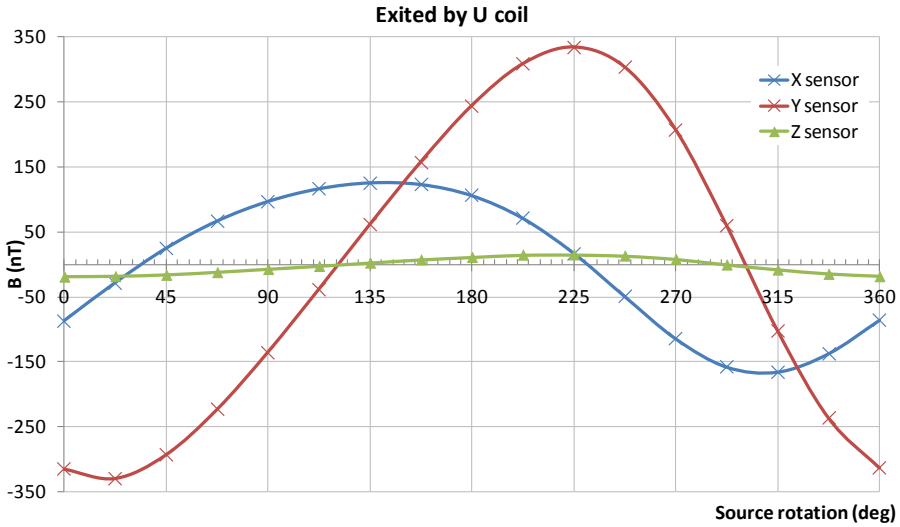

Figure 43. *The magnetic field during changing azimuth - coil U.*

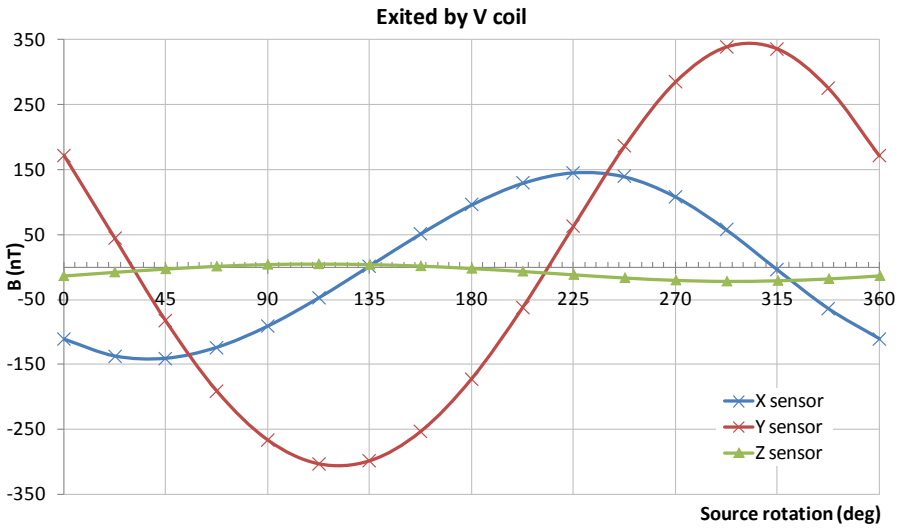

Figure 44. *The magnetic field during changing azimuth - coil V.*

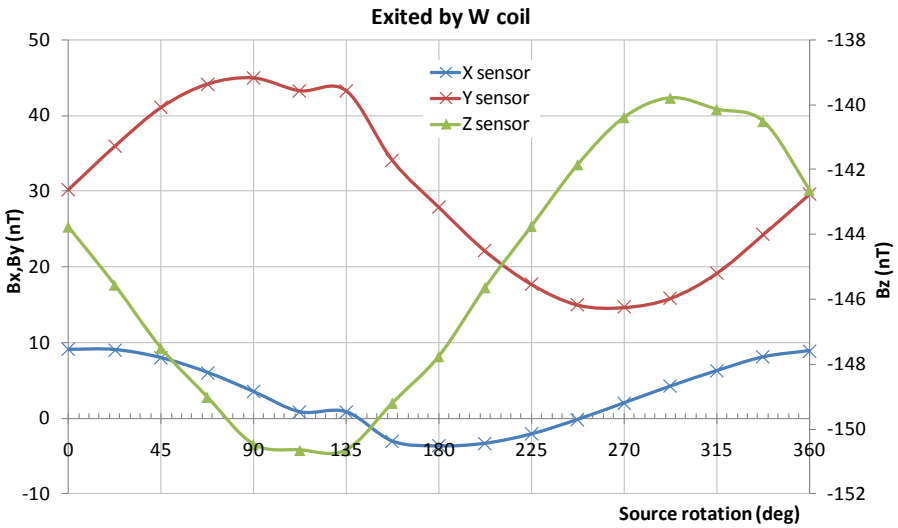

Figure 45. *The magnetic field during changing azimuth - coli W.*

The non-orthogonality of both source coils and magnetic sensors can be calculated from similar data because the shape of the wave should be a sine wave during rotation. There are other errors that should be considered before applying the calculation algorithm:

- differences between coil dipole moments and sensor sensitivities
- angular deviations of both triplets from orthogonality
- the triplets are not located in a single point
- the rotation axis is not exactly in the center of all sensors
- the center of magnetic sensor's triplet is not a one point
- the sensor is not small – it does not measure the magnetic field at a point.

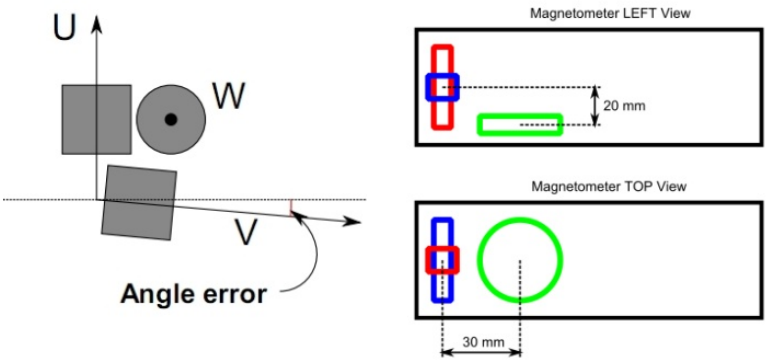

Figure 46. *Imperfection of a tri-axial magnetic sensor caused by the mechanical arrangement.*

The sensor offsets and their temperature drifts, normally the most severe problem with magnetic sensors, are suppressed by commuting of the source coil currents. The most significant source of error is therefore the fact that the individual coil centers are not located in the same point.

This imperfection can be mathematically corrected using the principle described in (Zikmund & Ripka, 2013), the parameters of construction errors are known and are included into the model, and the calculated distance error is reduced. The results of this procedure are shown in Figure 47 for a rotating field of the source.

The error caused by an off-axis center point of the magnetic sensor cannot be effectively suppressed in short distances because the source has a huge gradient. The third axis (shown in green in Figure 46) is therefore subjected to a much smaller magnetic field than the other two axes.

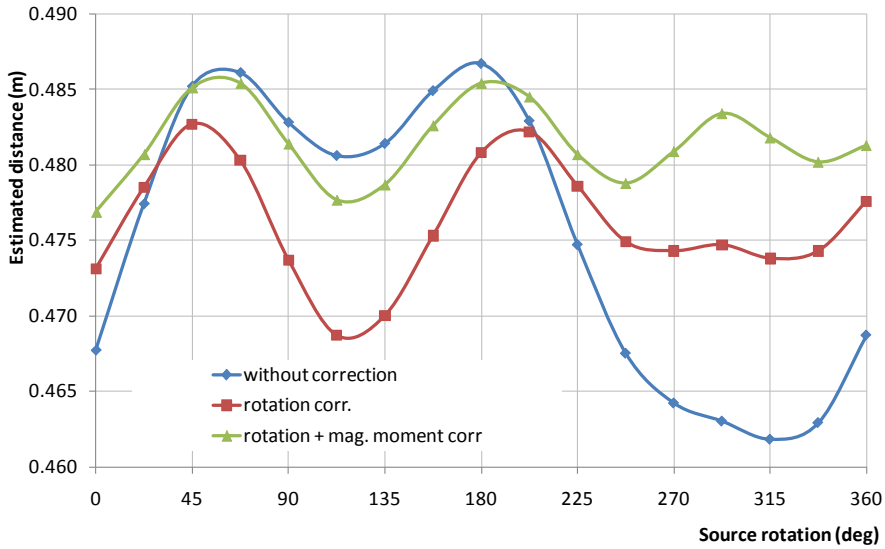

Figure 47. *Estimated distance with/without correction*

5.3 Magnetic tracker – hybrid system

In order to design the magnetic tracker, it is necessary to obtain additional information decreases the complexity of the problem. The rotational angles, which deteriorate the position estimation, can be measured with a gyro and a tri-axial accelerometer as an inertial measurement unit (IMU). Then the equations modeling the problem will have the form of equation 42 with only three unknown variables α, β and r.

$$M = T_\beta' T_\alpha' \frac{m}{2\pi r^3} \begin{bmatrix} 1 & 0 & 0 \\ 0 & -1/2 & 0 \\ 0 & 0 & -1/2 \end{bmatrix} T_\alpha T_\beta f_0 \qquad (42)$$

In this way, a hybrid tracker is created. The spatial position is established from the magnetic measurement and from the output IMU. Each part of this magnetic tracker therefore includes one IMU and the mutual rotational angle is calculated as their difference from the angles in the reference frame. This means (according to Figure 48)

$$\begin{bmatrix} yaw \\ pitch \\ roll \end{bmatrix} - \begin{bmatrix} yaw' \\ pitch' \\ roll' \end{bmatrix}$$

If this case is supposed, the model becomes not multimodal but unimodal in the meaning of the results. Since the mathematical expression has only three unknown parameters, the three-coil perpendicular setup can be reduced to only one coil generating the magnetic field. One coil supplemented by one IMU on one side and a magnetometer also supplemented by the inertial measurement unit on the other side form a hybrid magnetic tracker. Figure 48 presents a sketch of the system.

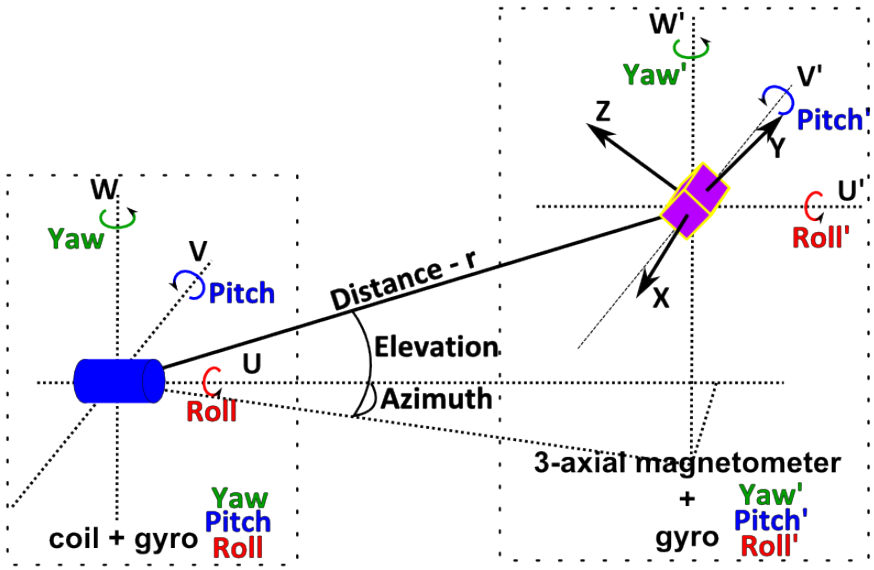

Figure 48. *Hybrid system – sketch of situation.*

Inertial measurement unit (IMU)

The IMU is related to the Earth's reference system. The north-south direction specifies a rotational axis for the roll angle (yaw), the east-west axis specifies the elevation angle (pitch) and vertical axis specifies the azimuth orientation (yaw).

The main impact on the resulting positions comes from the accuracy of the angle measurement, especially, over long distances. This is discussed in a later section, which focuses on the accuracy of the hybrid magnetic tracker.

The three angles have to be established from the gravity force and the angular speed of the Earth, because GPS and similar systems cannot be used in some applications, e.g. in horizontal drilling.

A fiber optical gyroscope which exploits the Sagnac effect is a very precise type of gyro. It can achieve precision of ±0.01 degree and it also suppresses some weak points of mechanical gyros.

Accelerometers measure the roll angle of IMU. MEMS accelerometers with electrostatic compensation form a very large group of accelerometers. MEMS accelerometers are manufactured on a silicon chip as individual electronic components that can be placed on the printed circuit board as a part of another electronic device. These accelerometers do not achieve the precision of a fiber optical gyroscope, but when they are properly calibrated they can achive near to 0.1 degree accuracy.

Coil – the source of the magnetic field

In our model, the magnetic field is assumed to be an ideal magnetic dipole, but it would be impossible to manufacture a coil generating this theoretical magnetic field. It can be shown that the ratio of coil dimensions (the coil radius/ the coil length) is around 0.67 provides the coil field that is closest to the ideal field of the dipole.

However, there are many effects conflicting with each other. Generally, the largest magnetic moment of the coil has to be designed to be able to measure over long distances. This requires a huge number of turns, a huge current or a coil cross-section according to equation 35. This means that the design of a coil for a magnetic tracker has to be optimized according to the following equation.

$$R = \rho \frac{l}{A_w} \ (\Omega) \tag{43}$$

$$I = \frac{U}{R} \ (\mathrm{A}) \tag{44}$$

$$l = 2N\pi r \text{ (m)} \quad (45)$$

$$A = \pi r^2 \quad (46)$$

The design of the coil is usually a compromise between possible size and power.

Symmetry problem

Even if the coil magnetic field is similar to the ideal magnetic dipole, the form of the symmetry is a problem. The magnetic field is centered symmetrically. This means that an arbitrary point has a symmetrical point on the opposite side of the coil (green vectors in Figure 49). During the calculation, we are therefore not able to distinguish which point is the right one Moreover, in a special case of the symmetry, if a point lies in the 2nd Gauss position (see the red arrow in Figure 49), the same magnetic vectors are on the circle surrounding the coil. We cannot say anything about the position in this case since the magnetic tracker problem theoretically has an infinite number of solutions. We therefore have to apply a more complex method to recognize the position.

The 1st Gauss position is also a specific case of the coil magnetic field, but it behaves like an arbitrary point. There are therefore only two possible solutions.

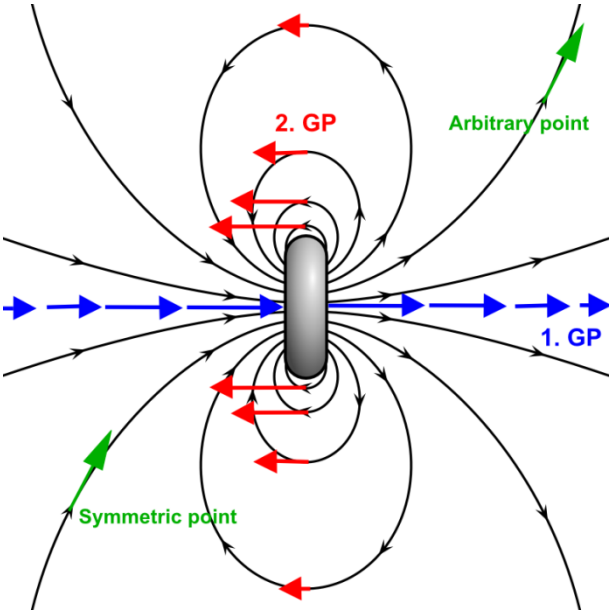

Figure 49. *Symmetry of the dipole magnetic field: green – centered symmetry: red – 2nd Gauss position and blue – 1st Gauss position.*

A calculation algorithm based on a numerical method can converge to a result that is opposite to the real position due to the symmetry. This situation affects changes to the sign of the position coordinates (for example point x=2, y=-3, z=0 is found as point x=-2, y=3, z=0). If the real position is close to the 2nd Gauss position the problem is more complicated, and the algorithm correctly calculates only the absolute distance r from the center. The Gauss positions can be detected from the values of the magnetic field, because in these positions the only one axis of magnetometer measures a signal.

The symmetry can be avoided by a simple trick. If we know the mutual orientation (the rotational angles) and the measurement is taken in two points

- by a coil or magnetometer movement of a known distance,
- by measurements with two magnetometers or two coils which are shifted by a known distance,

we can consider a possible solution and decide which is the real searched position. The known mutual distance, together with the rotational angles, defines the opposite point.

Let us assume the situation depicted in Figure 50. Magnetometer 1 (green cross) is placed in the real position. Since the rotation angle is known (in this case it is 0 degrees) and the magnetometer is placed at a distance of 1 meter it is clear that magnetometer 1 has to be closer to the coil than magnetometer 2, otherwise the mutual angle will not correspond with the measurement.

Practically, the principle works as follows. The magnetometers arrive at the real position that we want to measure. The measurement of the magnetic tracker is carried out and we get two possible solutions. Looking at the IMU, we obtain the mutual angle (e.g. 0 degrees) and we decide which is the right position on the basis of the mutual orientation of the magnetometer. With this arrangement (two magnetometers and two coils) we are able to avoid the second Gauss position, because in all possible instants, one of two magnetometers will be out of the specific situation.

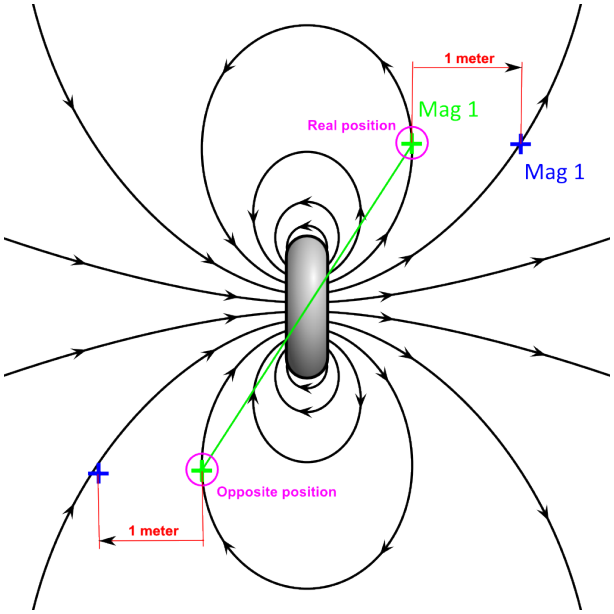

Figure 50. *Solution of the symmetry problem of the magnetic dipole field.*

Excitation sequence:

The excitation principle is the same as for the fully-magnetic tracker. The coils are fed with the square-wave current where both polarities of the pulse are applied to remove the Earth's field. The switching frequency of 3 Hz is chosen to avoid eddy currents.

Error analysis of the calculation

During measurements with the hybrid magnetic tracker, the results are loaded with many influences:

- angular error – caused by IMU uncertainty
- ambient magnetic field noise – caused by environmental disturbances of the magnetic field.

The calculated position therefore does not correspond with the real coordinates of the measured point.

Magnetic noise is present mainly in the vicinity of cities. It is created by moving ferromagnetic objects, or by electromagnetic interference from electric power networks.

The main influence on the error has the strength of the magnetic field excited by the coil (the signal-noise ratio). If the coil is designed to be strong enough to excite an appropriate magnetic field that is huge in relation to the noise, the error caused by

the noise will not have a major impact. In long distance measurements, in particular, the coil should be optimized according the noise in order to achieve the desired accuracy of the whole system.

A preliminary simulation was carried out for an ideal coil with a magnetic moment of 300 Am^2 to check the precision of the designed magnetic tracker with respect to influence of the noise. Figure 51 shows the influence of the ambient magnetic noise on the precision of the output. Magnetic noise manifests itself significantly when the signal from the coil is relatively low in comparison with the noise level B_n.

The angular error influences the calculated position linearly within the whole range, as is depicted in Figure 52.

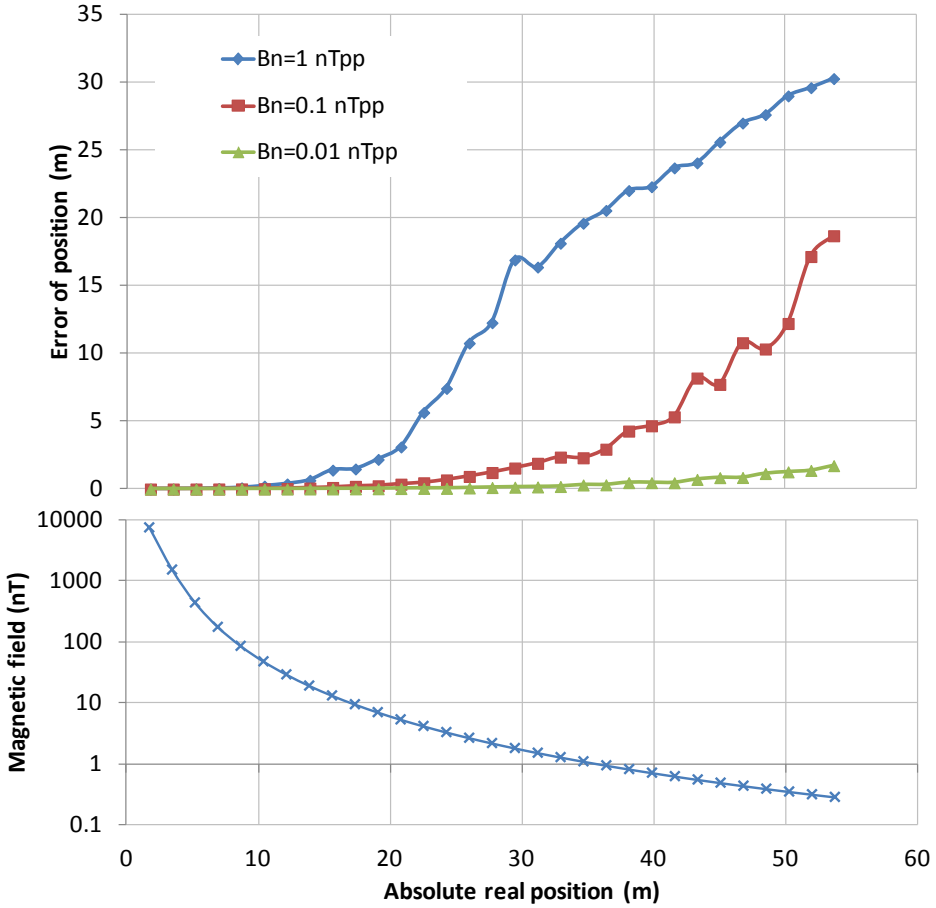

Figure 51. *Absolute error of position caused by magnetic field noise (The coil has a magnetic moment of 300 Am^2).*

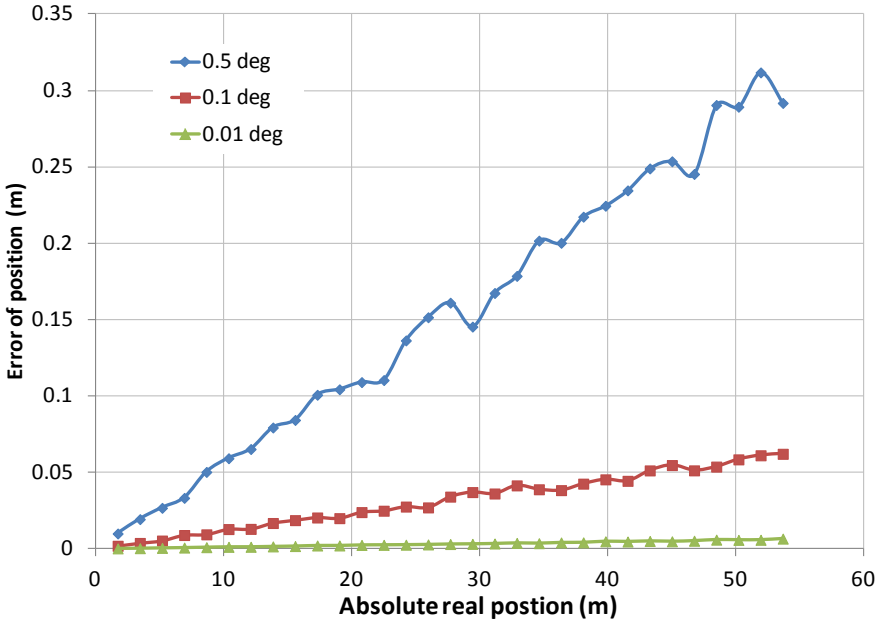

Figure 52. *Absolute error of position caused by an error of the rotational angles (The coil has a magnetic moment of 300 Am^2).*

5.4 Magnetic tracker for horizontal directional drilling (HDD) – system design

As was mentioned in the introduction to this chapter, horizontal drilling is an application area for the hybrid magnetic tracker. First, the direction of the drill head is calculated from the IMU placed in front of the drill setup. When it is necessary to drill from two sides, the magnetic tracker can find a mutual position of approaching drill heads.

The principle of navigation without a magnetic tracker is based on processing IMU data. The total length of the drilling pipe is known, as are the spatial angles. If the change in the length, while the pipe is being pushed into the ground, is integrated with respect to the known angles, the position of the drill heads is known at all times. Due to the limited accuracy of IMU, the error of the position increases with the drill length. Hitting the goal point is affected by the error, and the greater the total length, the more difficult it is to hit the target.

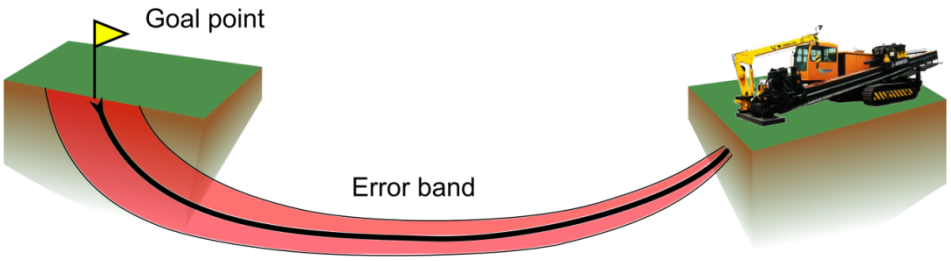

Figure 53. *Error band of positional horizontal drilling based on IMU.*

In some cases, it is very important to keep the goal point, and drilling from two sides is preferred even if this configuration increases the costs and the demands on the operator. An advantage of a two-side drilling setup is that there are decreased requirements on the drill during long jobs (up to 3 km). This is because the drill chain is enormously exposed to mechanical torque, which is lower for small distances. As was explained above, navigation is needed in order to hit both drill heads underground.

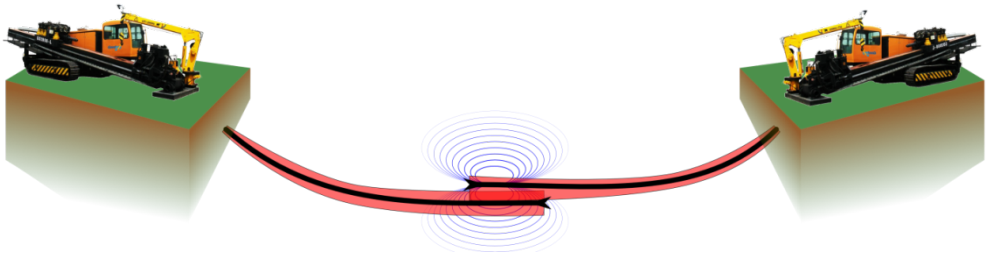

Figure 54. *Two-side positional horizontal drilling – error bands.*

The typical space where the two drill heads should approach each other is defined as a cube with an edge of five meters, which is established from the uncertainty of positional determination due to the IMU error. This is an important point in the design of a coil, because sufficient magnetic field strength has to be guaranteed in the maximum range of the possible space.

One solution to the HDD intersection problem is described in (Liu & Wang, 2011). The solution involves utilizing a permanent magnet as a magnetic field source that is fixed in the tube on the drill side. The opposite side of the drill consists of a tri-axial magnetometer and tri-axial accelerometers, which are able to determine the orientation. The magnetometer (opposite to the magnet) measures not only the Earth's magnetic field but also the response of the permanent magnet. Since the permanent magnet has a static magnetic field, the responses cannot be distinguished easily from the Earth's field. The method therefore exploits the mutual movement of

the drill pipes. The profile of the magnetic field is measured and the position is established with respect to the shape and strength of the signal.

The position is calculated according to the known magnetic properties of the magnet and the fitting principle is used.

Magnetized soils or rocks of any kind can distort the magnetic field, and this can depreciate the method. In addition, the method takes a long time for the measurements, for fitting and for analyzing the results. The Magnetic Ranging System, introduced in the previous chapter, is a more advantageous method (Vcelak, et al., 2012).

Power and communication

When the IMU system is used, power and communication are provided via a single wire (a powerline) and the communication signal is modulated at the power voltage. The negative pole of the power is an outer pipe, and the positive pole is led by a wire. The power supply voltage is 48 V, but losses on a long wire cause a drop in the output voltage. The units therefore also contain a battery pack, which allows work to proceed even if the power voltage is not optimal.

The power supply is also a limiting factor in the design of a magnetic tracker when the coil is to be excited with the maximum current.

Mechanical construction of the chain

During horizontal drilling, a bentonite mad is used as an abrasive mad that is pumped under huge pressure from the ground station to the head, where it is gushed to the rock and thus a new hole is scoured. This means that the mechanical construction should be adapted to this principle. There are three different types of pipes which:

1. carry torques and mad
2. carry torques, mad and IMU or a magnetic tracker, respectively
3. have a drill head that carries only the torque, and a mad flows inside.

The second pipe type is specially modified to be able to contain the electronic unit and batteries. It consists of two axially centered pipes. The outer pipe carries the torque and the inner pipe covers the electronic unit and other parts of the navigation system against the mad, which is pressurized in the space between these pipes.

The inner pipe has a defined diameter, which restricts the design of the magnetic tracker, mainly the coil.

Table 27. Types of pipes in the drilling chain.

Pipe type	1.	2.	3.
Outer diameter (mm)	100	120	180
Inner diameter (mm)	60	110	160
Material	C45	30CrNiMo4	30CrNiMo4
Relative permeability	1500	1000	1000

Each outer pipe has to be resistant to high torque, and high-quality materials are therefore used. The usual materials for these pipes are shown in Table 27Table 27. Most of them are magnetic, and they can influence the magnetic field. This fact is taken in account in the design of the final magnetic tracker.

Magnetic or even ferromagnetic parts can distort the magnetic field excited from the coil, and therefore they affect the result. Additionally, the pipes that are in front of the magnetic tracker and behind it concentrate the Earth's magnetic field, which can lead to over-range of the magnetometers. Finally, these parts cause a stronger response from the excitation coil, especially in the axial direction.

All these phenomena of the magnetic parts can distort the magnetic field generated by the coil. They can reduce the precision of the system due to the non-dipole shape of the field.

A simulation of this situation was made and the results were included in the mechanical design, mainly in the magnetometer unit.

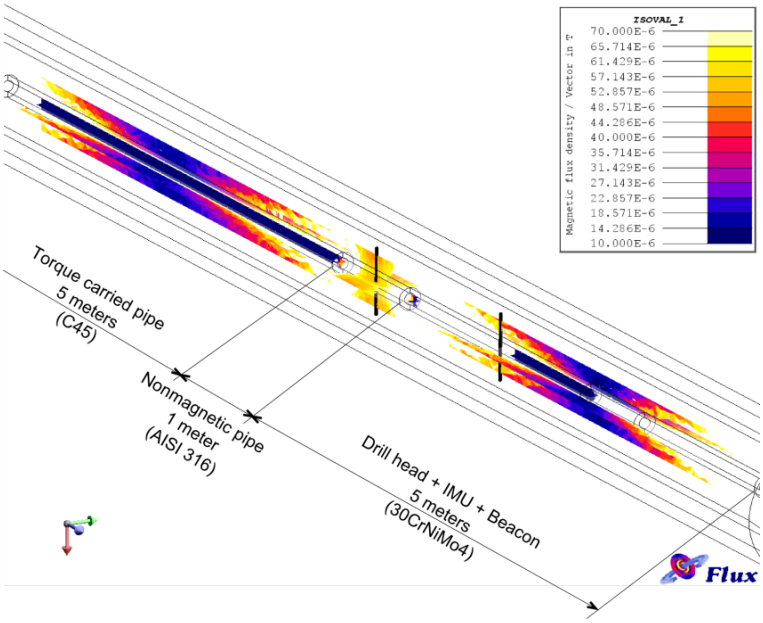

Figure 55. *Distortion of the Earth's magnetic field (axially) caused by the magnetic part of the drill chain.*

According to the simulation the pipes in front of and behind the magnetic tracker concentrate the magnetic field. If the Earth's field is oriented axially to the pipes, the magnetic field in the space, where the magnetometer unit should be, can over-range the magnetometers.

The magnetic tracker space has to be manufactured with a nonmagnetic material which also has to be resistant against the huge drilling torque. AISI316 alloy meets these conditions. Its permeability, provided by the manufacturer, is 1.1.

The simulations (see the example in Figure 55) indicate the minimum length of the nonmagnetic pipe which decreases the effect of magnetic pipes. For the simulation model, corresponding to the real situation, each magnetometer should be placed at least 350 mm from the magnetic part.

Even if the air gap is kept according to the simulation, the parameters of the pipes (mainly their permeability) can change during a drill job. It is a complex problem to estimate the permeability of magnetic alloys, so the mechanical part also contains a compensation coil around each magnetometer. The coil is oriented axially to the magnetometer, because the influence is mainly in the axial direction. If the magnetometer is overloaded the internal unit will react, and the magnetic field will be compensated by a coil current.

The conducting pipes distort the coil magnetic field through eddy current phenomena. This effect is suppressed by having a sufficient duration of the current pulses to let the eddy current decay before the measurement time.

The influences of the pipes were investigated during real measurement tests.

Magnetic tracker units

As has been mentioned above, each side of a drill job has a different type of unit. One side operates with a coil unit, and the opposite side measures with the magnetometer unit. The units have to be modified to fit inside the inner space of the pipe. PCBs have a shape that corresponds to this requirement. To keep to the original principle of the navigation system, the units of the magnetic tracker that is behind IMU also have to be able to share the powerline and so be able to work autonomously. Since the IMU also contains the batteries, powerline is mutually shared.

Both units contain the communication chip which transfers data (commands) up- or down-hole, but other parts differ.

Coil unit

The coil unit is connected to the powerline bus and continuously reads the data sent from the up-hole superior system. The up-hole system normally communicates with the IMU unit, which is in front of the coil unit and the coil unit is in the stand-by regime.

When the coil unit receives a special command from the up-hole unit to switch itself on, the GST (gyro steering tools, i.e., in fact the IMU) is disabled and the coil unit is fully connected to operate. This prevents the two units (IMU and the coil) transmitting at the same time and a collision occurring on the bus.

When the coil unit is fully controlled, it can excite the coils or charge the batteries. The control processor monitors the battery status, and if the battery level is below minimum, it is recharged for use as a source for excitation. The battery packs are manufactured as two custom batteries with nominal voltage of 22.8 V and a capacity of 3.2 Ah.

Since the powerline voltage is around 48 V, but can vary down to 30 V (depending on the length of the cable) it is necessary to separate the two packs during charging. This is arranged with a MOSFET switch, which also connects the batteries into series when the coil is to be excited.

The command for the excitation comes from the uphole unit. Currents injected into both coils are controlled by pulse width modulation in order to be able to change the amplitude of the currents. The electronic system of the coil unit is depicted in Figure 56.

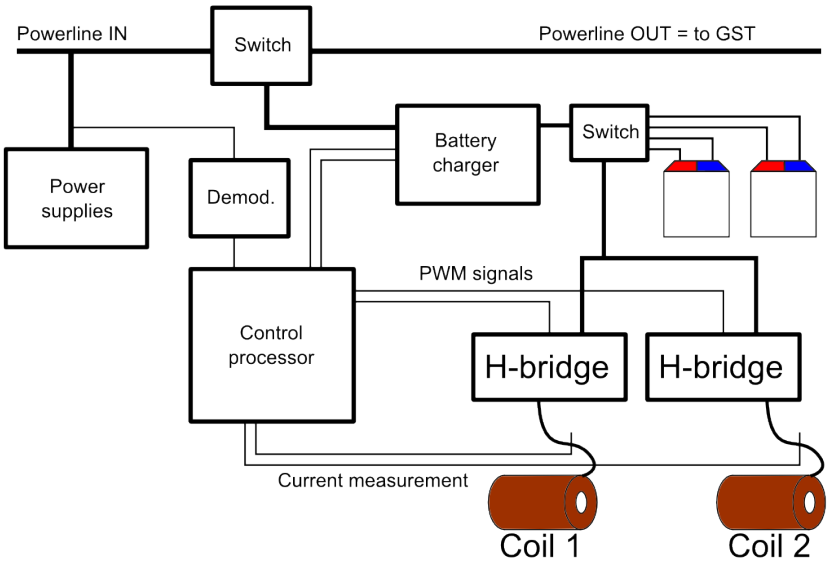

Figure 56. *Block diagram of the coil unit's electronics.*

The whole unit should be resistant against any vibrations created during drilling jobs. The electronics boards are designed with no relay and SMD components to prevent components breaking away from the board. High capacitance capacitors even need to be fixed with a sealant.

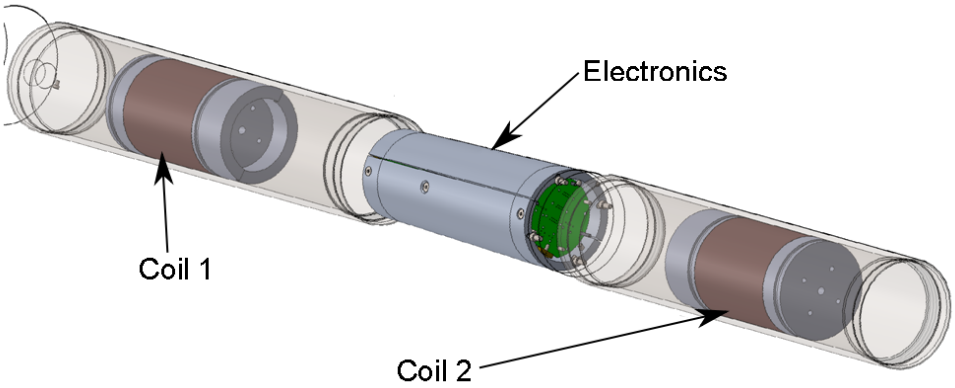

Figure 57. *Sketch of the coil unit without the outer pipes.*

With the development of the whole system, the coils were designed as two axial coils at a distance of around one meter apart. These coils were optimized for the maximum moment.

Table 28. HDD excitation coil parameters.

	Coil 1 and Coil 2
Turns	1007
Magnetic moment (per 1 A)	8.5 m^2
Maximum current	16 A
Resistance	3.1 Ohm
Approximate inductance	46mH
Magnetic field in 5 m (at ±10 A)	272 nT peak-peak
Magnetic field in 10 m (at ±10 A)	34 nT peak-peak

Magnetometer unit

On the opposite side of the drill job, there is a magnetometer unit at the end of the drill head. It communicates with the up-hole system in the same way as the coil unit. The principle of the switched powerline is also retained. However, this unit does not contain the batteries, because its power consumption is fully covered by the powerline energy.

The unit is equipped with two magnetometers axially placed in the tube according to Figure 58.

The output of each tri-axial magnetometer is sampled with a 24-bit analog-digital converter, and the data are transferred to the control processor via SPI. The sample rate is 5 ms, a value derived from potential of ADC and the whole processing system. Since six channels are sampled simultaneously, the processing system has high requirements on speed and memory space in order to record all necessary measurement data.

The unit also has a facility to compensate the axial magnetic field by controlling the current to the compensating coils if it detects any overranging of the magnetometers. A schematic diagram is presented in Figure 59.

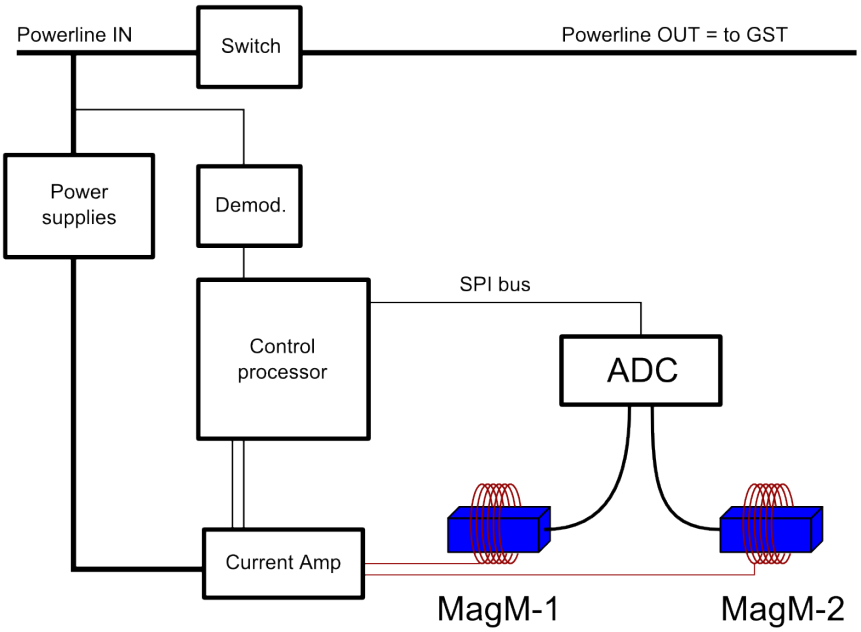

Figure 58. *Block diagram of the magnetometer unit's electronic.*

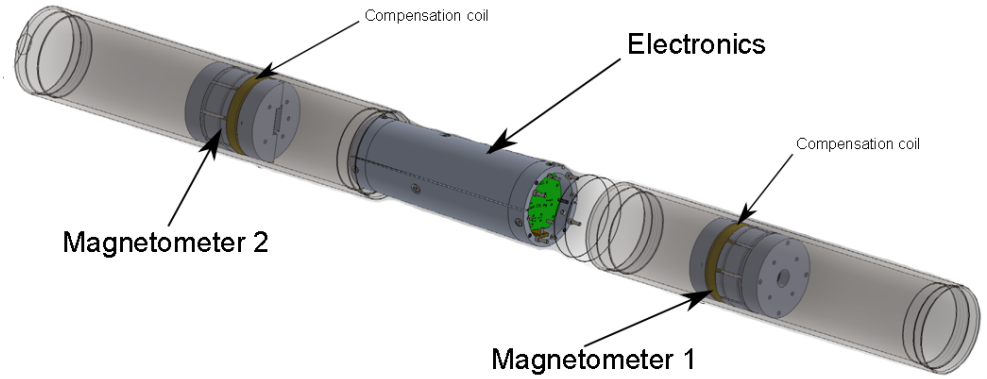

Figure 59. *Sketch of the magnetometer unit without the outer pipes.*

Excitation sequence

The power stored in the batteries is limited, so the length of the current sequence has to be modified to be able to excite at least ten times before needing to be recharged.

To avoid the eddy currents that can occur in underground rocks, sand or conducting structures (pipes), the rate of current changes should be as small as possible. In fact, the unit switches current flowing into the coil with the maximum speed, and then it waits for time when the current is settled. Thus the eddy currents are fade away at that time, and the measured magnetic field unit is only to the Earth's field and the coil field.

Bipolar excitation is used to subtract the Earth's magnetic field. The switch frequency is 1 Hz. This means 500 ms for positive pulse and 500 ms for the negative pulse. This is repeated at least five times to get enough measured data for averaging. Usually, the first coil is excited, and consequently the second one is excited. The excitation sequence is presented in Figure 60.

Synchronization

Synchronization of the two units is critical for the measurements. As stated above, the units work autonomously. They can only communicate and be controlled by the up-hole unit via a powerline bus. To obtain as many samples in the steady part of the pulse as possible, the synchronization should be within a time error of 20 ms. This is impossible using a powerline communication line, because the powerline bus response is very slow, or is even undetermined. The propagation time of the command from the uphole unit toward to the coil or magnetometer unit cannot be determined

due to the communication principle. The synchronization procedure is therefore based on a magnetic principle.

The procedure supposes that both units are oriented inversely, which is typically the case during a drilling job. The closest distance is between coil 1 and magnetometer 2 (the orientation is depicted in Figure 61). The magnetometers will therefore have the highest response when coil 1 is excited. In addition, the magnetic sync pulse signal is generated from the maximum current to catch the pattern even in long distances.

During synchronization, the magnetometer unit measures the magnetic field with both magnetometers and the unit periodically evaluates the magnetic data and seeks a well-defined synchronization pattern. When the pattern is recognized, it serves as a trigger signal to match the clock of the magnetometer unit according to the coil unit. The trigger signal should be detected by at least four of the six axes. This eliminates random triggering caused by noise. If the signal satisfies the condition of the trigger pulse, the magnetometer unit adapts its own clock.

After a short delay behind the trigger, the coil unit excites a regular signal sequence from which the magnetic field of the coil is measured. The order is always the same: a specific number of positive and negative pulses at coil 1 and then at coil 2.

The currents flowing in the coils are sampled, and also the magnetic field at the same time. Since the signal has a long settle time, there is a dead band when the signals are ignored. The whole measurement process is shown in Figure 60.

A weakness of the synchronization principle is that, it is very difficult to set the threshold for the triggering level in the huge magnetic field range that has to be detected. If the level is not high enough to detect weak signals properly, accident triggering of the system tends to occur.

The synchronization procedure was improved by using the correlation principle. The magnetometer unit samples the magnetic field and this signal is correlated with a known signal corresponding to the coil excitation. With this technique, the system is able to trigger a signal that is within the level of the noise.

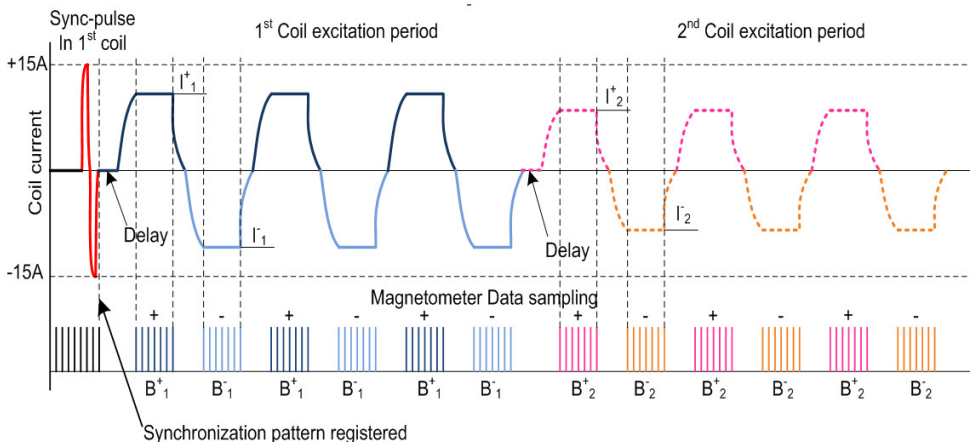

Figure 60. *The synchronization pattern and the excitation sequence.*

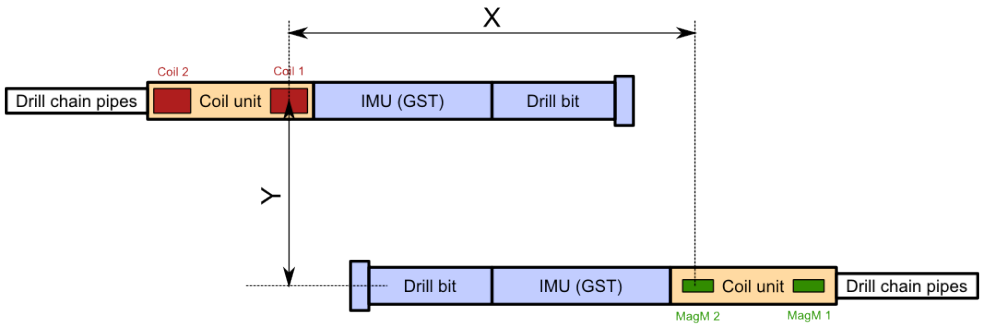

Figure 61. *Approaching drill chain – arrangement.*

Symmetry problem – horizontal directional drilling

The system is arranged as two excitation coils and two magnetometers. This provides an opportunity to solve to the symmetry problem. Figure 62 shows a typical case. The cross-results calculated from the measured data have to match to one point with respect to one coil. If the points are split, the algorithm approaches the opposite point. It is then very simple to distinguish the true value, and the software classifies itself.

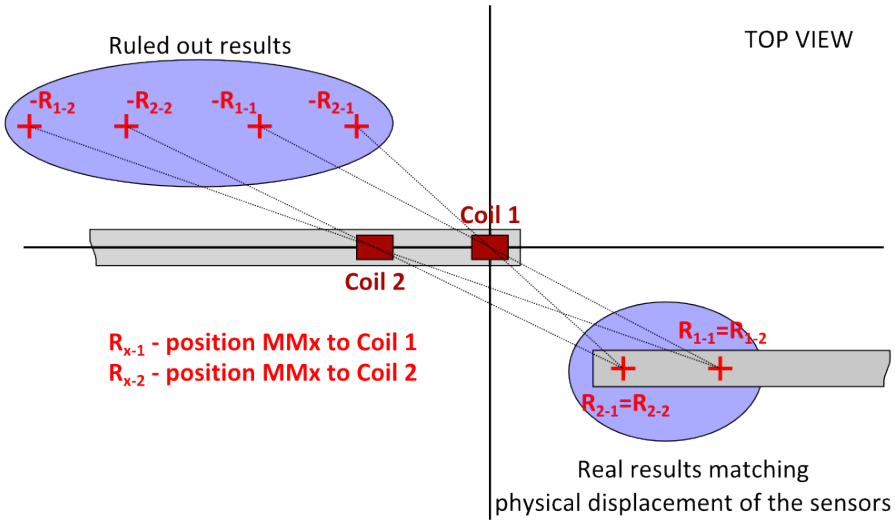

Figure 62. *Rule out the symmetry problem.*

Measurement procedure:

The procedure has to be split into two parallel tasks:

- a task for the magnetometer unit
- a further task for the coil unit.

In standard mode, the magnetometer unit measures the magnetic field in the slow mode, and periodically checks that the magnetometers are not overloaded. The spatial rotations are also measured. On the opposite side, the coil unit measures only the spatial rotation and checks whether the batteries are charged.

Then the operators stop drilling (when they think that the two sides are near to detecting each other) and they want to measure the mutual position. The process follows a number of steps:

1. Both operators agree to start the measurements and stop drilling.
2. The magnetometer unit is switched to attention mode (waiting for a trigger signal).
3. The coil unit is started, thus exciting the current sequence.
4. Detecting signal
    a. If the trigger signal is detected, the measured data are processed.
    b. If the trigger is not recognized, the timeout will report an error.
5. The computer collects all data
    a. Rotation angles of both units
    b. Excitation current

c. Magnetic field measured during excitation

6. The computer calculates the mutual position.
7. The measurements are repeated at least three times to ensure precision.

Precision of the hybrid magnetic tracker

After the whole system had been calibrated - which has to be done before each use - the system was tested in the factory environment (Vcelak, et al., 2013). Pictures from the tests are shown in Figure 63.

The coil unit was placed in a stable position, and the crane lifted the magnetometer unit. The magnetometer unit was positioned on known spatial points. The designed system was used to measure the positions in each point. As is shown in Figure 64, the error grows up with the distance. The error is below 1 meter if the real distances are up to 8 meters, because the signal is relatively high in comparison with the noise level. During the test, the noise level was below 0.1 nT in a time interval of 10 seconds. In long distances, about 15 meters, the signal is units of nT, and so the results are strongly influenced. The precision of the calculation of the rotation angle also has a fundamental impact.

Errors are caused by:

- the influence of ferromagnetic pipes
- synchronization jitter
- error in determining the rotation angles
- the influence of the ferromagnetic environment
- the influence of magnetic noise

Figure 63. *Factory testing of the hybrid magnetic tracker.*

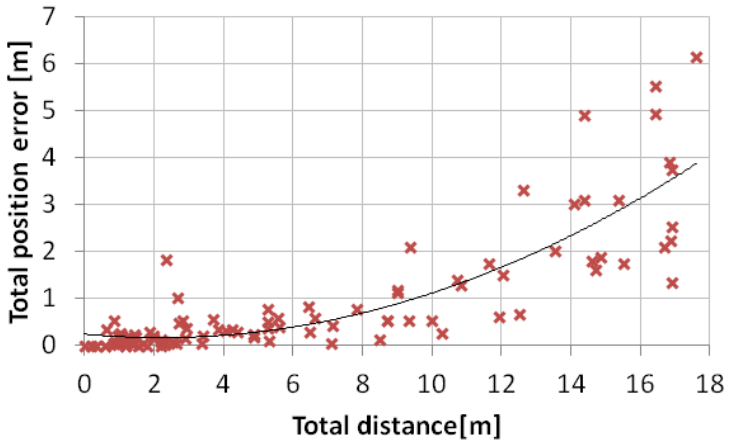

Figure 64. *The error of the hybrid magnetic navigation obtained during tests.*

The tests discovered potential errors made in the software or firmware. When the hybrid magnetic tracker was rebuilt in an additional upgrade, the some errors were found.

The main problem was the delay of the analog-digital (AD) converters used for the magnetometer measurements. They have a time delay due to the use of sigma-delta AD converters because the digital filter is at the output of the convertor. The original firmware continuously sampled the signal. When it found the edge, it waited for the specific AD conversion time to catch a further signal edge, but the edge was already buffered in the ADC. In this situation, continuous sampling, the AD delay has to be ignored. This is why we did not measure the magnetic field correctly.

We also discovered a huge error due to the presence of metal parts in the floor of the building in which we tested the magnetic tracker

We obtained better results when we corrected the errors, and moved the whole measurement setup out of the building for the final test. The magnetic tracker achieved precision of 0.4 meters in range 10 m. The error distribution is shown in Figure 65.

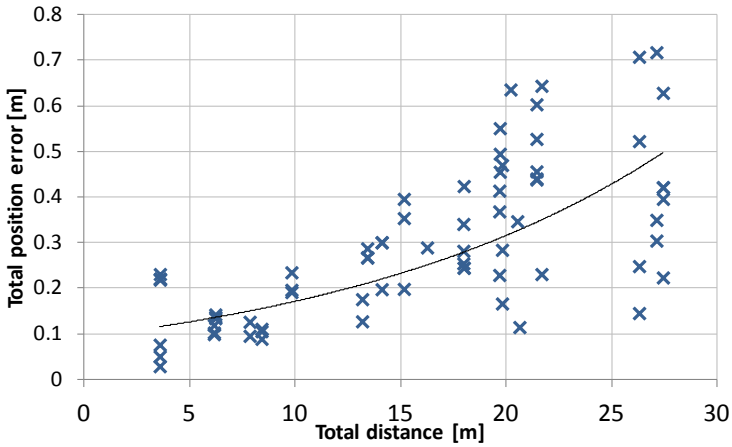

Figure 65. *The error of hybrid magnetic navigation – after improving the SW.*

6 Conclusions

6.1 Scalar calibration of the coil system

The scalar calibration principle that I have developed and described in this thesis significantly simplifies coil system calibration due to the use of a non-linear optimization method. Since the method uses the very precise Overhauser magnetometer and current measurements, it is affected only by two sources of uncertainty. Unlike the traditional method, it is not affected by the systematic error of cancelling the Earth's field.

The uncertainty of the method was expressed by the standard deviation of the measurement set, and optionally by the Monte Carlo method. Depending on the stability of the Earth's magnetic field the method can measure the coil sensitivity with uncertainty of 50 ppm and angular misalignment with uncertainty better than 0.02 degrees.

Our experiments have proved that the results are comparable with the standard method, and even have lower uncertainty. This method is applicable for very precise calibration of coil systems which serve for further calibration of magnetic sensors.

The only requirement for this method is that the coil system must have a homogeneous space big enough to obtain valid magnetic Overhauser data.

I also improved the calibration procedure of tri-axial magnetometers. A tri-axial coil system is not used as a cancellation system but the coil system only generates a sequence of currents and the Earth's field is simultaneously monitored with a scalar magnetometer. Even a solution of this problem has to be calculated by an optimization method, precision is not reduced. On the other hands, a magnetic gradient, or variation of direction of the ambient magnetic field, limits the uncertainty of the method.

The experiments that I carried out however show, that I can achieve uncertainty of 350 ppm for sensetitvities and 0.045 degree for the orthoginality eventhough I calibrated a digital magnetometer in relatively noisy envirnment.

6.2 Magnetic tracker

An arbitrary position can be established on the basis of magnetic measurements by using optimization algorithms, when the errors are effectively suppressed. When imperfections are present, see Chapter 4.2, the distance is only the reliable quantity

but it needs to be determined very precisely. The reason is that the optimization method does not converge properly.

After the errors had been minimized, the model magnetic tracker (distance sensor) achieved precision of 5 mm in the range of 1 m, even though the measurement was carried out in a very noisy laboratory environment.

If the spatial rotation angles are measured additionally, the optimization method solves only three unknown variables and converges very easily at all arbitrary positions, and the magnetic tracker can be used in a basic manner not only for the distance.

The accuracy of the tracker is then influenced by the imperfection of the magnetic source model, which is important for small distances, and by the magnetic noise.

Since the source of the magnetic tracker is a magnetic dipole, the solution is not unique but is a symmetrical with reference to the central point. The solution is to find the data in the right half of the space by using azimuth information, or using the double coil or use a double magnetometer configuration.

The designed hybrid magnetic tracker was exploited in horizontal directional drilling. Its procedures and its signal processing are unique, because the triggering is realized by a magnetic signal. However, the accuracy is limited due to the triggering condition and the number of excitation pulses from which the magnetic data are averaged. I achieved accuracy of 0.3 meters in the 10-meter range.

6.3 Achieved objectives

- The scalar calibration procedure has been described mathematically, and a suitable calculation algorithm was chosen in Chapter 3 that is able to establish the parameters of a 3D coil system.
- According to the selected principle, the measurement procedure was designed to obtain the required number of equations. The procedure was drawn up, and a step-by-step sequence and suitable measurement devices were discussed in Chapters 3.3 and 3.5.
- The calibration procedure was analyzed in Chapter 3.3 with a view to reduce the uncertainty. Preliminary tests of the method were carried out in the Pruhonice facility. The results are presented in Chapter 3.5.
- Very high-precision testing was carried out at PTB Braunschweig and at the GFZ Niemgk observatory, where minimum uncertainty was achieved. The results of these tests have been compared with results obtained using various calibration principle. The results are presented in Chapter 3.5.

- The magnetic dipole source was used as a mathematically known magnetic source. The spatial coordinates were derived from the dipole model in Chapter 5.1 to express them in solvable way.
- The problem was analyzed and the Levenberg-Marquardt optimization method was chosen. However, since the problem has no unique solution, convergence in the specific position was not declared. The full magnetic tracker was then degraded to a magnetic distance meter (Chapter 5.2) or, when the angular spatial orientation was known, to a hybrid magnetic tracker (Chapter 5.3).
- The designed measurement setup and also the excitation principle were developed, and are presented in Chapter 5.1. The current sequence is used for excitation and the magnetic field is synchronously measured with the fluxgate magnetometer.
- A hybrid magnetic tracker was adapted for horizontal directional drilling. The completed design (hardware and software) is presented in Chapter 5.4 for using the magnetic tracker in undersurface applications, e.g. for hit-point navigation.
- A real factory test was carried out to verify functionality and precision. The accuracy of the system has been summarized in the conclusions.

- The new method for calibration of tri-axial magnetometers was developed in this dissertation beyond the objectives of this dissertation.

6.4 Issues for further research

- exploit a different kind of optimization method e.g. stochastic algorithms to solve the case of the complex magnetic tracker.
- implement the magnetic principle for a surface navigation unit, to increase the detectable distance.

7 Publications, whit author's share in %

7.1 Peer reviewed publications – journals indexed in JCR

P[1]	Ripka, P. - Zikmund, A.: Testing and Calibration of Magnetic Sensors. Sensor Letters. 2013, vol. 11, no. 1, p. 44-49. ISSN 1546-198X.	50 %
P	Zikmund, A. - Ripka, P.: A Magnetic Distance Sensor with High Precision. Sensors and Actuators. 2012, vol. 186, p. 137-142. ISSN 0924-4247.	50 % C[2]=1
P	Zikmund, A. - Ripka, P.: Calibration of the 3D Coil System's Orthogonality. IEEE Transactions on Magnetics. 2013, vol. 49, no. 1, p. 66-68. ISSN 0018-9464.	50 % C=2
P	Tomek, J. - Platil, A. - Janosek, M. - Zikmund, A. - Ripka, P.: Suppression of Environmental Noise in Magnetopneumography by the use of Higher Order Gradients. IEEE Transactions on Magnetics. 2012, vol. 48, no. 4, p. 1317-1319. ISSN 0018-9464.	20 %
P	Janosek, M. - Vyhnanek, J. - Zikmund, A. - Butvin, P. - Butvinova, B.: Effects of Core Dimensions and Manufacturing Procedure on Fluxgate Noise. Acta Physica Polonica A. 2014, vol. 126, no. 1, p. 104-105. ISSN 1898-794X.	20 %
S[3]	Zikmund, A. - Ripka, P. - Ketzler, R. - Harcken, H. - Albrecht, M.: Precise scalar calibration of a tri-axial Braunbek coil system, IEEE Transaction on Magnetics	20 %
S	Zikmund, A. - Janosek, M. - Ulvr, M. - Kupec, J.: Precise calibration method for tri-axial magnetometers not requiring Earth's field compensation, IEEE Transactions on Instrumentation and Measurement	25 %
S	Vcelak, J. - Zikmund, A. - Ripka, P.: Long Range Magnetic Tracking System, IEEE Sensors Journal	33 %

[1] P=Published
[2] C=The number of citations
[3] S=Submitted

7.2 Publications in journals excerpted by WoS

P	Zikmund, A. - Ripka, P.: Magnetic Tracker with High Precision. Procedia Engineering [online]. 2011, vol. 25, no. 25, p. 1617-1620. Internet: http://www.sciencedirect.com/science/article/ pii/S1877705811060693. ISSN 1877-7058.	50 % C=1
P	Včelák, J. - Zikmund, A. - Král, J.: Long range magnetic localization - accuracy and range study. In Sensors & Their Applications XVII. Bristol: IOP Publishing Ltd, 2013, . ISSN 1742-6588.	33 %
P	Ripka, P. - Zikmund, A. - Vcelak, J.: Long-range magnetic tracking. In IEEE SENSORS 2012 - Proceedings. Piscataway: IEEE Service Center, 2012, p. 2094-2097. ISBN 978-1-4577-1765-9.	33 %
P	Vcelak, J. - Zikmund, A. - Kral, J.: Long range magnetic localization - accuracy and range study. In Sensors & Their Applications XVII. Bristol: IOP Publishing Ltd, 2013, . ISSN 1742-6588.	33 %
P	Zikmund A., - Janosek, M.: Calibration procedure for triaxial magnetometers without a compensating system or moving parts, (I2MTC 2014) Proceedings ; 2014, ISBN: 978-1-4673-6385-3, pp. 473-476	50 %

7.3 Other publications

P	Zikmund, A. - Ripka, P.: Scalar Calibration of the 3-D Coil System. Journal of Electrical Engineering. 2010, vol. 61, no. 7/s, p. 39-41. ISSN 1335-3632.	50 %
P	Zikmund, A. - Ripka, P.: Uncertainty Analysis of Calibration of the 3D Coil System. Journal of Electrical Engineering. 2012, vol. 63, p. 90-93. ISSN 1335-3632.	50 %

7.4 Projects

SGS – 161-821940C – Application of magnetic sensors for precise measurement

8 Bibliography

Angeles Herrador, M. & Gonzalez, A. G., 2004. Evaluation of measurement uncertainty in analytical assays by means of Monte-Carlo simulation. *Talanta,* Volume 64, pp. 415--422.

Avriel, M., 2003. *Nonlinear programming.* 1st ed. New Jersyey: Dover Publications.

Braunbek, W., 1934. Die Erzeugung weitgehend homogener Magnetfelder durch Kreisstraeme. *Zeitschrift fuer Physik,* Volume 88, pp. 399-402.

Bronaugh, E. L., 1990. *Helmholtz coils for emi immunity testing: stretching the uniform field area.* s.l., s.n., pp. 169--172.

Ding, L. et al., 2009. Equivalent magnetic noise limit of low-cost GMI magnetometer. *Sensors Journal, IEEE,* Volume 9, pp. 159--168.

Fanselau, G., 1929. The generation of large and homogenous magnetic field through circuits. *Z Phys,* Volume 54, pp. 260--269.

Firester, A. H., 1966. Design of square Helmholtz coil systems. *Review of Scientific Instruments,* Volume 37, pp. 1264--1265.

GUM, 1994. *Guide to the Expression of Uncertainties in Testing ,* Teddingtion: National Physical Laboratory.

Hakkinen, L. & Ryno, J., 1990. Measuring sensitivities and orthogonalities of magnetometer sensors in the Nurmijarvi coil hut. *Proceedings of the International Workshop on Geomagnetic Observatory Data Acquisition and Processing,* Volume 1, pp. 37-39.

Hakkinen, L., Ryno, J. & Sucksdorff, C., 1990. Coil system for the production of three-component uniform magnetic field at the Nurmijarvi observatory. *Proceedings of the International Workshop on Geomagnetic Observatory Data Acquisition and Processing,* Volume 1, pp. 17-22.

Heillig, B., 2012. Determining the orthogonality error of coil systems by means of a scalar magnetometer: application to delta inclination, delta declination (dIdD) magnetometers. *Meas. Sci. Technol,* Volume 23.

Hemshorn, A., Auster, H. & Fredow, M., 2009. DI-flux measurement of the geomagnetic field using a three-axial fluxgate sensor. *Measurement Science and Technology,* Volume 20, p. 027004.

Herceg, D., Juhas, A. & Milutinov, M., 2009. A design of a four square coil system for a biomagnetic experiment. *Facta universitatis-series: Electronics and Energetics,* Volume 22, pp. 285--292.

Jankowski, J. & Sucksdorff, C., 1996. Guide for magnetic measurements and observatory practice.

Kirschvink, J. L., 1992. Uniform magnetic fields and double-wrapped coil systems: Improved techniques for the design of bioelectromagnetic experiments. *Bioelectromagnetics,* Volume 13, pp. 401--411.

Liu, T. & Wang, B., 2011. Study of magnetic ranging technology in horizontal directional drilling. *Sensors and Actuators A: Physical,* Volume 171, pp. 186--190.

Liu, Y., Wang, Y., Yan, D. & Zhou, Y., 2004. *DPSD algorithm for AC magnetic tracking system.* s.l., s.n., pp. 101--106.

Malatek, M., Ripka, P. & Kraus, L., 2008. Temperature offset drift of GMI sensors. *Sensors and Actuators A: Physical,* Volume 147, pp. 415--418.

Marquardt, D. W., 1963. An algorithm for least-squares estimation of nonlinear parameters. *Journal of the Society for Industrial & Applied Mathematics,* Volume 11, pp. 431--441.

Meza, J. C., 2010. Steepest descent. *Wiley Interdisciplinary Reviews: Computational Statistics,* Volume 2, pp. 719--722.

Olsen, N. et al., 2003. Calibration of the Orsted vector magnetometer. *Earth Planets and Space,* Volume 55, pp. 11--18.

Raab, F. H., Blood, E. B., Steiner, T. O. & Jones, H. R., 1979. Magnetic position and orientation tracking system. *Aerospace and Electronic Systems, IEEE Transactions on,* pp. 709--718.

Ripka, P., 2001. *Magnetic sensors and magnetometers.* s.l.:Artech House.

Ripka, P., Tondra, M., Stokes, J. & Beech, R., 1999. AC-driven AMR and GMR magnetoresistors. *Sensors and Actuators A: Physical,* Volume 76, pp. 225--230.

Ripka, P. et al., 2003. AMR magnetometer. *Journal of magnetism and magnetic materials,* Volume 254, pp. 639--641.

Ripka, P. & Zikmund, A., 2013. Testing and Calibration of Magnetic Sensors. *Sensor Letters,* January, Volume 11, pp. 44--49.

Ripka, P., Zikmund, A. & Vcelak, J., 2012. *Long-range magnetic tracking.* s.l., IEEE Service Center, pp. 2094--2097.

Risbo, T. et al., 2003. Ã˜rsted pre-flight magnetometer calibration mission. *Measurement Science and Technology,* Volume 14, p. 674.

Roetenberg, D., Slycke, P., Ventevogel, A. & Veltink, P., 2007. A portable magnetic position and orientation tracker. *Sensors and Actuators A: Physical,* Volume 135, pp. 426--432.

Song, S. et al., 2013. An Electromagnetic Localization and Orientation Method Based on Rotating Magnetic Dipole.

Stupak Jr, J. J., 1995. *A method of calibrating Helmholtz coils for the measurement of permanent magnets.* s.l., s.n., p. 39.

Taylor, B. N., 2009. *Guidelines for Evaluating and Expressing the Uncertainty of NIST Measurement Results (rev.* s.l.:DIANE Publishing.

Tomek, J. et al., 2007. Gastric motility and volume sensing by implanted magnetic sensors. *Sensor Letters,* Volume 5, pp. 276--278.

Tomek, J. et al., 2008. The precision of gastric motility and volume sensing by implanted magnetic sensors. *Sensors and Actuators A: Physical,* Volume 142, pp. 34--39.

Vcelak, J., Zikmund, A. & Kral, J., 2013. *Long range magnetic localization - accuracy and range study.* s.l., IOP Publishing Ltd, pp. --.

Vcelak, J., Zikmund, A. & Ripka, P., 2012. *Magnetic Ranging System.* s.l., Slovak University of Technology, p. 17.

Waters, G. & Phillips, G., 1956. A new method of measuring the earths magnetic field. *Geophysical Prospecting,* Volume 4, pp. 1--9.

Zikmund, A. & Ripka, P., 2010. Scalar calibration of 3-D coil system. *J. Elect. Eng,* Volume 61, pp. 39--41.

Zikmund, A. & Ripka, P., 2011. Magnetic Tracker with High Precision. *Procedia Engineering,* 11, Volume 25, pp. 1617--1620.

Zikmund, A. & Ripka, P., 2012. A Magnetic Distance Sensor with High Precision. *Sensors and Actuators,* October, Volume 186, pp. 137--142.

Zikmund, A. & Ripka, P., 2012. Uncertainty Analysis of Calibration of the 3D Coil System. *Journal of Electrical Engineering,* December, Volume 63, pp. 90--93.

Zikmund, A. & Ripka, P., 2013. Calibration of the 3D Coil Systems Orthogonality. *IEEE Transactions on Magnetics,* January, Volume 49, pp. 66--68.

9 Abbreviations

AD	Analog-to-digital
ADC	Analog-to-digital converter
ESR	Electron spin resonance
GFZ	Geoforschungs Zentrum
GST	Gyro-steering tool
HDD	Horizontal directional drilling
IMU	Inertial measurement unit
MOSFET	Metal–oxide–semiconductor field-effect transistor
OVH	Overhauser
PCB	Printed circuit board
PTB	Physikalisch-Technische Bundesanstalt
RF	Radio frequency
SMD	Surface-mount device
SPI	Serial peripheral interface
ppm	Parts per million